ELECTROCHROMISM AND SOLUTION-PROCESSED POLYMER ELECTROCHROMIC DEVICES

by

Jiazhi He

A Dissertation

Submitted to the Faculty of Purdue University

In Partial Fulfillment of the Requirements for the degree of

Doctor of Philosophy

Department of Chemistry

West Lafayette, Indiana

December 2019

THE PURDUE UNIVERSITY GRADUATE SCHOOL
STATEMENT OF COMMITTEE APPROVAL

Dr. Jianguo Mei, Chair

Department of Chemistry

Dr. Shelley Claridge

Department of Chemistry

Dr. Chengde Mao

Department of Chemistry

Dr. Kejie Zhao

School of Mechanical Engineering

Approved by:

Dr. Christine A. Hrycyna

This dissertation is dedicated to my loving and supportive advisors, friends, and family.

ACKNOWLEDGMENTS

Thanks to my advisor Prof. Jianguo Mei for creating an open environment in the group, inspiring us for new ideas, and encouraging us to cooperate and stepping out from our comfort zone. I deeply appreciate your patience in guiding me and reminding me of details that I could have done better. Thank you for creating opportunities for me to take leadership on projects and ownership in the lab, which provides me the best preparations for my next stage.

Many thanks also go to my colleagues, William Mcnutt, Saadia T Chaudhry, Aristide Gumyusenge, Xuyi Luo, Dung T Tran, Kuluni Perera, Kaelon Athena Jenkins, Ke Chen, and Zhifan Ke, for many great times in Purdue and camping trips. To Dr. Yan Zhao, thank you for guiding me, giving me advice, and helping me in my most struggling time. Special thanks go to my friend, my teacher, and my teammate – Dr. Liyan You, without your support, I could not have explored broadly in this field. Thanks to my friend Dr. Rong Xu for teaching me electrochemistry and discussing scientific problems with me, for cooking great foods and hosting hot-pot parties.

Finally, I would like to thank my family. To father, you were my first teacher in 'science'. You always try to find the answers for the interesting phenomena in our daily lives and never give up until you can explain them in a scientific way, which inspires me and makes me stay curious for new knowledge. Thank you for giving me your support without any hesitation and reservation when I told you that I had a plan to study aboard. I do not know how much 'complaints' that you received from mother by sending her child away for six years. To mother, thank you for always being ready for my bad news and giving me the best courage to overcome them. Everything becomes easier after sharing with you. To Jiayingzi and my 'little' kitty – Mowga, thank for accompanying me through this unforgettable journey and being the warmest memories.

TABLE OF CONTENTS

LIST OF TABLES

LIST OF FIGURES

LIST OF SCHEMES

ABSTRACT

There are still technique hurdles that needed to be overcome in the commercialization of electrochromic devices (ECDs) for energy-saving smart windows. Among them, the long-term stability of ECDs and the high fabrication cost are the critical issues. The pricey ECDs can only be paid off through saving the energy for years, and their price will be dramatically lower if they can be solution-processed. Here, we studied the ions behaviors in the open-circuit state of electrochromic conjugated polymers (ECPs) which is important to the stability of ECDs during the operation. Moreover, we investigated the solution-processable ion storage layers and paired them with p-type ECPs and demonstrated the possibility of using them in the highly efficient roll-to-roll fabrication of ECD.

The crosslinkable non-color changing nitroxy radical-based polymer was investigated as the ion storage layer. With the applied of crosslinking strategy, the dissolution problems of radical polymers-based counter electrode in the electrolyte was suppressed, resulting in the enhancement of both performance and cycling stability of ECDs. Although p-type ion storage materials are widely studied as the ion storage layers for ECPs, they need to go through complicated pretreatment processes, including pre-oxidation, washing, and drying, before they can be paired with ECPs in an ECD. This complicated process greatly increases the fabrication cost.

In our last work, we applied the UV ozone (UVO) pretreatment to the solution-processed n-type niobium oxide and evaluated its potentials to be used as the ion storage layer for p-type ECPs. The UVO pretreatment generates strong oxidants like ozone or atomic oxygen which induce the photolysis of organic residues of ligands and organic solvent trapped in the solution-processed metal oxide layer led to the formation of free radical species. These highly reactive species promoted the formation of the amorphous metal−oxygen network. Following by low-temperature annealing (< 150 ^{o}C), the ion-storage properties of niobium oxide is comparable with the high temperature annealed (300 ^{o}C) niobium oxide. The method is successfully applied to fabricate niobium oxide on a flexible conductive substrate and demonstrate the capability to pair with p-type ECPs and fabricate high-performance ECDs without the need of any pretreatments. The low-temperature solution processing of both layers will significantly reduce the fabrication cost of ECDs.

CHAPTER 1. INTRODUCTION

1.1 Background

With rapid economic growth, energy demands increase dramatically (Figure 1.1).[1] Among these primary energy consumptions, over 40% is consumed by buildings in the US and Euro.[1] A large amount of the building energy is used for space heating/cooling and lighting. To mitigate the global energy crisis, the use of renewable energy including wind power, hydropower, solar energy, geothermal energy, and bioenergy needs to be increased.

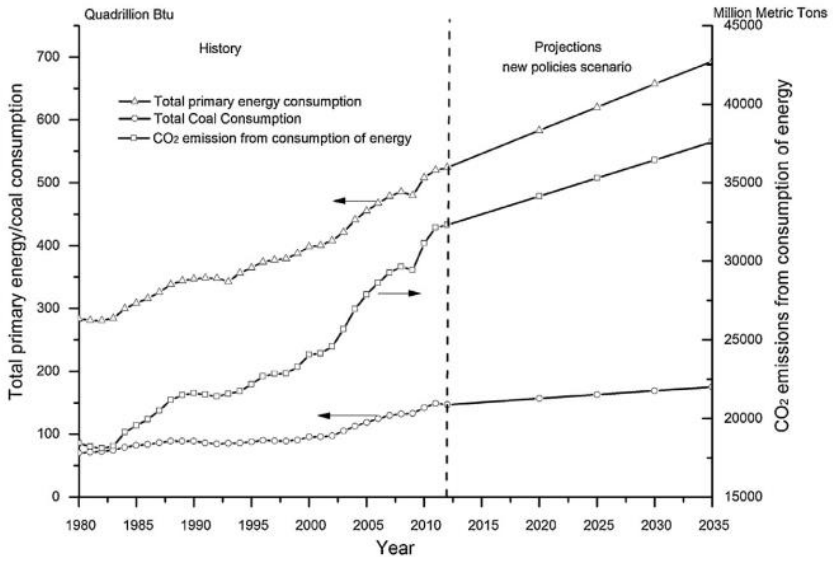

Figure 1.1 Global primary energy consumption, coal consumption and CO_2 emission from consumption of energy from 1980 to 2035. Reprinted from ref 1, Copyright 2016, with permission from Elsevier.

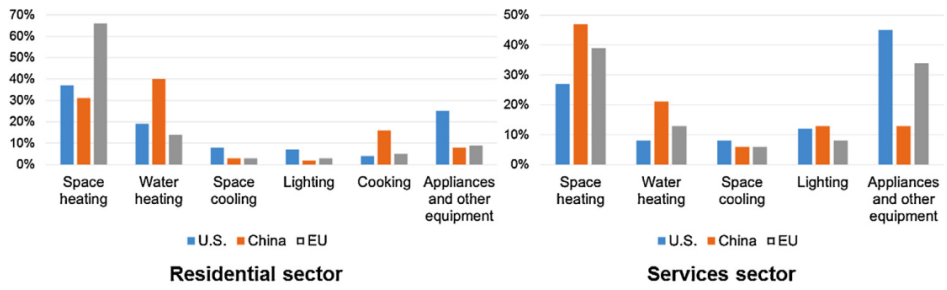

Figure 1.2 Percentage of building energy end-use in the U.S., China and the E.U., in 2010. Reprinted from ref 1, Copyright 2016, with permission from Elsevier.

Energy-saving electrochromic devices (ECDs) are very promising to be used in building windows to manage the solar light.[2] Annually, ~ 40 kWh m^{-2} of windows can be saved after replacing the regular windows with ECDs.[3] Considering the hundreds and thousands of skyscrapers using glass walls, the amount of energy saving could be enormous. When a small potential bias (< 2.5 V) was applied, the absorption of the electrochromic materials can be tuned due to the electrochemical doping resulting in the formation of polarons and bipolarons with smaller bandgaps. Thus, the absorption of the electrochromic materials shifts from visible light to the IR and NIR regions. By consuming a small amount of the energy, the interior lighting and temperature conditions, which are related to the visible light and IR and NIR light respectively, can be adjusted to obtain the desired visual and temperature comfort. However, the high fabrication cost has become one of the biggest obstacles for the market penetration of the energy-saving ECDs.[4] One way to compensate the high cost is to extend their lifespan and save energy in a long run. In general, more than 20 years of lifespan and 5 years of warranty are targeted for energy saving applications. If ECDs are switched twice a day, the optical contrast will be needed to be maintained for more than at least 15, 000 cycles to meet the needs. Another is to design electrochromic materials that can be highly efficient roll-to-roll (R2R) manufactured on flexible transparent conducting substrates, which can significantly lower the production cost compared to ECDs that are fabricated via magnetic sputtering on glasses under the conditions of high temperature and high vacuum.

1.2 Electrochromic Devices

ECDs usually comprise a stack of five layers – two transparent conducting layers and three major components in between, including the electrochromic layer (EC layer, also referred to working electrode (WE)), electrolyte, and ion storage layer (IS layer, also referred to counter electrode (CE)) (Figure 1.3a). There are also other configurations for ECDs. For example, the all-in-one ECDs that usually have one EC medium in between of two TCO layers (Figure 1.3b). The EC medium is made of mixtures of small molecules based electrochromic materials[5] (e.g. viologen[6] and transition-metal coordination complexes[7], and their derivatives), charge balancing small molecules, and electrolyte. They can be further fixed via the crosslinking in a polymer matrix to form an electrochromic gel. These devices usually are not bis-stable which means that they need extra power to maintain the states of ECDs, which is not ideal for saving energy. Another type of configuration is the lateral electrochromic device, in which the WE and CE are coated on separated TCO layer but the same substrate (Figure 1.3c). In this configuration, the color switching process of the WE and CE will not interfere each other, and it can be used to create all kind of colorful patterns.[8,9] However, if solid-state electrolyte is used in this configuration, it will be very difficult for ions to transport across the electrolyte that bridged the WE and CE layers. When it comes to the large-size ECDs e.g. 2 × 3 meters size used in building windows, the ions migration will become even more difficult. Thus, the ideal configuration for ECDs used in smart windows application is still the multilayer structure. In the inorganic multi-layer ECDs, the ECDs are fabricated by magnetron sputtering in the sequence of TCO/WE/electrolyte/CE/TCO on a glass.[10] The whole process usually required high vacuum and high-temperature annealing to achieve stable electrochromic performance. As a result, the capital expenditure (Capex) on the fabrication plants usually cost ~ $100 million. The high Capex and low-efficiency production line make the final price of the ECD extremely high (~ $ 800/m^2) and unaffordable for most of the commercial and residential buildings. We believed the only possible way to lower the process is to use low temperature (< 150 °C) solution-processable materials for both EC and IS layers. Thus, the following discussions in the thesis will be based on these promising materials.

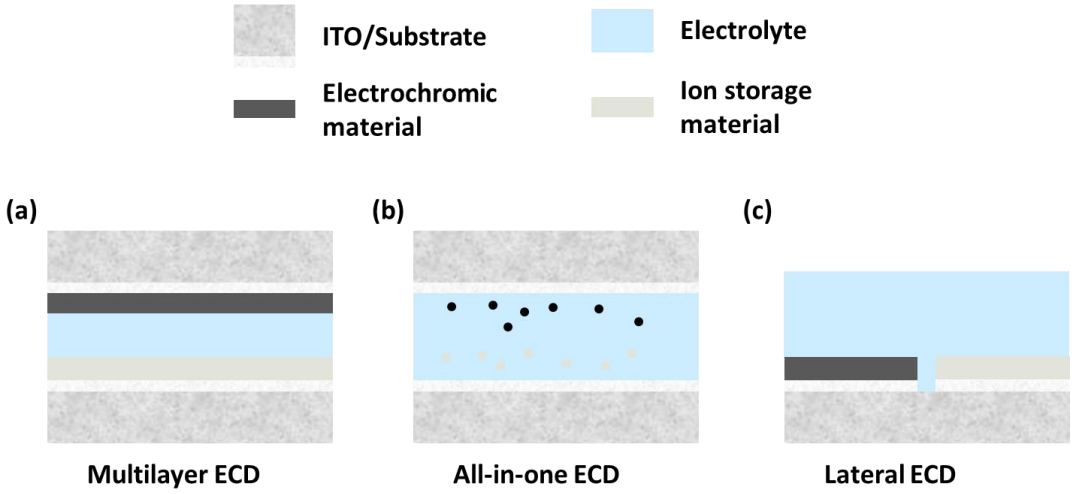

Figure 1.3 Electrochromic devices in different configurations: (a) multilayer, (b) all-in-one, (c) lateral.

1.3 Electrochromic layers

There are many types of electrochromic materials including inorganic metal oxides, organic small molecules, inorganic transition metal complex, etc.[5] Nevertheless, there are only a few examples of them being demonstrated in the roll-to-roll processing on the flexible substrate.[11] In contrast, Reynold *et al*. have developed a group of solution-processable electrochromic conjugated polymers that are able to be switched from the cyan, yellow, magenta, black color state to the transmissive state.[12] Compared with the inorganic electrochromic materials, electrochromic conjugated polymers (ECPs) usually have a higher coloration efficiency, a faster switching kinetics, and more color options.[13] The color switching of ECPs is controlled via the reversible electrochemical doping/de-doping process. Most of the well-studied ECPs belong to the category of P-type cathodically coloring polymers, which means the ECPs can only be switched between the color and bleach states via P-type (oxidation) doping and de-doping. Upon the oxidation process, ECPs lose electrons associated with anions insertion to maintain the charge neutrality and form polarons/bipolarons. (eq 1) These polarons and bipolarons generate new band structures with a narrower gap, which shifts the new absorption bands from visible wavelengths to near-infrared or infrared (Figure 1.4).[14] As a result, the ECPs change from a color to a transmissive state. During the reduction process, the P-doped ECPs (polarons and bipolarons) are recovered to the neutral states along with the absorption in the visible region. In contrast to the p-type ECPs, n-type ECPs

have faced stability issues in the n-doped states especially when exposed to water and oxygen. Lacking the studies of n-type ECPs limits the choice of materials used in ECDs, which will be discussed in the following section.

$$ECP + M^+ \cdot A^- \leftrightharpoons ECP^+ \cdot A^- + M^+ + e^- \quad (1)$$

In which *ECP* represents the electrochromic conjugated polymer, A^- is the counter anion, M^+ is the metal or organic cations, e^- is the electron, and the ECP^+A^- is the oxidized electrochromic conjugated polymer with the counter anion.

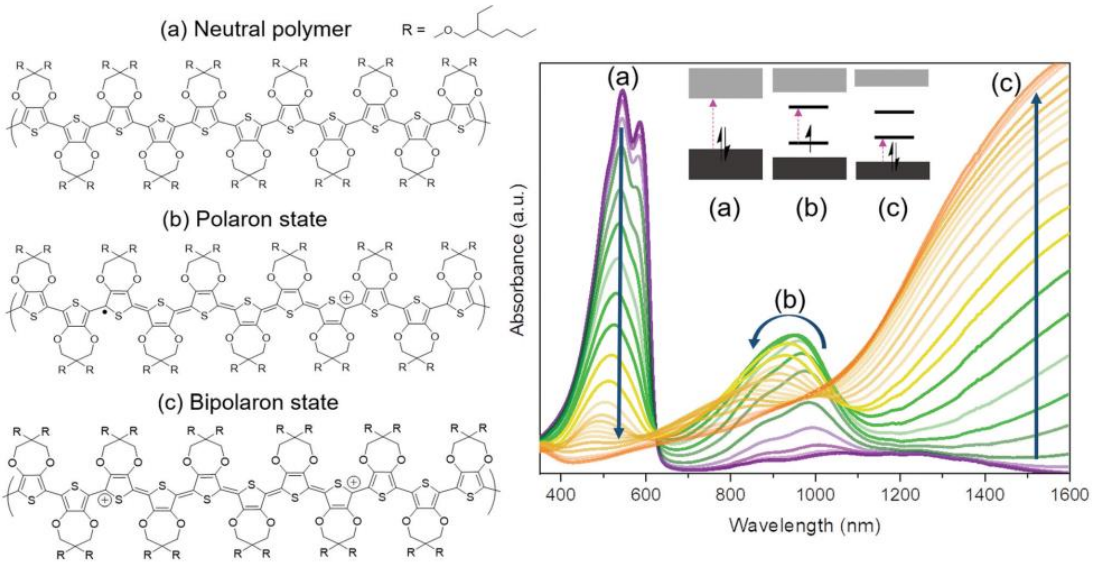

Figure 1.4 Molecular structures of poly(3,4-propylenedioxythiophene) (PProDOT) in (a) neutral state, (b) polaron state and (c) Bipolaron state and the UV-vis of the PProDot upon the small increment of the applied potential. Reproduced from Ref. 14 with permission from The Royal Society of Chemistry

1.4 Ion Storage Layers

The role of IS layers is to balance the charges in an ECD. For example, when an ECP is oxidized along with the intercalation of anions, in the meanwhile, the IS layer is reduced together with the intercalation of cations (Figure 1.5). Otherwise, side reactions will happen to compensate the charges consumed in the ECPs during the oxidation reactions leading to the poor cycling

stability of ECDs. To optimize the performance of ECDs, it is important to pair the electrochromic layer (EC layer) with an appropriate IS layer.

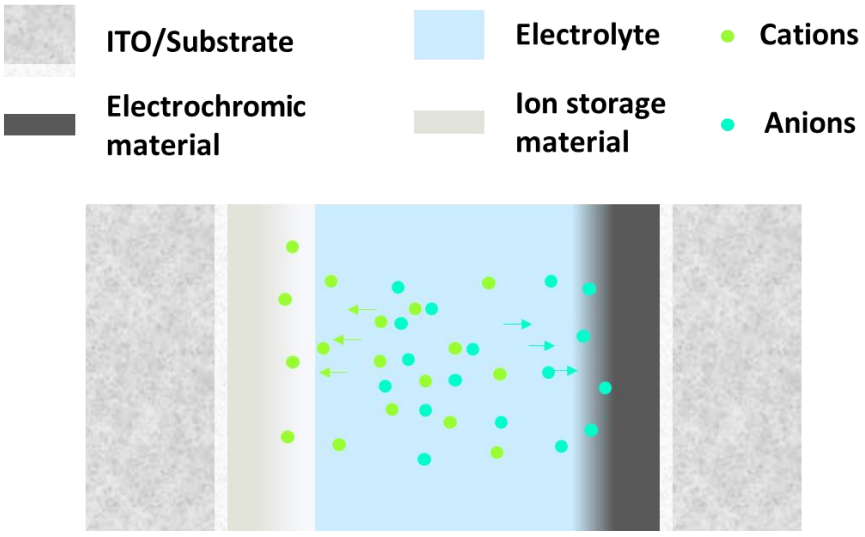

Figure 1.5 Ions intercalation in the operation of electrochromic devices

Based on the electrochromism of materials, there are mainly three types of IS layers namely complementary, non-color changing, and minimally color-changing IS layers. A complementary IS layer has the coloration efficiency that is comparable to the EC layer. For example, in the case of the most studied metal oxides ECDs – WO_3//NiO.[15] The coloration efficiency of NiO (~ 80 cm^2 C^{-1}) is on the bar with the EC materials WO_3. The color switching of them during the electrochemical reaction must match to give the best performance. WO_3 is n-type cathodically coloring materials that change from bleached to the colored state during the reduction. While NiO is the p-type anodically coloring materials that become colored during the oxidation. During the operation of ECD, they can be simultaneously switched from the bleached to colored state and vice versa.

In the case of non-color changing IS materials, the IS layer is electrochromic inactive in the visible wavelength region. The most studied example is the nitroxyl based radical polymers. The redox-active nitroxyl radical groups are attached to the non-conjugated polymer backbone so that the IS layer maintain highly transparent at both its radical and cation forms (Scheme 1.1).[16]

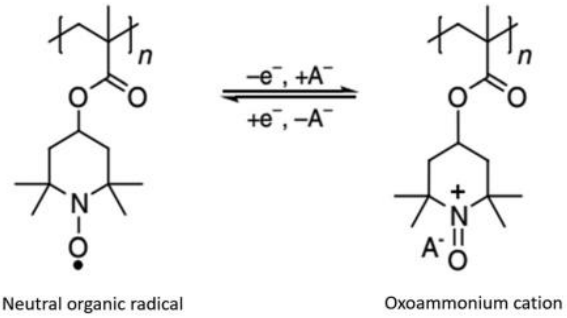

Scheme 1.1 Chemical structures of PTMA in its neutral radical and cationic states. Reprinted with permission from ref. 268. Copyright 2018 Springer Nature.

The last type is minimally color-changing IS layer. In this configuration, the IS layer is a 'poor' electrochromic material that has a low coloration efficiency in the visible wavelength region. The absorption of P-type N-alkyl-substituted PProDOPs locates at UV region in the neutral state and shifts to NIR wavelength region upon oxidation with the minimal color residue at both the neutral and P-doping states in the visible wavelength region (Figure 1.6).[17] Hence, it was used as the minimally color-changing counter electrode for ECPs. More detailed discussions on the advantages and disadvantages of using these three types of IS layer will be given in the following discussions.

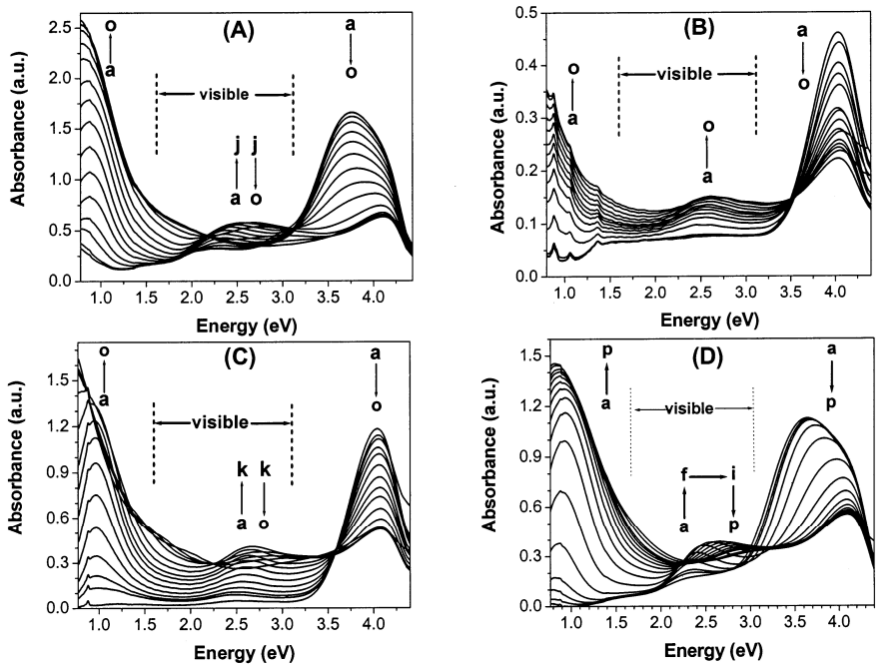

Figure 1.6 Spectroelectrochemistry of N-alkyl PProDOPs in 0.1 M $LiClO_4$/PC vs Fc/Fc^+: (a) N-Methyl PProDOP, (b) N-Pr PProDOP, (c) N-Gly PProDOP (d) N-PrS PProDOP upon small increment of potentials. Reprinted with permission from Ref 17. Copyright 2003 American Chemical Society.

1.5 Electrolytes

The electrolyte layer is used to physically separate the EC and IS layers and provide the ionic conduction. They can be fabricated in different forms including liquid, solid, and gel. The most preferable form in the application of smart windows is the solid electrolyte that has ionic conductivity over 10^{-7} S cm^{-1} and electron conductivity less than 10^{-12} S cm^{-1}.[18] During the fabrication of the ECDs, the solvent casting, and crosslinkable polymeric electrolyte can be used to further enhance the production efficiency. After WE and CE are coated, the gel electrolyte or the as-prepared crosslinkable electrolyte precursors comprising monomers, lithium salts, (plasticizers) can be applied to glue both electrodes together into the finally ECD via vacuum drying or photo-/thermal- crosslinking (Figure 1.7). This route can be integrated into the continuous inline production to further lower the production cost (Figure 1.8).

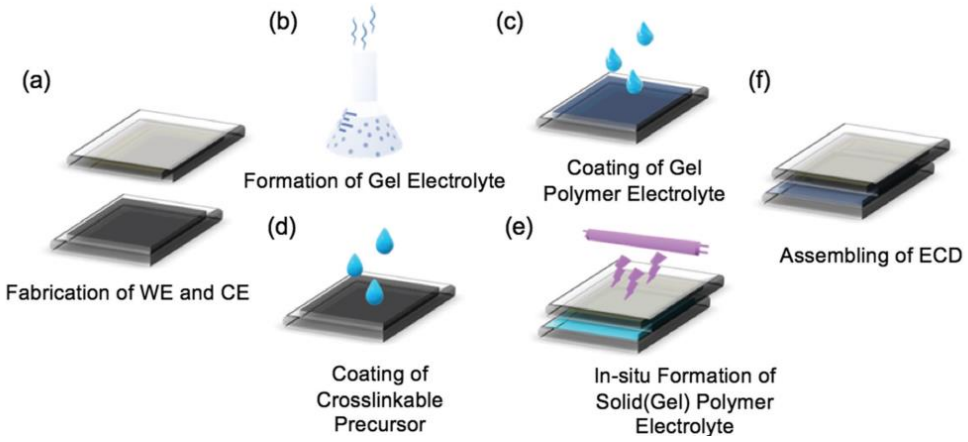

Figure 1.7 Schematic representation of steps followed when fabricating the electrolyte layer of an ECD. (a) As-fabricated WE and CE. (b) Evaporation of solvent to form gel electrolyte. (c) Gel polymer electrolyte applied on either WE or CE. (d) Coating of the cross-linkable electrolyte precursor. (e) Photo-/thermal crosslinking of cross-linkable precursor to form solid(gel) polymer electrolyte. (f) Assembling the working and counter electrodes on either side of the electrolyte to fabricate the ECD. Reproduced from Ref. 14 with permission from The Royal Society of Chemistry

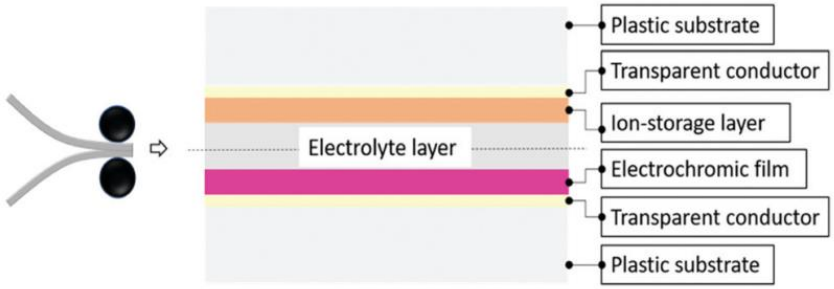

Figure 1.8 In-situ lamination approach enabling the roll-to-roll (R2R) manufacturing of ECDs. Reproduced from Ref. 14 with permission from The Royal Society of Chemistry

1.6 Characterizations

When new materials are designed, some routine characterizations and matrices are used to evaluate their performance. Herein, the characterization techniques will be discussed in the sequence of the experiments that are usually carried out to unveil the performance of new electrochromic materials in the lab.

1.6.1 Electrochemical Techniques

Electrochromic materials are essential redox-active materials. Understanding their electrochemical behaviors provide the necessary information to use in other characterization techniques, as well as the understanding of their electrochromism.

1.6.1.1 Electrochemical Cells

On the contrary to the application, a three-electrode liquid cell (a half-cell) is a better platform to understand the redox behavior of electrochromic materials. In a three-electrode liquid cell, the electrochromic material coated on the ITO/glass substrate is used as the WE. Although electrochromic materials coated on platinum is also often used in the three-electrode liquid cell to evaluate the electrochemical performance of EC materials, the work function of platinum and the adhesion of the EC materials on the platinum are different compared to the cases that used either the ITO/ or FTO/glass. The obtained results could make researchers draw the very different conclusions. A reference or quasi-reference electrode with a stable electrode potential (e.g. Ag, Ag/AgCl, Ag/Ag^{+}, etc.) is used to determine the electrochemical potentials of the WE with respect to them. A platinum counter electrode is used to complete the circuit of the cell and the current flow can be measured. The potential of the platinum counter electrode is adjusted to balance the electrochemical reactions in the working electrode. Hence, the potentials of the WE versus the reference electrode can be stabilized. The electrochemical reactions on WE at these potentials (vs. reference electrode) can be investigated. The electrolyte used in the cell is usually made of salts (usually lithium salts and ammonium salts) dissolved in polar solvents such as acetonitrile and propylene carbonates, etc.

1.6.1.2 Cyclic voltammetry (CV)

CV is a potential technique that scans the voltage in a constant rate between two potentials for certain cycles (Figure 1.9). The current responses at different potentials are collected for analysis. The electrochemical stable window can be used to set the potentials in the spectroelectrochemistry and double potential step chronoamperometry and chronoabsorptometry experiments. Moreover, the reversibility of the electrochromic materials can be evaluated by the following criteria:

a) the peak-to-peak separation ($\Delta E = E_{pa} - E_{pc}$) needs to be within 59/n mV, where n represents the number of electrons involved in the electrochemical reaction, E_{pa} and E_{pc} are the anodic and cathodic peak potentials, respectively;

b) the positions of peak voltage do not alter as a function of voltage scan rate;

c) the ratio of the cathodic and anodic peak currents ($\frac{I_{pa}}{I_{pc}} \approx 1$) is equal to one, where I_{pa} and I_{pc} are anodic and cathodic peak currents, respectively.

d) the peak currents are proportional to the square root of the scan rate; According to the Randles–Sevcik equation:

$$I_p = 0.4463nFAC(\frac{nFvD}{RT})^{\frac{1}{2}} \quad (2)$$

in which *F* is the Faraday constant, *A* is the electrode area, *C* is the concentration, *D* is the diffusion coefficient, *R* is the gas constant, *T* is the temperature.

According to the eq 2, the diffusion coefficient (*D*) of ions involved in the electrochemical reactions can be derived from the slope of the peak current vs. square root of the scan rate curve (Figure 1.10).

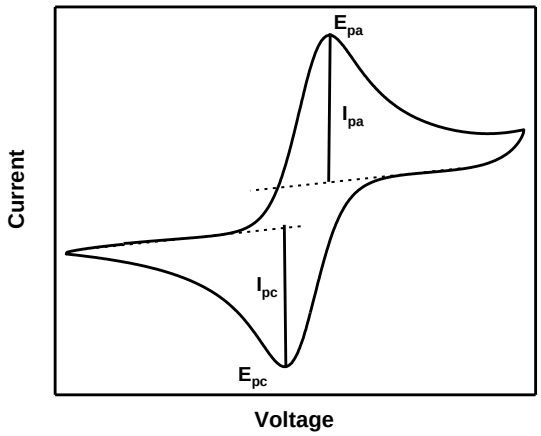

Figure 1.9 Cyclic voltammograms with peak potentials and currents labeled.

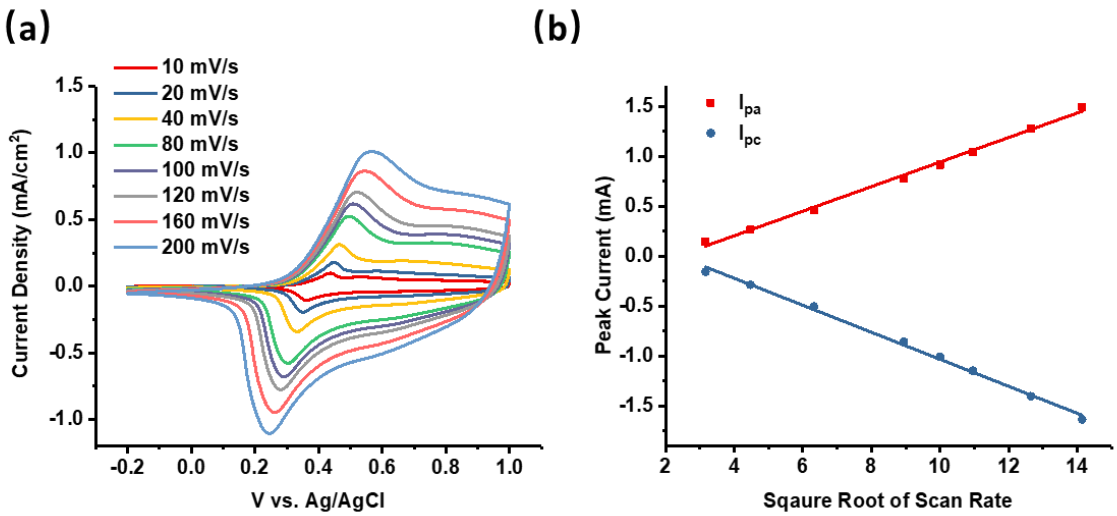

Figure 1.10 (a) Cyclic voltammetry of a conjugate polymer at different scan rates ranging from 10mV/s to 200 mV/s. (b)The peak current vs. square root of scan rate.

1.6.1.3 Electrochemical Impedance Spectroscopy (EIS)

EIS is an impedance technique used to characterize the impedance of the electrochemical reactions including the electrochemical double layer formed at the electrode and electrolyte interfaces, charge transfer, diffusion of counterions into the bulk, etc. In the EIS experiment, a small sinusoidal potential (with an amplitude of ~ 10 mV) over a frequency range of 10^{-1} - 10^{6} Hz is applied to the electrochemical system. The potentiostat automatically converts the obtained current signals to impedance ($Z = \frac{E}{I}$) which can be further represented as complex numbers and plotted in a Nyquist plot (Figure 1.11a). Or the impedance can be plotted versus frequency to obtain the Bode plot (Figure 1.11b).

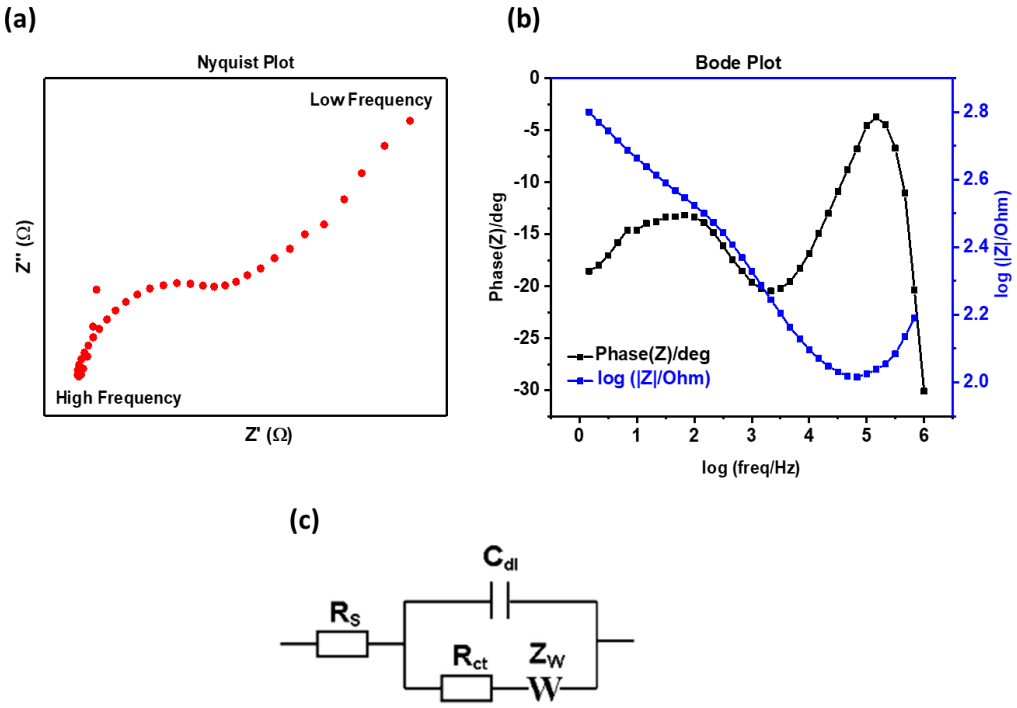

Figure 1.11 (a) Nyquist plot and (b) Bode plot of an electrochemical cell. (c) A Randles circuit.

To obtain the exact impedance values related to the electrochemical processes in the Nyquist plot, an equivalent electrical circuit is used to fit the raw data. For instance, in the typical Randle circuit (Figure 1.11c), R_s is the solution resistance, R_{ct} is the charge transfer resistance, C_{dl} is the double layer capacitance, Z_w is the Warburg diffusion impedance. After fitting, the obtained values can be used to evaluate the electrochemical performance of materials.

1.6.2 Spectroelectrochemistry

Spectroelectrochemistry is usually carried out to characterize a serious of electrochemical reactions of an analyte. In the multilayer ECDs, the color change is stepless tinting process controlled by the applied potential. Thus, the spectra of the EC layers that are at neutral, polarons, and bipolarons or mixed states can be captured when a small potential was applied in a small increment. The transition processes from neutral to polarons and finally bipolarons along with their colors changing can be investigated (Figure 1.4).

1.6.3 Double Potential Step chronoamperometry and chronoabsorptometry (DPSC)

DPSC is a chronoamperometry technique that cycled between step potentials with a certain holding period and the current signals are collected by potentiostat while the absorbance/transmittance change at certain wavelength over time was collected by UV-vis spectrophotometer (Figure 1.12).

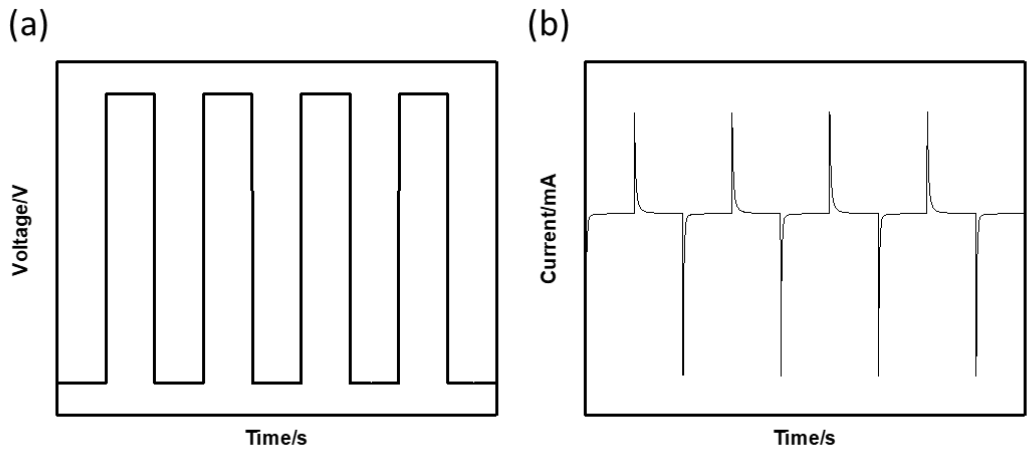

Figure 1.12 (a) A square wave of potentials. (b) The current signals under the applied square wave of potentials.

1.6.3.1 Optical Contrast

A square-wave absorbance/ transmittance usually can be obtained during the DPSC experiments when the kinetics of the electrochemical reactions are fast enough compared to the holding period. The optical contrast (ΔT) can be obtained from the difference of the highest transmittance (T_H)and the lowest transmittance (T_L).

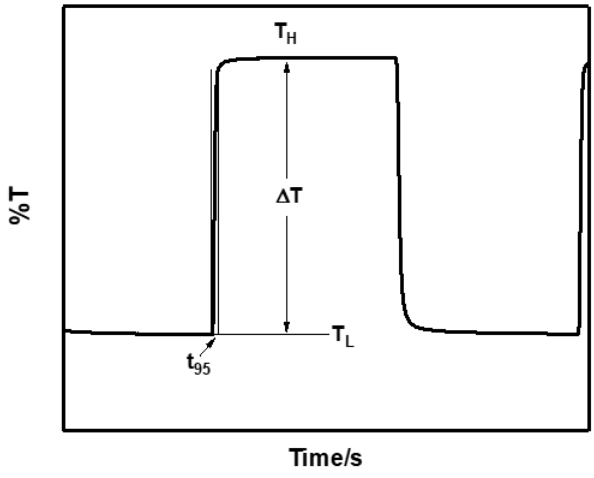

Figure 1.13 Transmittance of the electrochromic cell under the applied square wave of potentials.

1.6.3.2 Switching time

The switching time is usually set to be time taken to switch from the T_L to a percentage of the optical contrast. For example, the time to switch 95% of the ΔT is indicated in Figure 1.13.

1.6.4 Coloration efficiency

The cumulative charge density over time can be obtained from the integration of the current over time curve in the chronoamperometry experiment. In the meanwhile, the change of the optical density can be obtained from the chronoabsorptometry experiment. Then, they can be replotted in the change of the optical density versus the charge density (Q) curve by coordinating the time axis and the coloration efficiency can be obtained from the slope (Figure 1.14).

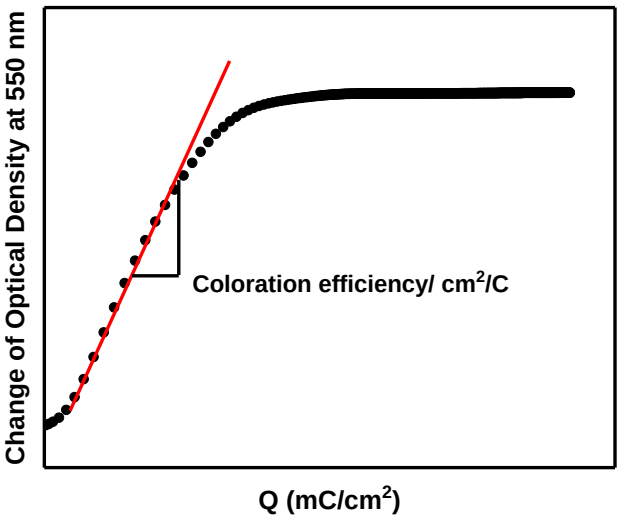

Figure 1.14 Change of optical density vs. charge density.

1.7 Atomic Force Microscopy (AFM)

AFM is a scanning probe imaging tool that can capture surface morphological features (in nm scale) of electrochromic thin films. Another important application of AFM is to measure the thickness of the electrochromic materials in a step height measurement; the electrochromic materials are pre-scratched with needles and the height difference of the scratched area and the un-scratched films were measured to obtain the thickness (Figure 1.15).

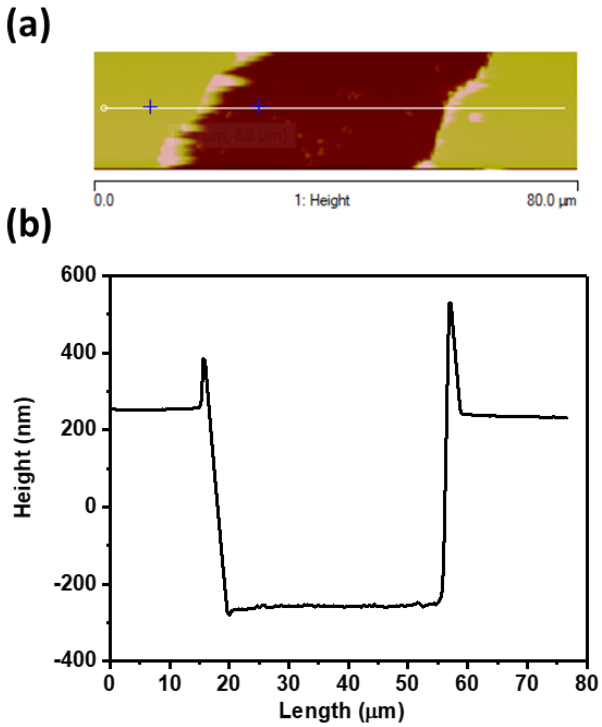

Figure 1.15 (a) AFM image and (b) step height measurement of the scratched thin-films.

CHAPTER 2. SELF-BLEACHING BEHAVIORS OF ELECTROCHROMIC CONJUGATED POLYMERS

This chapter was adapted with permission from the manuscript published in ACS Applied Materials & Interfaces: He, J.; You, L.; Mei, J. Self-Bleaching Behaviors in Black-to-Transmissive Electrochromic Polymer Thin Films. ACS Appl. Mater. Interfaces 2017, 9 (39), 34122–34130.

2.1 Abstract

Polymer-based electrochromic smart window is an emerging energy-saving technology. There are several technological hurdles in the development of organic electrochromics. In this article, self-bleaching behaviors of a black electrochromic polymer (ECP-black) thin film were investigated. We found that the electrochemical break-in process led to a less dense morphology and the increased free volume facilitated ion permeation in the ECP-black thin films. The polarized interface between polymer thin film and transparent indium-tin-oxide (ITO) electrode made charge transfer accessible, which caused the self-bleaching behaviors. Herein, we proposed two approaches to study and mitigate the self-bleaching phenomenon. First, a densely-packed morphology was regenerated by increasing the cathodic polarization time under open-circuit conditions (V_{off}). The second involved the modification of the electrode (ITO) surface with a partial coverage of octadecyltrichlorosilane (OTS) layer. The combination of the two approaches rendered ECP-black thin film capable of maintaining the colored state up to 900 s. To extend the scope of our studies, self-bleaching of ECP-magenta and ECP-blue thin films were also tested and suppressed by using these two methods. Additionally, the cycling stability of the ECP-black has been improved from ~ 600 cycles up to 2300 cycles without a noticeable decay of optical contrast.

2.2 Introduction

Electrochromic thin films whose light transmission can be manipulated by switching a small voltage bias to oxidize/reduce the active materials have been developed for decades. Various types of active materials, including inorganic materials (e.g. WO_3, MoO_3, V_2O_5, Nb_2O_5, etc.),[19] small molecules (e.g. viologens,[20] Prussian blue,[21] etc.), conjugated polymers[12,13,20] and inorganic-

organic hybrids[22] have been explored. Among them, conjugated polymers present many attractive properties such as fast coloring-bleaching time, low cost, and flexibility.[13] However, there are a few obstacles in the commercialization of polymer electrochromics, including cycling stability,[23,24] photostability,[25] optical memory,[21,26] etc.

The optical memory is the ability of an electrochromic material to maintain its colored/ bleached state under V_{off}. Although conjugated polymer thin films generally have good adhesion on device electrodes,[13] the self-bleaching behaviors of conjugated polymers are often observed,[26] thus limiting the applications of electrochromic windows. For instance, the transmissivity of smart windows is required to be precisely controlled based on the variation of solar radiation.[27,28] Because of the self-bleaching behaviors, the automatic control becomes more challenging. Therefore, it is important to understand and inhibit the self-bleaching behaviors of electrochromic polymer thin films.

Shin, et al.[26] suggested that in the case of conjugated polymers with a HOMO level higher than -5 eV, the electrons spontaneously transferred from conjugated polymers to the electrode (ITO) at the interfaces, leading to the self-bleaching of electrochromic windows under V_{off}.[26] By redesigning the side chain of the poly(3,4-ethylenedioxythiophene), the HOMO of the conjugated polymer was lowered down to -5.15 eV. Subsequently, the degree of self-bleaching was dramatically mitigated. However, changing the side chains of conjugated polymers also led to the change of their absorption spectra and higher oxidation potentials were required to oxidize the polymers.[26]

As it is shown in eq 1 below, self-bleaching also involves ion motion. During the self-bleaching process, positive charges (polarons and bipolarons) are generated on the polymer backbone. To maintain the overall electroneutrality of the electrochromic polymer (ECP) thin film, the permeation of counterions is a necessity and can be controlled by the compactness of conjugated polymer thin films.[29,30] If a compact polymer thin film was regenerated after electrochemical processes, the self-bleaching behaviors could be suppressed.

$$ECP + M^+ \cdot A^- \leftrightharpoons ECP^+ \cdot A^- + M^+ + e^- \quad (1)$$

Where ECP represents electrochromic polymer thin film, $M^+ \cdot A^-$ represents the electrolyte, M^+ is for metal or organic cation, and A^- is for the counter anion of the electrolyte, $ECP^+ \cdot A^-$ represent the oxidized conjugated polymer thin film whose charge is compensated by the endosmotic anions.

In previous works, Otero et al. and Odin et al. showed that the compactness of conjugated polymers under V_{off} was related to the cathodic polarization time in a logarithmic relationship, reflected by the retardant observations in both anodic chronoamperograms and voltammograms.[29,31,32] The work proposed electrochemically stimulated conformational relaxation (ESCR) model to describe this relationship. In the ESCR model, the electrochemical behavior of conjugated polymers is treated as the conformation relaxation.[29] In the oxidation process, electrons are taken away from polymer chains and polarons and bipolarons are formed consequently. The electrostatic repulsions between the positive charges result in opening channels for the swelling of counter-ions and electrolyte into the polymer thin film. In the reverse process, when the polymer is reduced back to the neutral state, the counter-ions and electrolyte are expelled. A closed and compact polymer network is regenerated. These conformation relaxations - opening and closing of the ion channels, are essentially related to the latter electrochemical response of the conjugated polymers.[33] Thus, the compact polymer thin film generated by the cathodic polarization can be used to inhibit the self-bleaching behaviors of ECP thin film under V_{off}.

Herein, we studied the electrochemical processes of ECP-black[34,35] thin films in association with self-bleaching behaviors. First, the impact of the break-in process was probed. Then, we investigated the effect of cathodic polarization time on the self-bleaching behaviors of ECP-black thin films. Additionally, we modified ITO with a partial coverage of octadecyltrichlorosilane (POTS) to impede the spontaneous charge transfer at interfaces. Finally, combing a long cathodic polarization (300 s) and POTS-modified surface, we demonstrated that self-bleaching of ECP-black can be suppressed to a large degree. These approaches are general and applicable to ECP-magenta, and ECP-blue[36] thin films as well. We also found that the cycling stability of the ECP-black thin film on surface-modified ITO was significantly improved.

2.3 Results and Discussion

The HOMO energy level of the ECP-black (Figure 2.1b) was estimated to be - 4.8 eV by using the empirical formula (eq 2). Thus, the self-bleaching of ECP-black polymer could occur under V_{off} due to the interface electron transfer (IET) according to the previous work.[26]

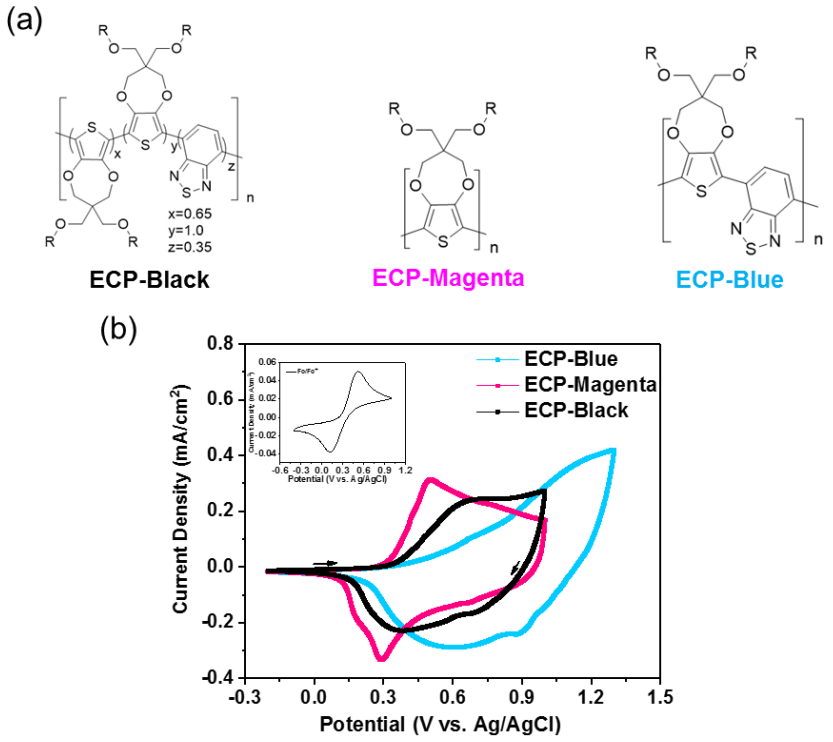

Figure 2.1 (a) Chemical structures and (b) cyclic voltammograms of the ECP-black, ECP-magenta, and ECP-blue. R = 2-ethylhexyl. (Inset: the cyclic voltammogram of ferrocene)

$$E_{HOMO} = - [4.8 + (E_{ox} - E_{1/2(ferrocene)})] \text{ eV} \quad (2)$$

where the E_{HOMO} is the HOMO energy level of the conjugated polymer; the E_{ox} is the onset oxidation potential of the conjugated polymer obtained from the CV (Figure 2.1b) of the ECP-black thin film, which is comparable to the E_{ox} in the DPV (Figure 2.2); the $E_{1/2(ferrocene)}$ is the half-wave potential of ferrocene.

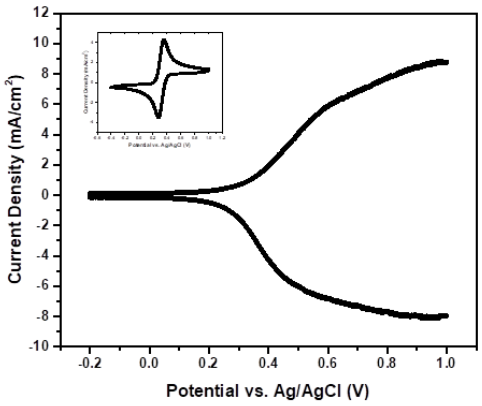

Figure 2.2 DPV of ECP-black on platinum (inset: the CV of ferrocene in 0.1 M $TBAPF_6$ PC)

The optical memory of the pristine ECP-black thin film was evaluated by recording the optical density at ~ λ_{max} (640nm) for 900 s under V_{off}. (Figure 2.3a). It was found that the absorption of the pristine film remained unchanged, suggesting that the pristine thin-film did not undergo self-bleaching within the observation period. This observation does not follow the early report that conjugated polymers with HOMO levels higher than – 5 eV will undergo self-bleaching on the ITO substrate.[26] We then applied 15 cycles of break-in to the ECP-black thin film by cycling from -0.2 V to 1.0 V at 40 mV/s (Figure 2.4). Thereafter, the ECP-black thin film was first oxidized to its bleached state. The pre-oxidized thin film was then subjected to 1.0 V for 30 s, and the potential was switched off from the 30th to 150th second. The optical density of the bleached ECP-black thin film had little change, indicating that the self-coloring was absent. Subsequently, the ECP-black thin film was reduced back to its colored state by applying a reverse bias at -0.2 V for 30 s. When the cathodic voltage bias was removed, we immediately observed that the optical density of the colored thin film started to decay (Figure 2.3b). The ECP-black thin film can be reversely switched from transmissive state to its original black-blue color state, suggesting that the polymer thin film did not decompose during the break-in process. Therefore, we hypothesized that the activation of the self-bleaching behaviors can be ascribed to the conformational changes of the ECP-black thin film during the redox processes.

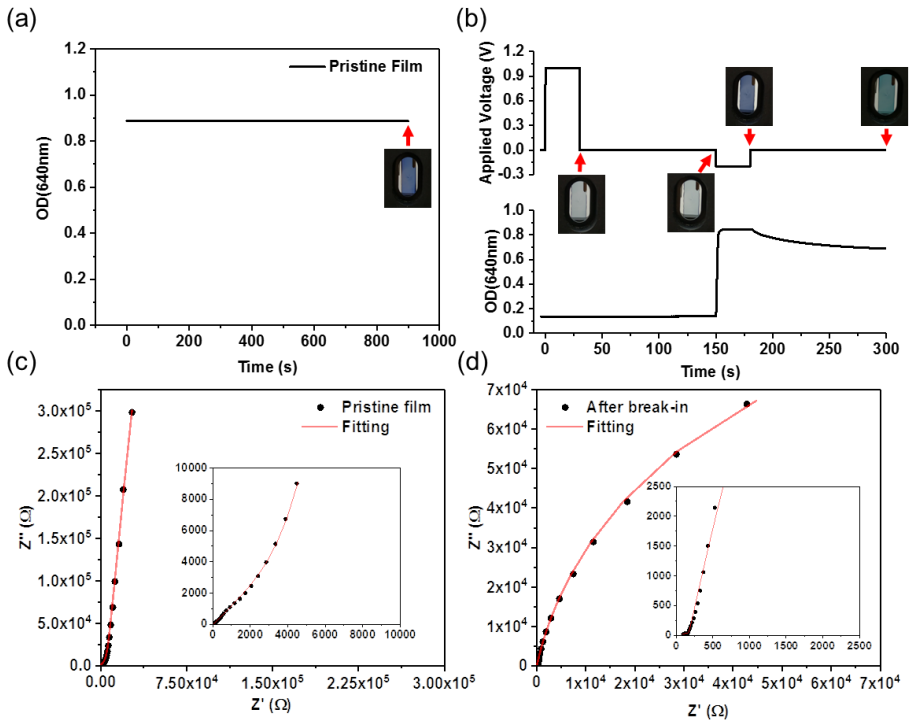

Figure 2.3 In-situ OD (640nm) measurements of the ECP-black thin film: (a) at the pristine state (inset: a photograph of the pristine film) and (b) after break-in and at different potentials (inset: photographs of the ECP-black film at different states). EIS measurements from 1Hz to 1MHz of the ECP-black thin film (c) at the pristine state (inset: the enlarged EIS spectrum), and (d) after break-in and with 300 s cathodic polarization (inset: the enlarged EIS spectrum).

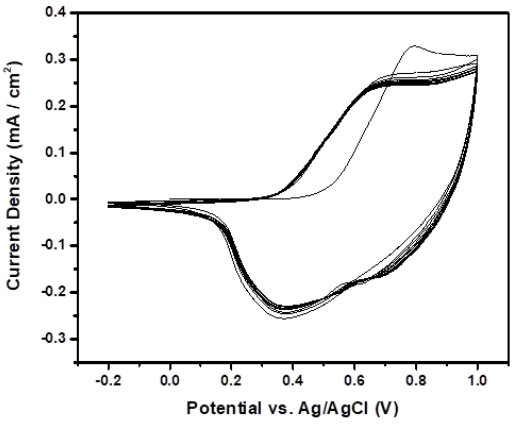

Figure 2.4 Typical CVs (15 cycles) of the break-in process.

To validate our hypothesis, atomic-force microscopy (AFM) and electrochemical impedance spectroscopy (EIS) experiments were conducted to probe the structural changes of the ECP-black thin film after the break-in. Indeed, looser surface morphologies were observed for ECP-black thin films after the break-in process from the AFM images (Figure 2.4). The resulted loose surface morphologies would facilitate the diffusion of solvated ions to compensate the positive charges generated on the polymer backbone during the self-bleaching process. Dramatically structural changes for the pristine film were also observed in a previous report on the volume changes of polypyrrole (dodecylbenzenesulfonate) (PPy(DBS)) during redox cycles by using in-situ AFM experiments.[37] The volume changes of the first cycle were between 60 - 100%, whereas only 30 - 40% volume changes were obtained in the following cycles. The differences of volume changes indicated the pristine compactness of the PPy(DBS) thin films cannot be recovered. Wang et. al also observed the slow ion diffusion in the first reduction of PPy (DBS) due to exceptionally compactness of the as-deposited film.[38] Our results are in good agreement with these previous studies which state that initial electrochemical processes can cause the conformational changes of the pristine conjugated polymer thin films to facilitate ion diffusion.

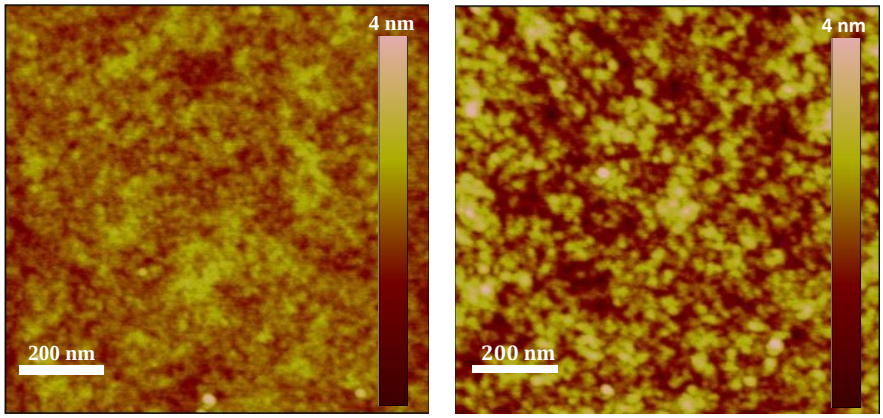

Figure 2.5 AFM images of a ECP-black thin film before (left) and after break-in (right).

The conformational changes of the ECP-black caused by the break-in were further confirmed by EIS measurements. First, the EIS of the ECP-black film was obtained before break-in (Figure 2.3c). Then, the break-in process was carried out, followed by a 300 s cathodic polarization potential (-0.2 V) that was applied to reset the ECP-black thin film back to its color state. Right after the cathodic polarization, the EIS of the broken-in thin film was taken (Figure

2.3d). In the EIS experiment, because the electrode was coated with the neutral semiconducting polymer thin film, the counterions needed to penetrate through the polymer thin film to reach the interfaces where the charge transfer occurs.[29,39] The EIS results can hence be fitted by the $R_s(Q_{film}R_{film})(Q_{dl}R_{ct})$,[39–43] where R_s is the solution resistance; Q_{film} and R_{film} are the capacitance and resistance of the thin film; Q_{dl} and R_{ct} are double layer capacitance and charge transfer resistance at the ECP-black film/ ITO interfaces. The fitted results were summarized in Supporting Information (Table. 2.1). Both the R_{film} and R_{ct} decreased dramatically for the broken in thin film, even after applying 300 s cathodic prepolarization to reset the film. This implied that the ECP-black thin film became looser, which would be easier for the counter-ions to permeate through and facilitate the self-bleaching reactions (eq 1).

Table 2.1 The R(QR)(QR) fitting results of EIS spectrums of the pristine film and the thin film after break-in followed by 300 s polarization

	Pristine Film	**Thin film (after break-in + 300s polarization)**
R_s / Ω	52.72	59.93
Q_{film} / F · s $^{(a-1)}$	0.5713×10^{-6}	2.04×10^{-6}
a_{film}	0.959	0.8896
R_{film} / Ω	45.97×10^{6}	1.97×10^{5}
Q_{dl} / F · s $^{(a-1)}$	4.313×10^{-6}	2.461×10^{-6}
a_{dl}	0.5649	0.6049
R_{ct} / Ω	6693	111.4

Next, the relationship between the cathodic polarization and the degree of the self-bleaching of the ECP-black thin film was explored. The degree of self-bleaching is quantified as the percentage change of the optical density (ΔOD/OD (%)) under V_{off}. It is shown in Figure 2.6 that the degree of self-bleaching within 120 s decreased on increasing the cathodic polarization time. The result matches the ESCR model. The longer the cathodic polarization, the more counterions/ electrolyte were expelled out from the polymer matrix, and the polymer matrix became more condensed due to the electroosmotic processes.[30–32] After the voltage was turned off, the degree of self-bleaching became lower because it was more difficult for ions to penetrate into the thin film matrix to compensate the positive charges generated in the self-bleaching process. These results suggest that the permeation of the counterions is necessary for the self-bleaching

processes and can be potentially used to mediate the degree of the self-bleaching. Also, it is consistent with the previous observation (Figure 2.3) that the self-bleaching behaviors only occur when the ECP-black thin film presents a loose structure that has resulted from the break-in process.

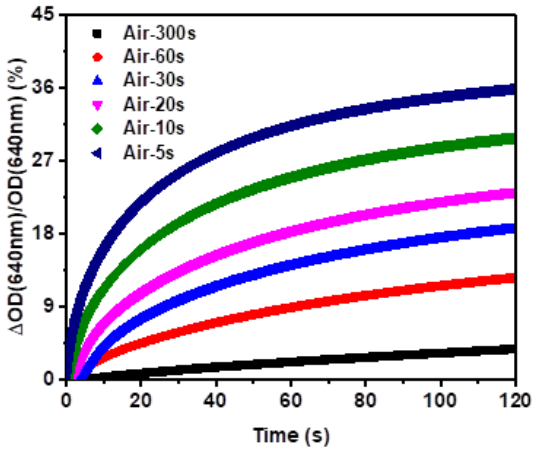

Figure 2.6 Short-term percentage change of optical density after different durations of reverse bias (-0.2 V) in ambient environment.

A more rigorous procedure was adopted to rule out the effect of oxidant (e.g., molecular oxygen in the air) that might cause the self-bleaching of ECP-black (Figure 2.7). The freeze pump treatment was applied to get rid of the oxygen residue inside the propylene carbonate electrolyte. The cuvette was sealed by Teflon tape and parafilm inside the N_2 glove box. The spectral measurement was conducted under the N_2 protection. The result (Figure 2.7) suggested that cathodic polarization still played a role in controlling the degree of self-bleaching, similar to the results obtained under the ambient conditions. The degree of self-bleaching decreased when increasing the duration of cathodic polarization. In addition, if the existence of the oxidant was the dominant factor that caused the self-bleaching of the black-ECP thin film, then the self-bleaching would be observed for the pristine film before any electrochemical experiments (Figure 2.3a).[44] Thus, we believe that the self-bleaching of the broken-in ECP-black thin films is due to the spontaneous electron transfer from the ECP-black thin film to ITO electrode, instead of the effect of oxidants.

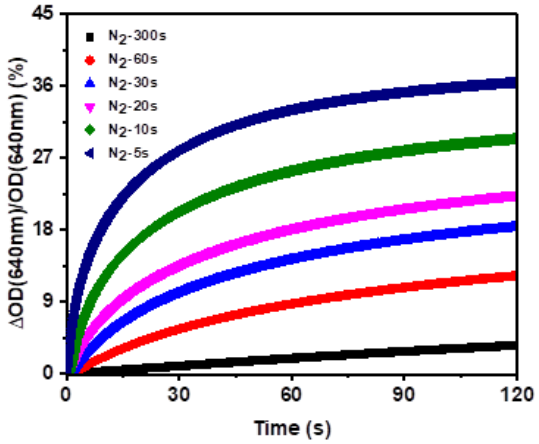

Figure 2.7 Short-term percentage change of optical density after different durations of reverse bias (-0.2 V) under nitrogen flow with 10 L/min flow rate.

To mitigate the self-bleaching problem, interfacial engineering was proposed to evade the need for redesigning the polymer structure. Octadecyltrichlorosilane (OTS) modification has been widely used in the field of organic field effect transistor to increase the adhesion of the organic layer (e.g. pentacene) to the substrate (Si wafer/ ITO).[45–47] For electrochromic devices, the insulated nature of OTS could be used to impede the spontaneous electron transfer associated with the self-bleaching of ECP thin films.[48] However, the electrochemical processes of ECP thin films could be hampered at the same time. Therefore, we chose to make ITO partially covered by OTS (POTS) to mitigate the self-bleaching of ECP thin film. To generate a partial coverage of OTS on ITO, both the roughness and the immersion time of the ITO in OTS solution are critical.[49] For unpolished ITO substrates, it generally takes longer time (~15 hrs) to form a condensed self-assembled monolayer (SAM) layer.[48] Kept under 1 vol% OTS hexane solution for a short time (80 mins), ITO substrates were expected to be partially modified by OTS.

To evaluate the coverage of the as-formed SAM layer, cyclic voltammetry experiments of 0.1 M ferrocene in 0.1 M $TBAPF_6$ propylene carbonate solution were conducted by using a bare ITO and an OTS-modified ITO, respectively. For OTS-modified ITO, the voltammogram of ferrocene showed a lower peak current density, and a larger distance between cathodic and anodic peaks, as compared to the bare ITO (Figure 2.8a). The surface coverage (θ) of the POTS-ITO was estimated to be 0.22 by using eq 3.[48,50] By extending the absorption time to 15 h, a more densely

packed OTS (DOTS) layer formed on ITO, which was indicated by the extremely small current from the CV of ferrocene. The θ of DOTS-ITO was estimated to be 0.99. The CV studies demonstrated that the ITO was partially covered by OTS at which electron transfer was interfered but could proceed with the aid of external potential.

$$\theta = 1 - (I_{p'} / I_p) \quad (3)$$

where I_p and $I_{p'}$ are the peak current densities of the CVs of ferrocene using bare ITO and OTS-modified ITO electrodes, respectively.

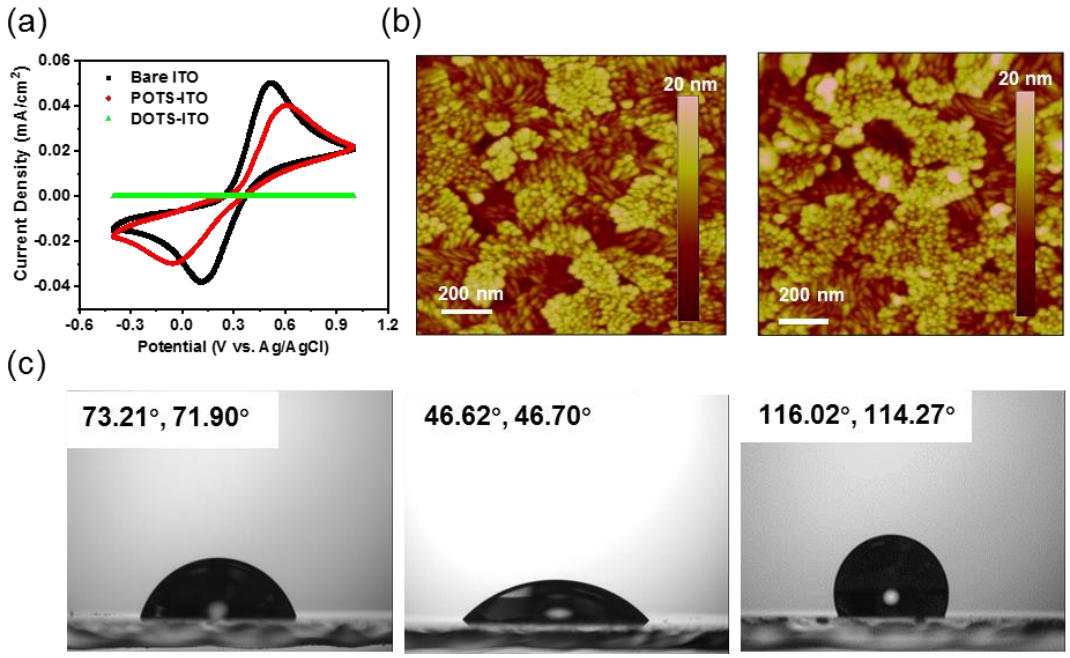

Figure 2.8 (a) Cyclic voltammograms of 0.1M ferrocene in 0.1M $TBAPF_6$ propylene carbonate solution using POTS-ITO, DOTS-ITO, and bare ITO as the working electrode. (b) AFM images of the bare ITO (left) and POTS-ITO (right). (c) Contact angle images of bare ITO, UV-ozone treated ITO and POTS-ITO.

To further study the formation of POTS layer on the ITO, the contact angle and AFM measurements were performed. In the contact angle measurements, 5 ul of deionized water was titrated on top of each substrate, and images were taken immediately. The substrates were cleaned by UV-ozone ahead of OTS modification. The surface wettability of bare ITO, UV- ozone cleaned ITO, and partially OTS modified ITO (POTS-ITO) were determined by their contact angles, respectively. The typical images of contact angle measurements of bare ITO, UV-ozone treated ITO, and POTS-ITO are shown in Figure 2.8c. The average contact angle values were obtained

from measurements at four different positions (Table. 2.2). After the UV-ozone treatment, the ITO surface became more hydrophilic with a small average contact angle ~49°.[51] Compared with the UV-ozone treated ITO, the OTS-modified ITO has a larger average contact angle of 116°, indicating the formation of hydrophobic OTS layer on the ITO surface. From the AFM measurements, the average R_q increased slightly from 2.93 to 3.38 nm which suggested that a self-assembled monolayer was formed on most of the surfaces (Figure 2.8b).

Table 2.2 Average contact angles of bare-ITO, ITO treated by UV-ozone, POTS-ITO

Bare ITO		**UV-Ozone-ITO**		**POTS-ITO**	
79.87 ± 5.91	80.02 ± 6.30	49.12 ± 2.43	49.04 ± 3.27	115.95 ± 2.09	115.46 ± 1.63

To test the effect of the POTS layer on the self-bleaching behaviors of the broken-in ECP-black thin films, the percentage change of optical density was measured for ECP-black thin films on both bare ITO and POTS-ITO. From the first derivative of OD (640 nm) of ECP-black with respect to time during the self-bleaching process, the change of the OD (640 nm) is negligible after ~ 500 s indicated by a small value of the decay rate (dOD/dt) (Figure 2.9). Thus, 900 s was sufficient to monitor the degree of self-bleaching. In Figure 2.10a, the degree of self-bleaching was observed to decrease from 27.6% ± 4.6% to 15.5 ± 2.98% (the average and standard deviation were calculated based on three individual experiments) after using the POTS-ITO and 60 s cathodic polarization. This is because that the spontaneous electron transfer was disturbed by the insulated POTS layer.[52] By extending the cathodic polarization time to 300 s, the degree of self-bleaching can be further reduced to 7.6% ± 1.4%. This phenomenon also supports that the self-bleaching behaviors of the ECP-black thin film are primarily caused by the IET at the organic/ITO interfaces.

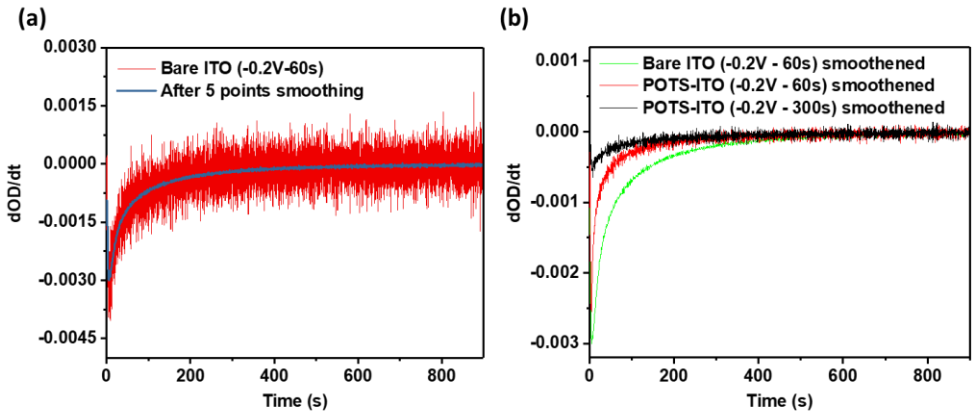

Figure 2.9 (a) An example of the first derivative of OD (640nm) of ECP-black with respect to time during self-bleaching processes before and after 5 points FFT smoothing. (b). The smoothened first derivative curve of OD (640nm) of ECP-black on bare ITO with 60 s cathodic polarization, and POTS-ITO with 60 s cathodic polarization and 300 s cathodic polarization.

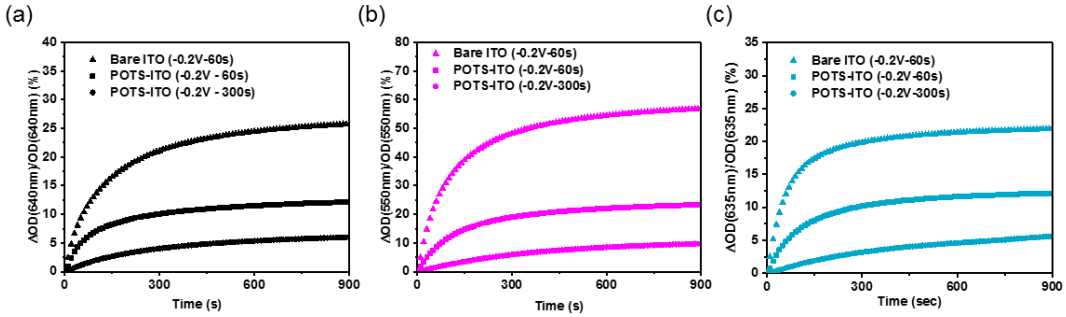

Figure 2.10 Long-term percentage change of optical density of (a) ECP-black on bare ITO after 60 s cathodic polarization, and on POTS-ITO after 60 s and 300s cathodic polarization， (b) ECP-magenta on bare ITO after 60 s cathodic polarization, and on POTS-ITO after 60 s and 300 s cathodic polarization， and (c) ECP-blue on bare ITO after 60 s cathodic polarization, and on POTS-ITO after 60 s and 300 s cathodic polarization.

To demonstrate the universality of POTS layer and cathodic polarization on the suppression of self-bleaching, ECP-magenta, and ECP-blue polymers were also selected to measure the degree of self-bleaching after break-in on both bare ITO and POTS-ITO. Both ECP-magenta and ECP-blue underwent self-bleaching because of their high HOMO levels, which was calculated to be - 4.79 eV and - 4.95 eV, respectively (Figure 2.1b). By using POTS-ITO and

applied long cathodic polarization, the degree of self-bleaching can be reduced from 56.78% to 9.75% for the broken-in ECP-magenta thin film, and from 21.92% to 5.56% for the broken in ECP-blue thin film (Figure 2.10b, c). Therefore, POTS modification and cathodic polarization are able to suppress the self-bleaching behaviors of ECPs. Additionally, the spectroelectrochemical behaviors and electrochromic switching of the ECP-black thin film on POTS-ITO are studied (Figure 2.11). There is no obvious difference compared with the ECP-black thin film on bare ITO (Table 2.3). Because the ITO surface is partially covered by OTS, electrochemical oxidation/reduction can still progress when driven by external potential. From the energy point of view, the coloration efficiency measurements were carried out for broken in thin films of ECP-black on both substrates. The coloration efficiency (CE) of the bleaching process can be calculated from the slope of the curve made by ΔOD VS. ejected charge density. Compared to the ECP-black on bare ITO (203.23 cm^2/C), the slope of the ECP-black on POTS-ITO (473.4 cm^2/C) is more inclined at the beginning but starts to gradually decrease till the end (Figure 2.12a). The initial larger values of the CE might be due to the better contact between the polymer thin film and ITO electrode, so the electron transfer driven by externally applied voltage was more efficient at the beginning. However, due to the existing of insulated POTS on the surfaces of ITO, it consumed more charge to completely oxidize the whole ECP-black thin film.

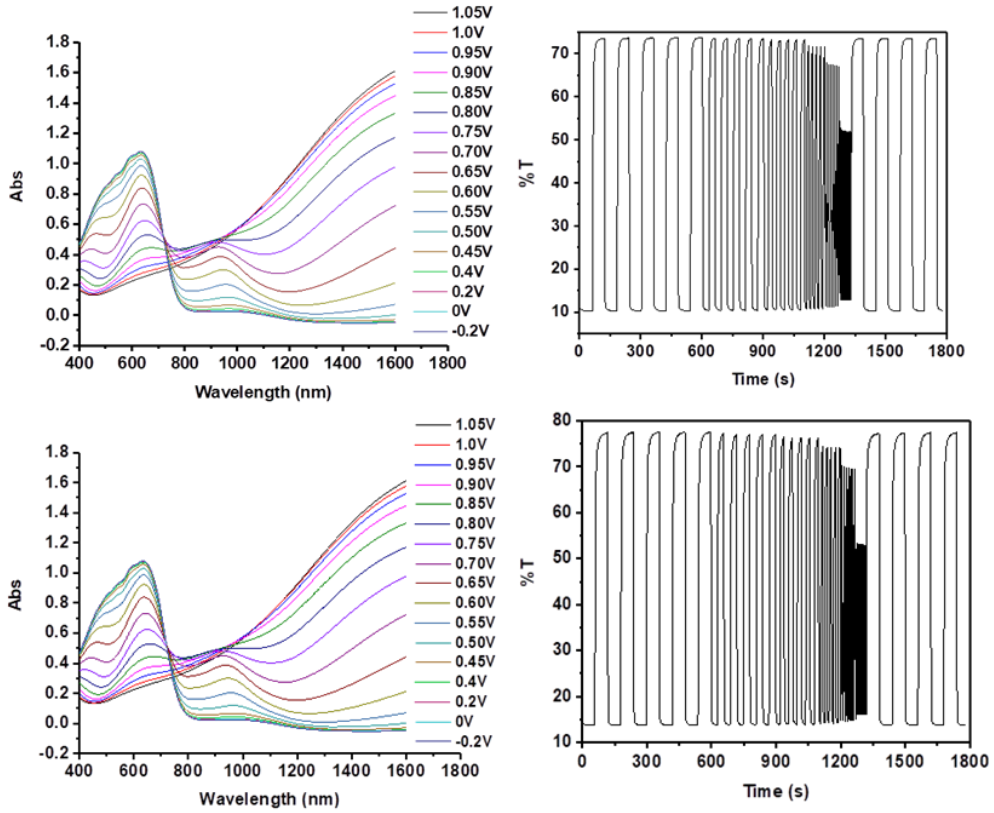

Figure 2.11 Spectroelectrochromic behaviors and double potential step chronoamperometric experiments (T% at 640nm) of ECP-black on the POTS-ITO (top) and bare ITO (bottom).

Table 2.3. Comparison of ECP-black thin films on bare ITO and POTS-ITO

Substrate	ΔT/ %	t_b(95%)/ s	t_c(95%)/ s	CE/ cm^2/C
Bare ITO	63	11.5	3.3	203.23[a]
POTS-ITO	63	9.5	5.6	473.4[a]

a) Coloration efficiency is calculated based on the initial slope highlighted in Figure 6a.

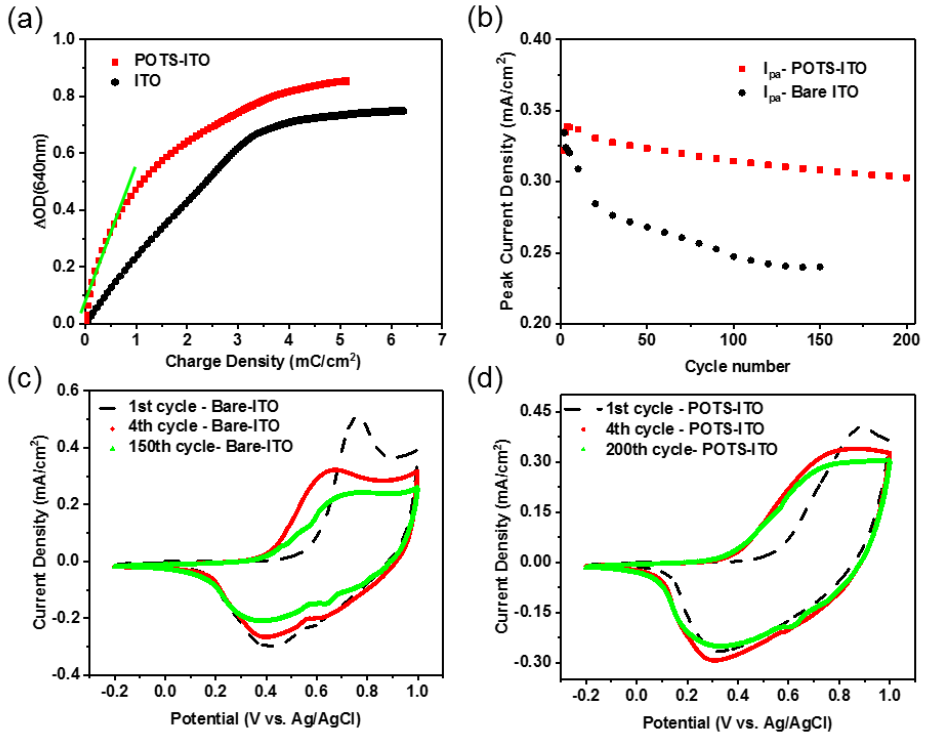

Figure 2.12 (a) Coloration efficiency of ECP-black thin films on bare ITO and POTS-ITO. (b) The development of anodic peak current density of ECP-black thin films on POTS-ITO and bare ITO versus number of cycles (the first cycle is not included). Selected cyclic voltammograms of ECP-black thin films on (c) bare ITO and (d) POTS-ITO.

Finally, the cycling stability of the ECP-black on POTS-ITO was tested by cyclic voltammetry (CV) and double potential step chronoamperometric (DPSC). The CV cycling test can access the adhesion of the ECP-black thin film on the substrate by monitoring the development of the voltammogram and peak current density of each cycle. On the other hand, DPSC cycling experiments can provide in-situ transmittance change at an on-off switching mode. However, the transmittance measurement is based on one spot where the light penetrates through, so the result might not represent the conditions of the entire film. Therefore, we combined these two methods to evaluate the effect of POTS on the cycling stability. The CV cycling experiments were scanned between -0.2 V to 1.0 V at a scan rate of 40 mV/s. The development of the anodic peak current density (I_{pa}) of CV was summarized in Figure 2.12b. The voltammogram of initial cycle, fourth cycle, and the last cycle were shown in Figure 2.12c, d for ECP-black on POTS-ITO and bare ITO, respectively. The I_{pa} of first scan (dash line) was excluded due to the first scan effect as shown in Figure 2.12c,d.[53] For the ECP-black on bare ITO, the I_{pa} of CV decreased rapidly and the shape of

CV changed dramatically with more and more cycles, indicated by the delamination of ECP-black from bare ITO. During the redox cycles, electrochromic thin films on ITO are expanded/contracted due to the incorporation and extraction of solvated ions.[37,54] The hydrophilic surface of the ITO cannot provide enough adhesion to hydrophobic conjugated polymer thin films to overcome the volume change. It led to the delamination of the thin film, indicated by 28% decrease (from 2nd cycle to 150th cycle) of the value of I_{pa}. For the CV of the ECP-black on POTS-ITO, the position of anodic peak slightly moved towards higher potential while the oxidation onset was comparable, which supports our hypothesis that electron transfer is partially impeded. The I_{pa} for the ECP-black on POTS-ITO increased slightly from the 1st to 4th cycle, because the thin film became looser for solvated ions to permeate into and more materials could get involved in the reaction. Then, the I_{pa} decreased 10% from 4th cycle to 200th cycle (Figure 2.12b). The overall shape of CV only changed slightly for 200 cycles, which indicated that the ECP-black on POTS-ITO can maintain its adhesion via the hydrophobic interaction (Figure 2.12d) resulting in the improvement of cycling stability. In the DPSC measurement, the potential was switched between -0.2 V and 1.0 V with a 10 s time interval. The optical contrast of ECP-black thin film on POTS-ITO can be maintained up to 2300 cycles with losing only 5% of its original contrast. After ~ 4300 cycles, most part of the ECP-black thin film can remain a good adhesion on POTS-ITO (Figure 2.13a). As a comparison, the losses of optical contrast can be observed for the ECP-black thin film on bare ITO at ~ 600 cycles and increased to ~ 35 % of its original contrast after ~ 1800 cycles, which indicated the delamination of the thin film. After 3300 cycles, the ECP-black thin film delaminated from the bare ITO and was not capable of being fully reduced back to black-blue, as shown in the photograph (Figure 2.13b).

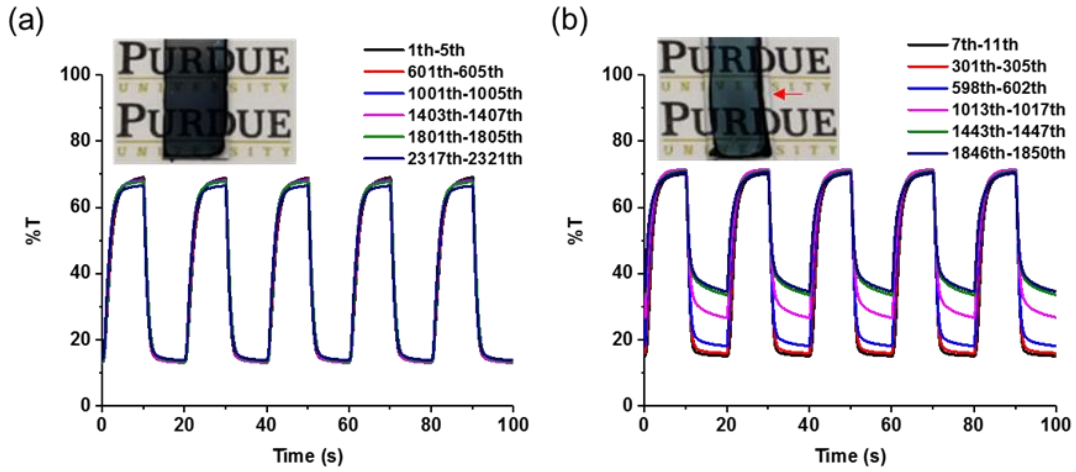

Figure 2.13 Transmittance at 640 nm of ECP-black thin films on (a) POTS-ITO (The inset is the photography of the thin film after 4300 cycles) and (b) bare ITO (The inset is the photography of the thin film after 3300 cycles) under double potential step chronoamperometric experiments switching between 1.0 V and -0.2 V VS. Ag/AgCl.

2.4 Conclusions

We adopted two approaches, partial OTS surface modification and cathodic polarization, to probe and study the self-bleaching behaviors of ECP-black. Taking advantages of these two approaches, we have successfully mitigated the self-bleaching problem of ECP thin films. Moreover, compared with the bare ITO, the POTS-ITO has a more hydrophobic surface which provides stronger adhesion to conjugated polymer thin films. As a result, cycling stability of the ECP-black thin film on POTS-ITO can be enhanced dramatically.

In the future work, we envisage to investigate an appropriate SAM layer that can induce an interfacial dipole to increase the work function of ITO so that the electron transfer at the ITO/ECP interfaces can be prevented under V_{off}.[55,56] Meanwhile, it is important to improve the adhesion of thin film on the ITO surface to enhance the cycling stability. By introducing the SAM-modified ITO, other properties including switching time, coloration efficiency, and color contrast, should be also taken into consideration. This work provides more insight into the self-bleaching behaviors of electrochromic polymers and offers solutions towards reliable automation control of electrochromic windows. For instance, the colored state of the electrochromic windows can be maintained by refreshing cathodic bias at a low frequency and with a minimum energy consumption.

2.5 Acknowledgement

The authors would like to thank Prof. Ritural Borgohain for the use of the contact angle goniometer, and Dr. Yan Zhao for the assistance on the OTS modification.

2.6 Experiments

ITO slides (CG-501N-CUV) were purchased from delta technologies, LTD. Anhydrous propylene carbonate (PC), Tetrabutylammonium hexafluorophosphate ($TBAPF_6$) (≥ 99.0%, for electrochemical analysis), silver wire (≥ 99.0%) with 1.5 mm diameter, platinum wire (99.0%) with 0.5 mm in diameter were purchased from Sigma-Aldrich.

The ECP-black, ECP-magenta, ECP-blue were synthesized by following the published procedures (Figure 2.14-2.16).[57,58]

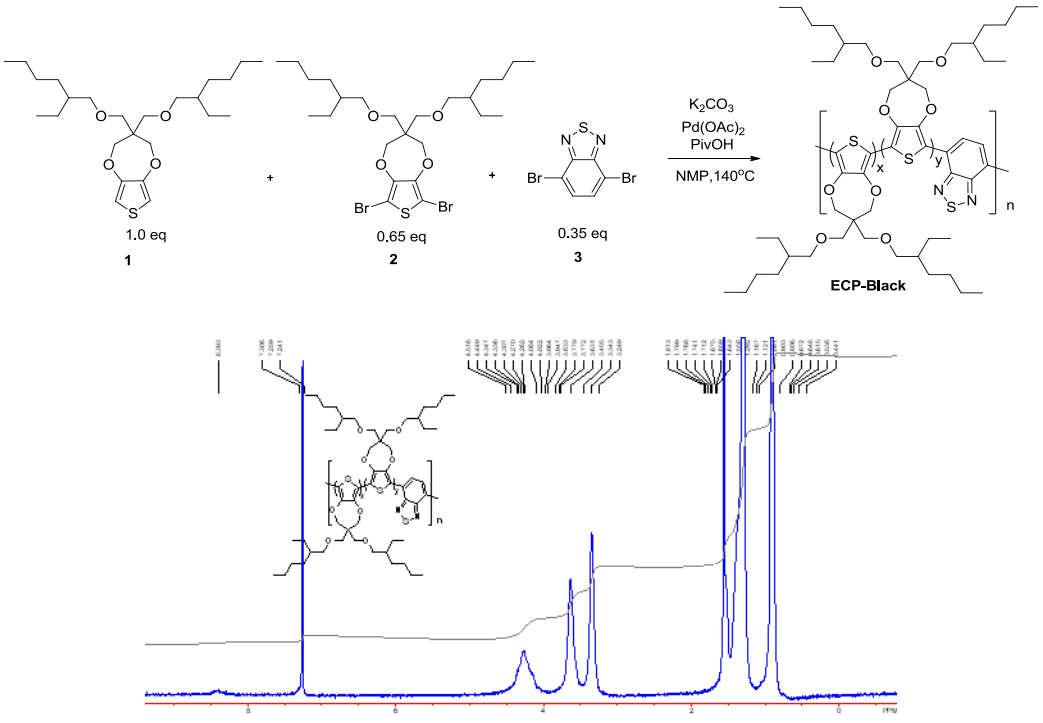

Figure 2.14 Synthesis and ^{1}H NMR spectrum of ECP-black.

^{1}HNMR (300 MHz, $CDCl_3$) δ 8.44-8.20 (m, 1H), 4.52-4.26 (m, 10H), 3.63 (bs, 10H), 3.34 (bs, 10H), 1.55-1.29 (m, 45H), 0.90 (bs, 30H).

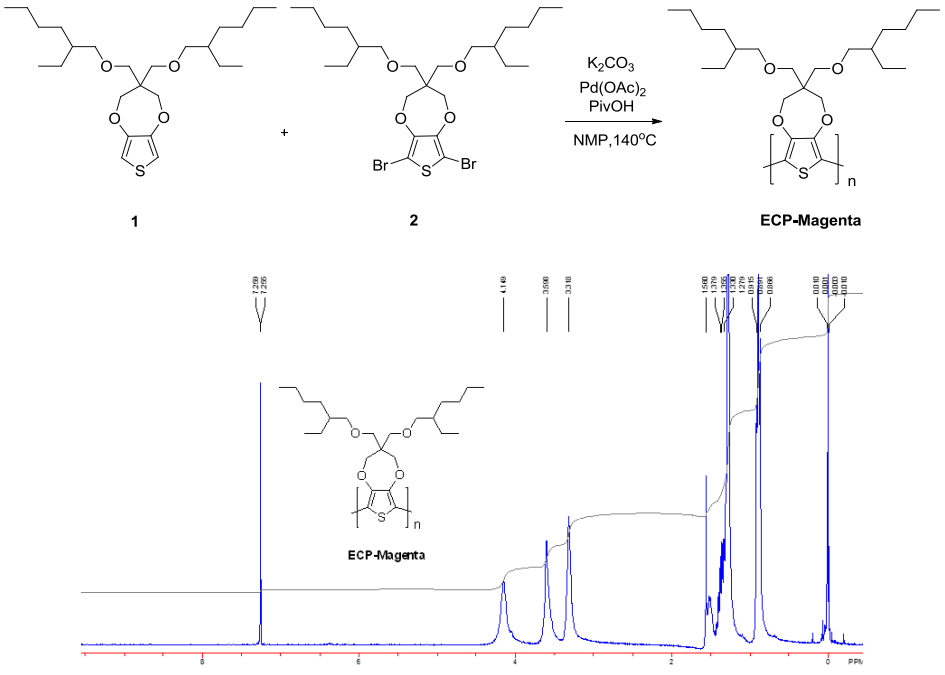

Figure 2.15 Synthesis and ^{1}H NMR spectrum of ECP-magenta.

^{1}HNMR (300 MHz, $CDCl_3$) δ4.15 (br, 4H), 3.60 (br, 4H), 3.32 (br, 4H), 1.56-1.33 (m, 18H), 0.92-0.87 (bs, 12H).

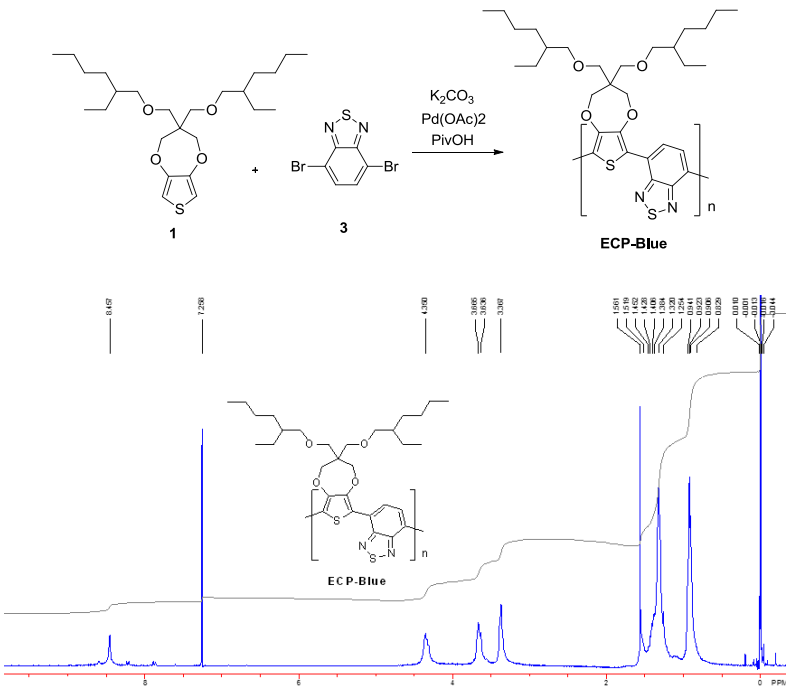

Figure 2.16 Synthesis and ^{1}H NMR spectrum of ECP-blue.

^{1}HNMR (300 MHz, $CDCl_3$) δ 8.46 (br, 2H), 4.35 (br, 4H), 3.64-3.67 (m, 4H), 3.37 (br, 4H), 1.56-1.25 (m, 18H), 0.94-0.83 (bs, 12H).

Instrumentation

All the electrochemistry related experiments were performed using BioLogic SP-150. The UV-vis spectrum and the optical memory measurement were obtained from Agilent Cary 5000 UV-Vis-NIR spectrophotometer. The AFM images were taken by using the Veeco dimension 3100. Contact Angle measurements were carried out by using Ramé-Hart Model 790.

Cyclic Voltammetry (CV) experiments were carried out by using a conventional three-electrode system. The working electrode is ITO coated by the polymer thin film; the pseudoreference electrode is an Ag wire coated by AgCl;[59] the counter electrode is the platinum wire; the electrolyte is 0.2 M $TBAPF_6$ in PC. The thin film of polymer was made by spin-coating ~ 0.1 ml of 40 mg/ml solution on top of the ITO with a 1500 rpm/s spin rate to form a film with ~ 375 nm thick which shows the highest optical contrast (Figure 2.11).[60–62] The voltage is scanned from -0.2 V to 1.0 V at a 40 mV/s scan rate for ECP-black and ECP-magenta, and from -0.2V to

1.3V at a 40 mV/s scan rate for ECP-blue. Same set-up and parameters were also used for the CV cycling stability test. The anodic peak current density in the voltammogram was used to indicate the cycling stability of the polymer thin film. Moreover, 15 cycles of break-in were applied before the characterizations of the polymer thin films unless otherwise mentioned.

Differential Pulse Voltammetry (DPV) measurements were done by using a platinum bottom as a working electrode. A thin polymer layer was coated on top of the platinum bottom by drop casting the 3 - 5 mg/ml solution. All other set-ups were same as CV experiments unless otherwise mentioned. 20 mV pulse height, 50 ms pulse width, 1.0 mV step height, and 100 ms step time were used. The potential range for the experiment was set between -0.2 V and 1.0 V.

The degree of Self-bleaching was quantified as the percentage change of optical density of the thin films under open circuit conditions. The broken in thin films were oxidized by applying 1.0 V for 30 s for ECP-black and ECP-magenta, and 1.3 V for 30s for ECP-blue. Then, the percentage change of optical density at bleached state was recorded for 2 mins. Right after 2 mins, a - 0.2 V cathodic potential was applied for certain time (5 s, 10 s, 20 s, 30 s, 60 s, 300 s). Finally, the potential was switched to voltage off and the percentage change of optical density at colored state was recorded for 120 s for short-term measurement, and 900 s for long-term measurement. The detailed processes of the experiments were shown in the Scheme 2.1. For the measurement under the N_2 protection, N_2 was pre-purged into the chamber of the Cary 5000 for 30 mins at 10 L/mins before the experiments and was continuous supplying in the rest of the experiments.

Partial OTS Surface Modification: ITO substrates were washed by ultrasonic bath in the order of ethanol, acetone, ethanol for 10 mins each. The washed ITO substrates were dried by nitrogen blowing. Then, the conducting sides of the ITO slides were treated for 20 mins in a UV-ozone chamber. ITO were partially covered by OTS (POTS) monolayer after immersing in a 1 vol% OTS hexane solution for 80 mins.

Ferrocene/ferrocenium redox couple was used as electrochemical probe to exam the formation of POTS monolayer. The CV experiments were done in a propylene carbonate solution with 0.1 M of ferrocene and 0.1 M of $TBAPF_6$. The potential was scan from -0.4 V to 1.0 V vs. Ag/AgCl at 40 mV/s.

Electrochemical Impedance Spectroscopy & AFM: the EIS experiments were obtained using a 20 mV perturbation amplitude (V_{rms} = 14.4 mV) in a frequency ranging from 1.0 Hz to 1.0 MHz. The data was fitted by a R(QR)(QR) Equivalent circuit (Scheme 2.2). AFM images were obtained in a tapping mode at a 0.5 Hz scan rate. The average R_q was calculated based on three different images.

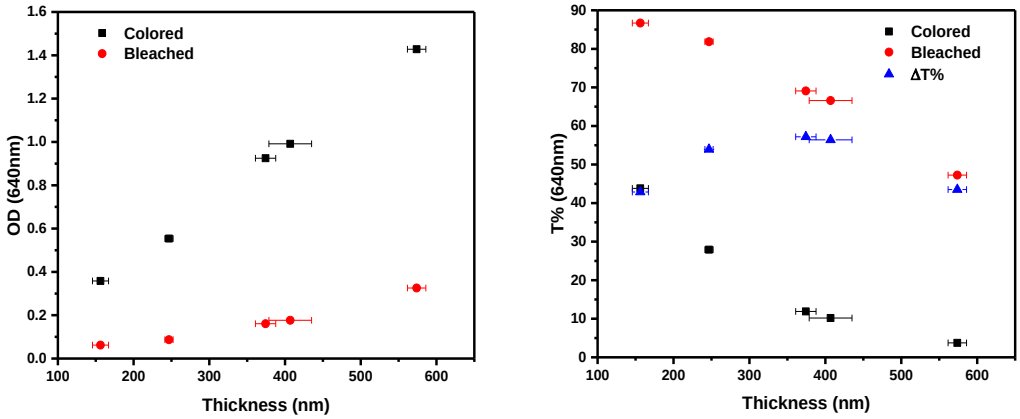

Figure 2.17 Optical density and transmittance of ECP-black thin films with different thicknesses

The ECP-black thin films with different thicknesses were obtained by spin coating ECP-black solution with different concentrations including 20 mg/ml, 30 mg/ml, 40mg/ml, 50 mg/ml, 60 mg/ml at 1500 rpm. The results showed that the highest contrast can be achieved by the ECP-black thin film with ~ 375 nm obtained from the 40 mg/ml solution (Figure 2.17). Thus, the 40 mg/ml ECP-black solution was used in our studies for fabricating thin films unless otherwise mentioned.

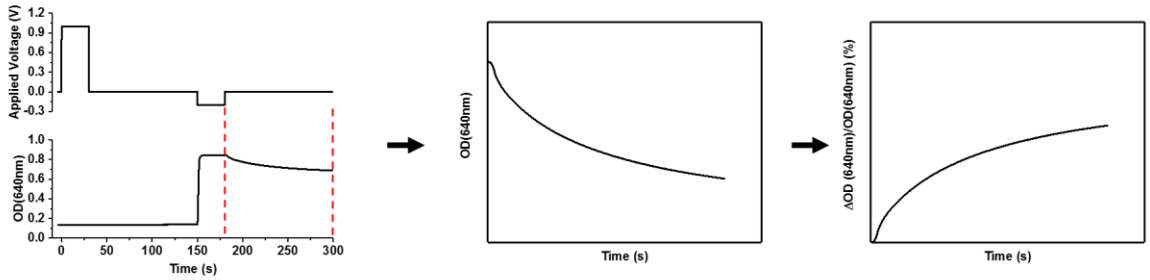

Scheme 2.1 The procedure for obtaining the degree of self-bleaching from UV-vis optical density measurement

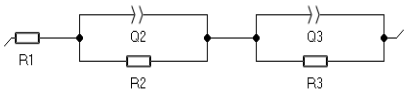

Scheme 2.2 R(QR)(QR) Equivalent circuit

CHAPTER 3. HIGHLY TRANSPARENT CROSSLINKABLE RADICAL POLYMER AS THE ION STORAGE LAYER

This chapter was adapted with permisson from the manuscript published in ACS Applied Materials & Interfaces: He, J.; Mukherjee, S.; Zhu, X.; You, L.; Boudouris, B. W.; Mei, J. A Highly Transparent Crosslinkable Radical Copolymer Thin Film as the Ion Storage Layer in Organic Electrochromic Devices. ACS Appl. Mater. Interfaces 2018, 10 (22), 18956–18963.

3.1 Abstract

A highly transparent crosslinkable thin film made of the radical polymer poly (2,2,6,6-tetramethyl-4-piperidinyloxy methacrylate)-*co*-(4-benzoylphenyl methacrylate (PTMA-*co*-BP) has been developed as the ion storage layer in electrochromic devices (ECDs). After photo-crosslinking, the dissolution of PTMA-*co*-BP in electrolytes was mitigated, which results in an enhanced electrochemical stability compared with the homopolymer PTMA thin film. Moreover, the redox capacity of PTMA-*co*-BP increased because of the formation of a crosslinked network. By matching the redox capacity of the PTMA-*co*-BP thin film and bis(alkoxy)-substituted poly(propylenedioxythiophene), the ECD achieved an optical contrast of 72% in a small potential window of 2.55 V (i.e., switching between +1.2 V and –1.35 V), and it was cycled up to 1800 cycles. The ECD showed an excellent optical memory as its transmittance decayed by less than 3% in both the colored and bleached states while operating for over 30 min under open circuit conditions. Use of crosslinkable radical polymers as the transparent ion storage layer opens up a new venue for the fabrication of transmissive-mode organic ECDs.

3.2 Introduction

Polymer-based electrochromic devices (ECDs) have a great potential in a number of applications that range from smart windows to transmissive-mode displays.[63] A great deal of effort has been devoted to electrochromic materials and resulted in a vast library of redox polymers with various color states that span the whole color wheel.[5,13] Typically, a full ECD has minimally three layers, namely the electrochromic layer, the electrolyte, and the counter electrode (i.e., the ion storage layer). In stark contrast to the electrochromic layer, the ion storage layer has rarely been

systematically studied.[13] A bare transparent metal oxide conductor [e.g., tin-doped indium oxide (ITO)] is often directly used as the ion storage layer.[64] In order to balance the charge generated in the electrochromic layer, an overpotential (> -1.5 V vs. Ag/Ag^+) needs to be applied to reduce the ITO electrode, and this is an irreversible process.[64] The irreversible reduction of the ITO electrode leads to a serve decay of the optical contrast of ECDs during the cycling test. Thus, it is crucial to develop a robust ion storage layer for ECDs. A few electrode materials have been utilized in this fashion, and they include metal oxides (e.g., NiO, TiO_2, and WO_3); conjugated polymers [e.g., poly(3,4-ethylenedioxythiophene) polystyrene sulfonate (PEDOT: PSS) and N-C_{18} substituted poly(3,4-propylenedioxypyrrole (PProDOP)], and radical polymers [e.g., poly (2,2,6,6-tetramethyl-4-piperidinyloxy methacrylate) (PTMA) and poly(2,3-bis(2',2',6',6'-tetramethylpiperidinyl- N-oxyl-4'-oxycarbonyl)-5-norbornene) (PTNB)]. Among these materials, WO_3 and PEDOT: PSS have absorption in the visible light region after being reduced, which affects the color purity of ECDs. Moreover, Padilla et al. suggested that the contrast of a dual electrochromic system was lower than either of the optical contrast that can be achieved by the individual material, based on the mathematical calculation of the electrochromic system that obeys the Lambert-Beer's law.[65] Therefore, a highly transparent and nonelectrochromic ion storage material is desired to achieve a high optical contrast. Kim et al. recently used a highly transparent TiO_2 film as the counter electrode and obtained a high contrast.[66] However, the processing of metal oxides-based thin film counter electrodes is rather sophisticated and costly. It often involves high vacuum or high-temperature annealing (> 500 °C) when solution processing is adopted.[66–69]

Polymers with highly transmissive neutral and doped states are attractive as counter electrodes in ECDs, including both semiconducting polymers and radical polymers. For instance, PProDOP has an absorbance in the near ultraviolet (UV) region in its neutral state, and this absorption band directly shifts to the near-IR region upon oxidation. Reynolds *et al.* studied such a minimal color-changing polymer (MCCP) – PProDOP – as a counter electrode and obtained a high optical contrast.[70] It is noted that the synthesis of PProDOP is nontrivial and multiple reactions are involved. Radical polymers attract a lot of attention as the active materials for energy storage devices and organic electronics.[71–77] Few attempts have also been made to use radical polymers as active materials of the counter electrode for ECDs, as they have negligible absorption in the visible region. However, they present significant disadvantages. For instance, when Nishide et al. used PTNB as the counter electrode to couple with Prussian blue and poly(decylviologen)-

poly(styrenesulfonate) (PV10-PSS) and constructed ECDs, the devices did not achieve a high contrast and were not robust during the cycling test.[78] One possible explanation is the dissolution of radical polymers, which results in an unmatched redox capacity between PTNB and PV10-PSS. To mitigate the dissolution of radical polymers, Vasilyeva *et al.* reported that the PTMA/ poly(methyl methacrylate) (PMMA) (1:3 molar ratio) polymer blend can increase the redox stability of the radical polymer, and the ECP-Magenta device can achieve a contrast of over 70% with a fast switching rate and a high cycle stability.[79] Nevertheless, 75% of the PTMA/PMMA blend was PMMA, which is not a redox active material. To compensate for the charge involved in the color switching of the electrochromic active layer, a thick PTMA/PMMA layer was used, which led to a large ohmic resistance of the ECDs.[66] As a result, a high anodic potential (2.35 V) was adopted to achieve a large optical contrast. Moreover, a long annealing time was required to obtain a homogeneous polymer blend that has a good electrochemical stability. Therefore, an alternative strategy is needed to address the dissolution of radical polymers in electrolytes without sacrificing the ion storage capacity of radical polymers.

A crosslinking strategy has been applied to make stable radical polymers as the cathode-active materials in energy storage devices.[80] Here, we turned to using a radical polymer-based material that includes a small number of copolymerized repeat units that are capable of undergoing photo-crosslinking. Specifically, we used the photo-crosslinkable radical random copolymer PTMA-*co*-(4-benzoylphenyl methacrylate) (PTMA-*co*-BP) as the counter electrode for ECDs. The effects of crosslinking and the associated electrolytes on the electrochemical behavior of PTMA-*co*-BP were established. By using the optimized thicknesses of each layer and using 0.2 M 1-ethyl-3-methylimidazolium bis(trifluoromethylsulfonyl)imide (EMI-TFSI) in propylene carbonate (PC) as electrolytes, the bis(alkoxy)-substituted poly(propylenedioxythiophene) (ECP-magenta)/PTMA-*co*-BP device had a high optical contrast of ~72 % at a wavelength of 550 nm, and the composite coloration efficiency was calculated to be ~754.0 cm^2 C^{-1}. The high composite coloration efficiency suggests that the device can achieve a high optical contrast by consuming a small amount of charge. Moreover, the device can be switched using a small potential bias of 2.55 V and cycled for more than 1800 cycles in a reversible manner. Last but not the least, the device maintained its colored/bleached state for 30 min at open circuit with a minimum color change.

3.3 Experiments

Reagents and Materials. All reagents were purchased from Sigma-Aldrich, and they were used as received unless otherwise specified. The synthetic procedure for the preparation of PTMA-*co*-BP has been published earlier elsewhere.[21] ITO/glass substrates (CG-501N-CUV) were purchased from Delta technologies, Ltd. The leakless miniature Ag/AgCl electrode ET072 was purchased from eDAQ. EMI-TFSI was purchased from Millipore Sigma.

UV Crosslinking. PTMA-*co*-BP thin films were spin-coated onto ITO substrates at a spin speed of 1500 rpm. Then, the thin films were transferred into the N_2 glove box and crosslinked by Thermo Scientific Pierce UVP ultraviolet lamps (8-watt) that emit at 254 nm for 30 mins. Longer exposure time causes the formation of a highly crosslinking network which could impede the ion diffusion.

Instrumentation. Electrochemical experiments were performed using a BioLogic SP-150 potentiostat. The UV-Vis spectra and the optical memory measurements were obtained from an Agilent Cary 5000 UV-Vis-NIR spectrophotometer. The thickness of thin films was measured by a Veeco dimension 3100 atomic force microscope (AFM).

Thin Film Characterization. The three-electrode cyclic voltammetry (CV) experiments were carried out to calculate the redox capacity of ECP-magenta and PTMA-*co*-BP thin films with different thicknesses. The working electrode is an ITO substrate coated by the ECP-magenta/ PTMA-*co*-BP thin film; the reference electrode is an ET072 leakless miniature Ag/AgCl electrode; the counter electrode is a platinum wire; and the electrolytes used are 0.2 M $TBAPF_6$ in PC or acetonitrile (ACN), or 0.2 M EMI-TFSI in PC. The voltage was scanned from -0.2 to 1.0 V at a scan rate of 40 mV/s for ECP-Magenta. For PTMA-*co*-BP, the voltage was scanned from -0.2 to 1.0, 1.4, 1.5, or 1.6 V at a scan rate of 40 mV/s. The anodic voltage was adjusted when different electrolytes and film thicknesses were used. The same setup was also used for the CV cycling stability test. The anodic and cathodic peak current densities in the voltammogram were used to indicate the cycling stability of the polymer thin film. Moreover, all the thin films were preconditioned by the CV cycling before characterizations of the polymer thin films unless otherwise mentioned. The two-electrode CV experiments were carried out to study the appropriate ratio of redox capacity of the PTMA-*co*-BP thin film to the ECP-magenta magenta. All the thin films were made by spin-coating of the solutions on ITO substrates at a spin speed of 1500 rpm. The thickness of PTMA-*co*-BP can be controlled by varying the concentrations of the solutions in

the range from 5 – 26.7 mg/mL. ECP-magenta solutions (30 mg/mL) were used for spin-coating, resulting in a thin film with a thickness of ~ 240 nm. To assemble a two-electrode cell, a PTMA-*co*-BP coated ITO substrate and an ECP-magenta-coated ITO substrate were inserted into a precut plastic cap parallelly, and then they were immersed in the electrolyte housed in a UV cuvette. The two-electrode CV experiments were carried out between -1.35 V to 1.2 V at a scan rate 40 mV/s. Chronoabsorptometry experiments were performed between -1.35 and 1.2 V, and the absorbance spectra were recorded between 350 and 1200 nm after each potential was applied. The background absorbance was corrected by a reference cell that has two bare ITO substrates immersed in the same electrolyte. AFM images were obtained in a tapping mode at a 0.3 Hz scan rate. The thickness was measured by scanning across a scratch in the samples. The average step height was calculated from four different measurements. The EIS experiments were obtained using a 20 mV perturbation amplitude (V_{rms} = 14.4 mV) in a frequency ranging from 1.0 Hz to 1.0 MHz. The stray points with a negative value in high frequency and the deviated points in low frequency were removed before data fitting.

3.4 Results and Discussion

A crosslinkable radical polymer PTMA-*co*-BP was synthesized via radical polymerization using a previously reported procedure (Figure 3.1a).[81] From the ^{1}H NMR, the ratio between the radical and the benzophenone moieties was approximately about 85:15. By incorporating the benzophenone moieties, the PTMA-*co*-BP can undergo photo-crosslinking reaction by proton subtraction under the UV irradiation, leading to the formation of a crosslinked network which prevents the dissolution of PTMA-*co*-BP thin films. The CV of the crosslinked PTMA-*co*-BP thin film in 0.2 M $TBAPF_6$ ACN shows a pair of redox peaks at +0.93 V and +0.49 V (Figure 3.1a). These signals are associated with the reversible redox property of the conversion of the nitroxide radical to the oxoammonium cation (and vice versa on the reverse sweep). The UV-vis light absorption measurements show that the spectra of the PTMA-*co*-BP thin film with a thickness of ~ 180 nm are similar in both radical and cation states. (Figure 3.1b) Moreover, transmittances of both are above ~ 94% from 350 to 1,000 nm. Therefore, PTMA-*co*-BP can be an excellent candidate as a noncolor change ion storage layer for ECDs.

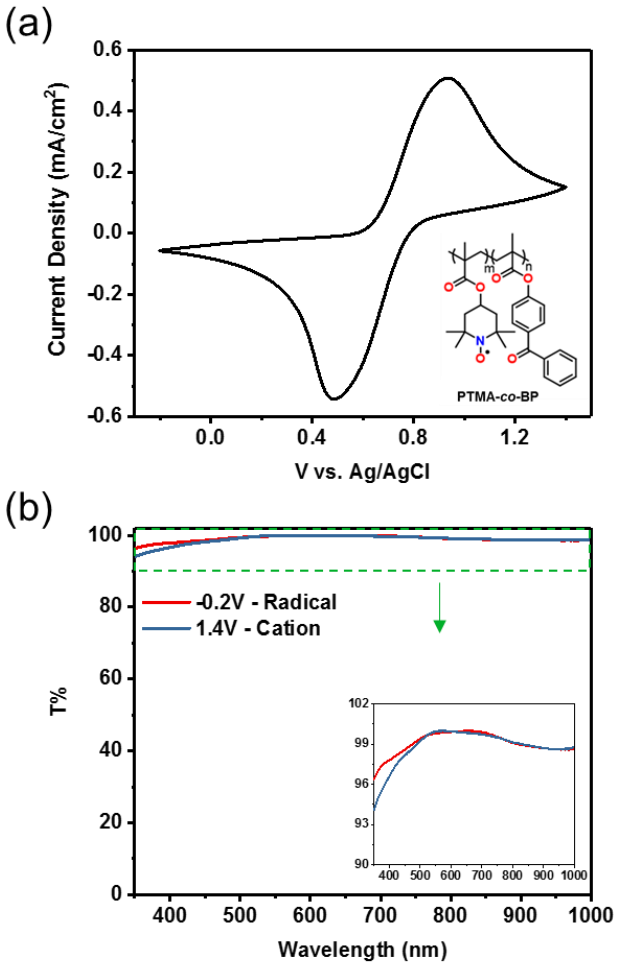

Figure 3.1 (a) Cyclic voltammogram of PTMA-*co*-BP (inset: molecular structure of PTMA-*co*-BP). (b) UV-vis transmittance spectra of PTMA-*co*-BP in the radical and cation forms (inset: the enlarge plot).

UV-vis and CV measurements were performed to determine the effect of the crosslinking on the optical and electrochemical properties of the PTMA-*co*-BP thin films. From the UV-vis measurements, the peak at ~250 nm is associated with the BP moieties in the PTMA-*co*-BP thin film (Figure 3.2a). The intensity decreases after UV light irradiation and remains the same with longer exposure, indicating that the consumption of benzoylphenyl group was complete within 60 minutes of exposure. The CV results show an increase in the current density after crosslinking, resulting in a higher redox capacity (Figure 3.2b). The increase of redox capacity is believed to be due to two factors. First, the electrochemical stability of PTMA-*co*-BP was improved after crosslinking. Second, the polymer chains formed a semi-locked conformation after crosslinking,

which resulted in an increase of current generated from a diffusional dependent double-layer charging process.[82]

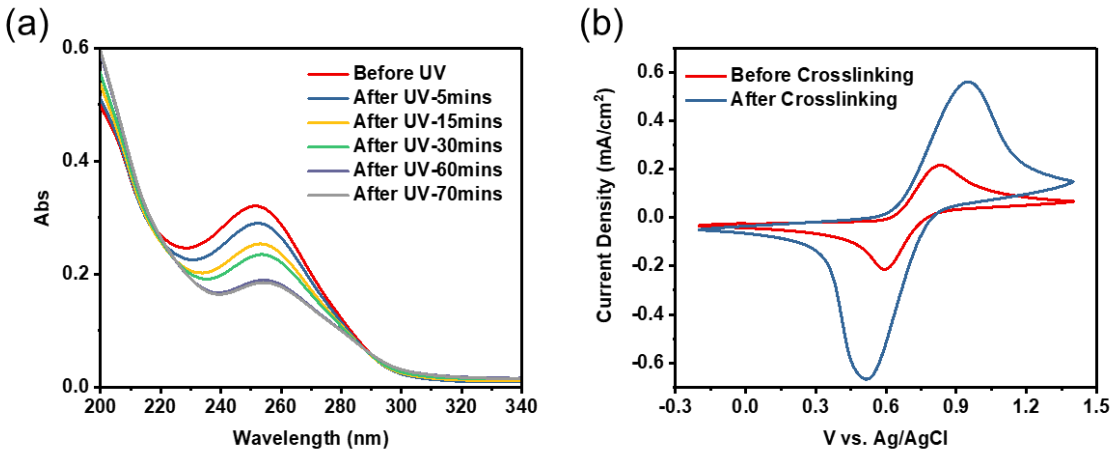

Figure 3.2 (a) UV-vis absorption spectra of PTMA-*co*-BP thin films with a thickness of ~ 180 nm before and after UV irradiation for different time intervals. (b) Cyclic voltammograms of the PTMA-*co*-BP thin film before and after UV crosslinking.

CV cycle tests were performed to confirm the electrochemical stability of PTMA-*co*-BP after photo-crosslinking. A thin layer of PTMA and PTMA-*co*-BP was coated on two different ITO substrates. Then, CV cycle tests were scanned at a rate of 40 mV s^{-1} in a 0.2 M $TBAPF_6$ in ACN. The thin film of PTMA-*co*-BP went through a break-in process during which the I_{pa} increased from the 1st to the 50th cycle (Figure 3.3a). Relative to the CV profile of the homopolymer PTMA thin film, a broad plateau around 0.7 V can be observed in the CV of PTMA-*co*-BP, which became sharper with extended cycles (Figure 3.3a, b). The broader redox processes also suggested that the PTMA-*co*-BP thin film was indeed crosslinked.[82] The I_{pa} of PTMA-*co*-BP lost 9.3% upon the 250th cycle after the break-in process, while the I_{pa} of PTMA thin film lost 84% after 150 cycles (Figure 3.3c). Therefore, the crosslinking strategy can effectively prevent the dissolution of PTMA-*co*-BP thin films.

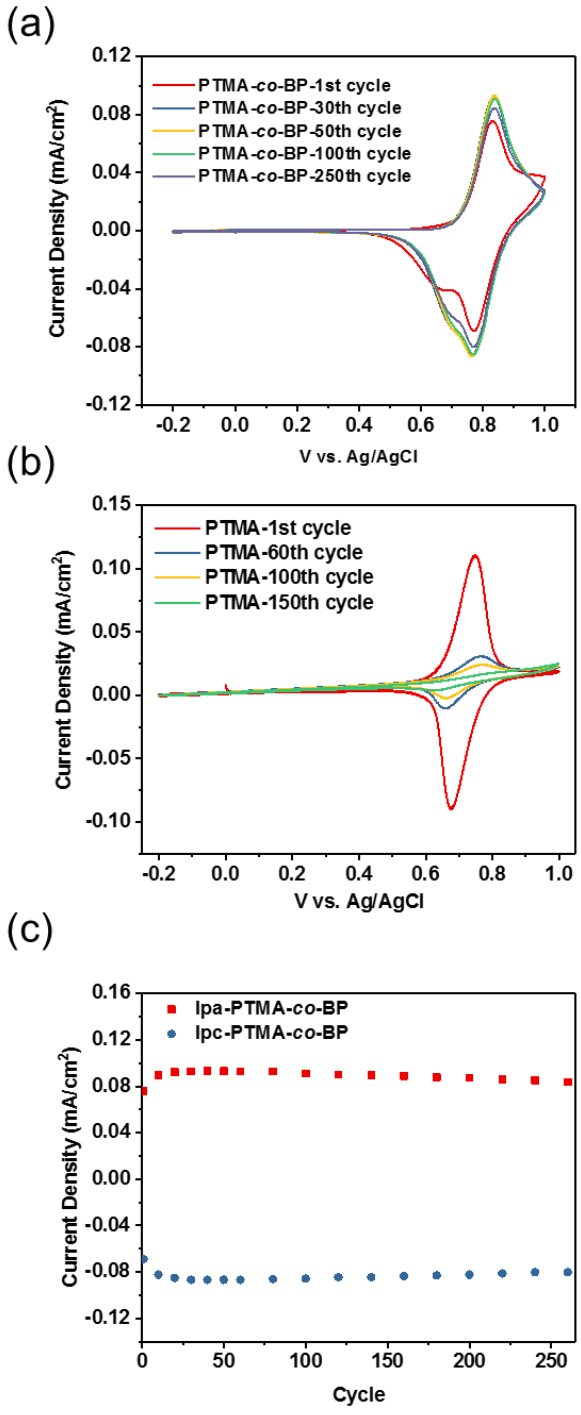

Figure 3.3 Cyclic voltammograms of (a) PTMA-*co*-BP and (b) PTMA. (c) I_{pa} and I_{pc} of the cyclic voltammograms of the PTMA-*co*-BP thin film vs the number of cycles.

The electrochemical impedance of PTMA-BP before and after crosslinking was also evaluated by EIS measurements (Figure 3.4). Both EIS measurements show small semi-circle in the high-frequency region which is related to the double layer capacitance and charge transfer resistance. In the low-frequency region, the impedance plots show a line approaching 90°. While coming to the lower frequency ~ 10 Hz, they start to deviate and appear like an arc shape. (Figure 3.10) Thus, a modified Randles circuit with a restricted linear diffusion element was used as the equivalent circuit to model the EIS spectra after removing the deviation points.[95] (Scheme 3.1) From the fitting results, the R_{ct} for PTMA and PTMA-*co*-BP are 14.2 Ω and 15.7 Ω, respectively. The similar values of R_{ct} suggest the crosslinking of PTMA-*co*-BP thin films did not result in an increase of ionic resistances.

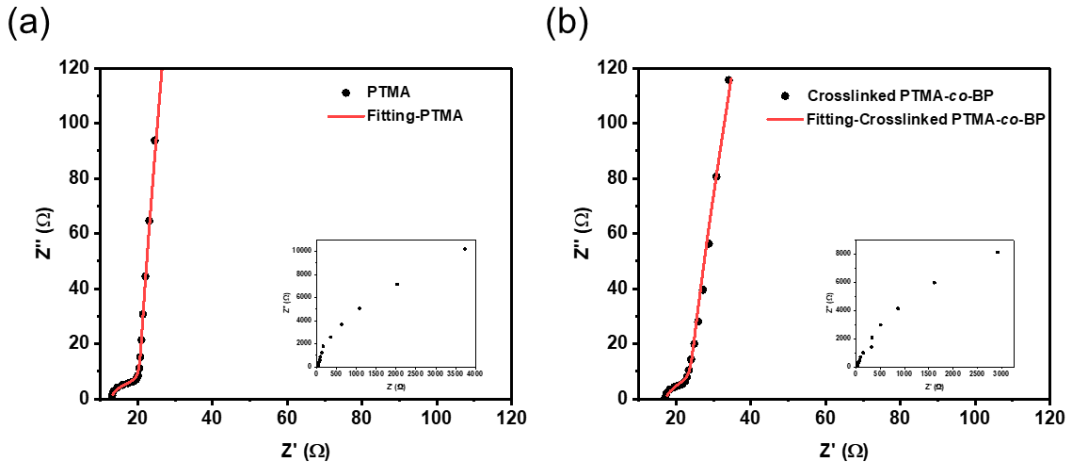

Figure 3.4 (a)EIS measurements of the PTMA thin film (inset: the full spectrum of EIS), and (b) the crosslinked PTMA-*co*-BP thin film (inset: the full spectrum EIS).

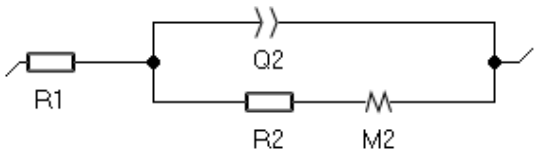

Scheme 3.1. R(Q(RM)) Equivalent Circuit

Next, we investigated the effect of electrolytes on the electrochemical behaviors of PTMA-*co*-BP as electrolyte anions were found to assist the charge transportation in the PTMA gel previously.[83] Moreover, different electrolyte anions have different diffusion coefficients in the charge transportation that occurs within the PTMA matrix, and this affects the discharging rate characteristics of the organic radical battery.[84] When radical polymers were used as the ion storage layer in ECDs, the diffusion coefficient of solvated anions within the electrodes determined the accessibility of redox sites of electrodes. As a result, the redox capacity of radical polymers might have a variation in different electrolytes. Selecting the appropriate electrolytes could be the key factor to enhancing the performance of radical polymers-based ECDs. The redox capacity of PTMA-*co*-BP thin films was calculated from the CV at a scan rate of 40 mV s^{-1} in a three-electrode setup with a platinum wire serving as the counter electrode and Ag/AgCl serving as the reference electrode. The CV experiments of PTMA-*co*-BP thin films with similar thicknesses were carried out in 0.2 M $TBAPF_6$ PC and ACN. The thickness of the thin films was controlled by spin-coating of the same solution at the same spin speed. The redox capacity of the PTMA-*co*-BP thin film, which was smaller in PC (~ 0.8 mC/cm^2) compared to the thin film with a similar thickness in ACN (~ 5.6 mC/cm^2) (Figure 3.5a). CV experiments at different scan rates ranging from 10 to 200 mV/s were performed in both electrolytes. The square root of the scan rate has a linear correlation with the anodic peak current of the CVs of PTMA-*co*-BP thin films in both PC and ACN, which indicated a diffusion-controlled process (Figure 3.5b). The diffusion coefficients of the solvated PF_6^- can be calculated from the slope of anodic peak current vs. square root of scan rates, which were 7.18×10^{-9} and 2.41×10^{-6} cm^2/s for the PTMA-*co*-BP thin film in PC and ACN, respectively (Figure 3.5b). The diffusion coefficient of the solvated PF_6^- in the PTMA-*co*-BP thin film was about 3 orders of magnitude larger in ACN than in PC. Therefore, the smaller redox capacity of PTMA-*co*-BP in PC was due to the slow diffusion of the solvated counterions. The low redox capacity of PTMA-*co*-BP in 0.2 M $TBAPF_6$ PC made it insufficient to balance the redox capacity of the electrochromic layer, resulting in a low optical contrast of the ECD (Figure 3.6). Although PTMA-*co*-BP thin films have a larger redox capacity in ACN, ACN is highly volatile and not suitable for device fabrications. We investigated the nonvolatile electrolyte 0.2 M EMI-TFSI in PC. After the break-in, the PTMA-*co*-BP thin film in 0.2 M EMI-TFSI PC had a redox capacity of ~ 3.9 mC cm^{-2}, and the diffusion coefficient of the solvated $TFSI^-$ was calculated to be ~ 8.29×10^{-7} cm^2 s^{-1} (Figure 3.5b). We believed that the increased redox capacity of PTMA-*co*-BP thin

films in PC was due to the higher diffusion coefficient of the solvated $TFSI^-$ counterions.[84] Thus, 0.2 M EMI-TFSI PC was used in the following studies.

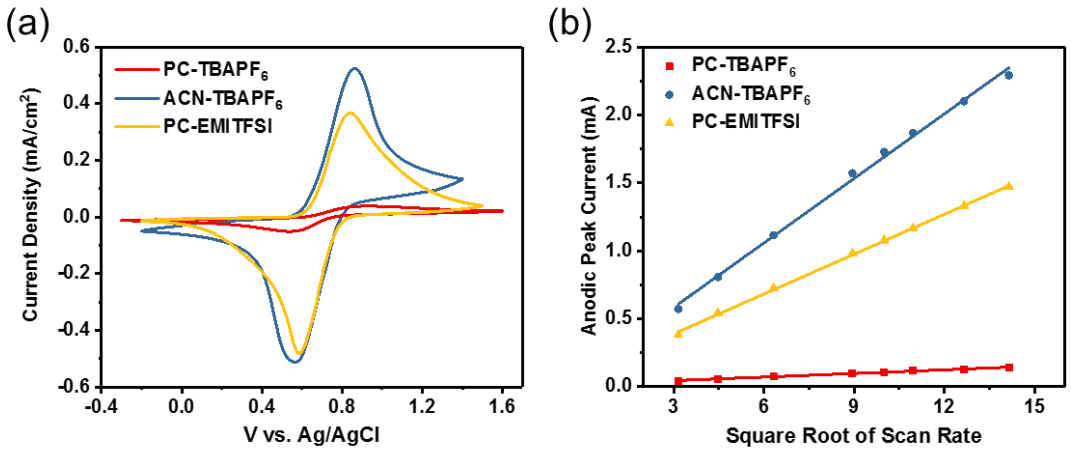

Figure 3.5 (a) Cyclic voltammograms of PTMA-*co*-BP thin films in 0.2 M $TBAPF_6$ PC, 0.2 M $TBAPF_6$ ACN, and 0.2 M EMI-TFSI PC. (b) Anodic peak current of PTMA-*co*-BP thin films obtained from the cyclic voltammograms in 0.2 M $TBAPF_6$ PC, 0.2 M $TBAPF_6$ ACN, and 0.2 M EMI-TFSI PC vs. square-root of scan rate.

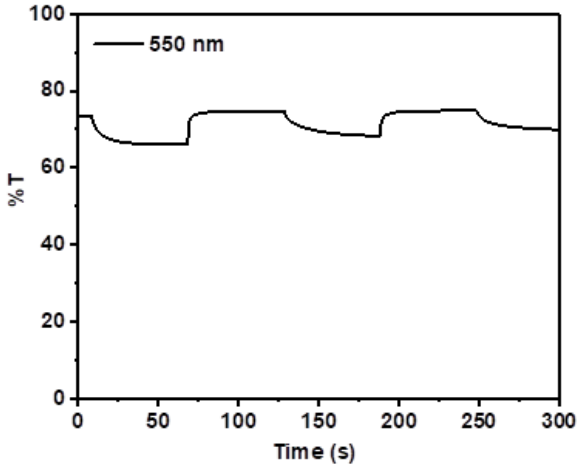

Figure 3.6 Double-potential step chronoamperometry of a two-electrode cell of PTMA-*co*-BP and pre-oxidized ECP-magenta. The voltage was switched between -1.0 V and 2.2 V.

Two-electrode cells were assembled to further evaluate the PTMA-*co*-BP as the ion storage layer of electrochromic materials (Figure 3.7a). ECP-magenta that can be switched between magenta (neutral state) and a highly transmissive state (oxidized state) was used as the electrochromic layer (Figure 3.7a). The two electrodes were inserted into the plastic cap such that they were parallel, and they were then immersed in a 0.2 M EMI-TFSI PC electrolyte, which was housed in a UV cuvette cell (Figure 3.7a). Because both PTMA-*co*-BP and ECP-magenta are P-type materials and will only undergo reversible oxidation reactions, the PTMA-*co*-BP layer was oxidized first before being assembled into two-electrode cells. In an ECD, the redox capacity of the counter electrode determined whether the charges generated in the electrochromic layer can be balanced to accomplish a color switching. Hence, by changing the thickness of the counter electrode, the redox capacity of the counter electrode can be varied to optimize the performance of the electrochromic layer. The redox capacity of each layer was estimated from the CV at a scan rate of 40 mV s^{-1} in a three-electrode setup before assembling the materials into a two-electrode cell. The thickness of the ECP-magenta layer was fixed at ~ 240 nm with a redox capacity ~ 2.56 mC/cm^2. The thicknesses of PTMA-*co*-BP layers were varied from ~ 40 nm to ~ 220 nm by spin coating of solutions with different concentrations (Table 1). The redox capacity of PTMA-*co*-BP layer increased with the increase of thickness. In addition, the ratio of the redox capacity of PTMA-*co*-BP layer to ECP-magenta layer (R_q) can be adjusted from 0.22 to 2.00 (Table 1). Figure 3.7b shows the CVs of two-electrode cells of PTMA-*co*-BP/ECP-magenta with different R_q. The CVs show a pair of broad peaks around ~ - 0.5 and ~ - 0.2 V, suggesting that the reversible electrochemical reactions occurred within this electrochemical window (-1.35 - 1.2 V). When R_q is smaller than 1.0, the shape of the CVs is more like the CV of PTMA-*co*-BP. On increasing the R_q of PTMA-*co*-BP to ECP-Magenta to over 1.0, CVs show more obvious capacitive-like plateaus appearing at both forward and backward scans, which are similar to the CV of the ECP-magenta (Figure 3.7). These capacitive-like plateaus were believed to be the faradaic redox processes during the charging/discharging of redox-active polymer thin films.[85] Then, -1.35 and 1.2 V were selected as the potentials in the double-potential-step chronoabsorptometry (DPSC) experiments during which the transmittance was measured at 550 nm (Figure 3.7c). The results are summarized in Table 3.1. When the R_q was ~ 0.22, the charge capacity of the PTMA-*co*-BP layer could not balance the charge consumed in the ECP-magenta layer during the color switching. As a result, the two-electrode cell could only have optical contrast (ΔT) of 37.8 %. With increasing the R_q to

~ 1.59, the ΔT of the two-electrode cells reached a maximum value of 72.1 % and decreased to 64.8 % at the R_q of 2.00. Although the switching time at the R_q of 1.59 is the longest, the two electrodes cell can still reach 95% of its colored/bleached state within 10 s. Additionally, composites coloration efficiencies at 95% change of optical contrast ($\eta_{95\%}$) during the bleaching process were calculated based on a previously reported method (Figure 3.7d).[86] The composite coloration efficiency reached a maximum at the R_q of 0.77. This is because the thinner films generate less capacitive current during the redox processes, and thus, most of the charge injection/extraction is due to the color switching of the electrochromic layer. However, the charge consumed in the ECP-magenta layer had not been balanced completely, and the optical contrast was not optimized. With the increase of the R_q to 1.00, the ΔT did not have an obvious change and more charge generated from the capacitive charging, resulting in a lower value of the composite coloration efficiency. At the R_q of 1.59, the doping level of ECP-Magenta was further increased, which was indicated by the higher transmissive at 550nm. The sufficient doping of the ECP-magenta layer led to a higher composite coloration efficiency of 754.0 cm^2C^{-1}. The further increase of the R_q caused the decrease of ΔT and coloration efficiency. The thicker layer of PTMA-*co*-BP might lead to an increase of resistance and capacitive charge, resulting in an inefficiency charge consumption of the ECD.[66] Therefore, the R_q of PTMA-*co*-BP to ECP-magenta was kept at ~ 1.59 in the spectroelectrochemical study and the cycling test. The optimized ECD has an optical contrast of 72%, which is higher than the previously reported value of 66% for the ECD made by ECP-magenta and PMMA/PTMA, and their coloration efficiencies are comparable.[79] The slower switching time in this work could be due to the smaller working potential.

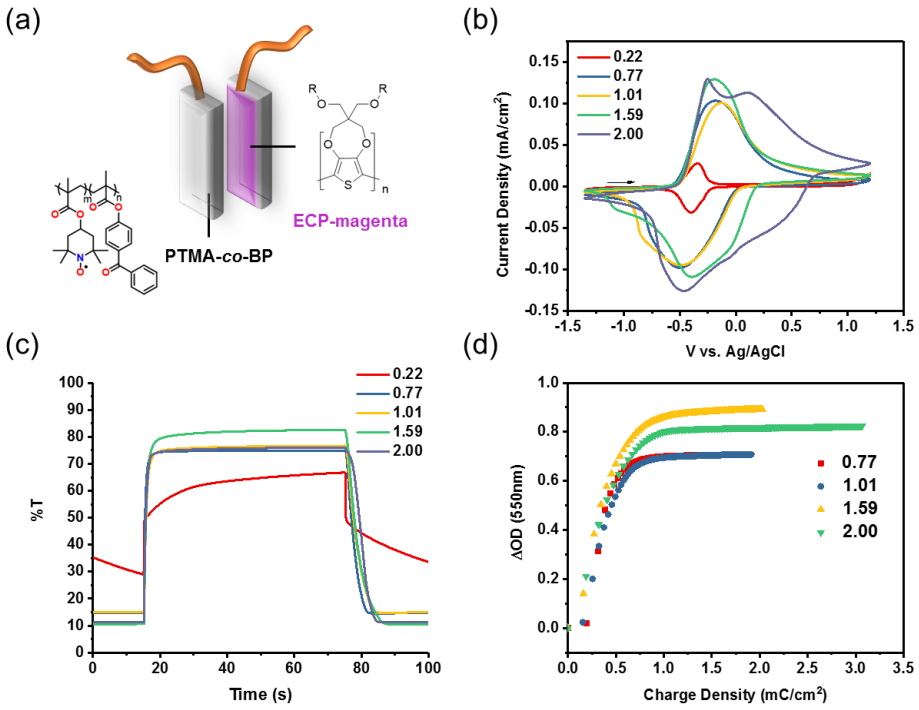

Figure 3.7 (a) A schematic demonstration of two-electrode cells and the structures of PTMA-*co*-BP and ECP-magenta. (b) Cyclic voltammograms, (c) double-potential step chronoamperometry, and (d) the plots of change of the optical density at 550 nm vs. charge density of two-electrode cells with different ratios of redox capacity of PTMA-*co*-BP to ECP-magenta.

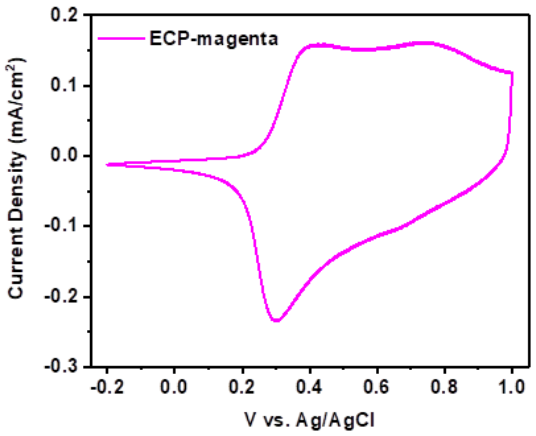

Figure 3.8 Cyclic voltammogram of ECP-magenta with a thickness of ~ 240 nm at the scan rate of 40 mV s^{-1}.

Table 3.1 The thickness of PTMA-*co*-BP, optical contrast, switching time that achieved 95% of optical contrast, and composites coloration efficiencies of two-electrode cells with different ratios of redox capacity of PTMA-*co*-BP to ECP-magenta.

R_q[a)]	PTMA-*co*-BP Thickness/nm	ΔT[b)]	t_b (95%)[c)]/s	t_c (95%)[c)]/s	$\eta_{95\%}$[d)]/cm^2C^{-1}
0.22	42.61 ± 4.90	37.8	/	/	/
0.77	85.69 ± 3.76	60.1	1.8	5.6	880.5
1.00	159.19 ± 10.77	61.7	3.4	7.7	713.5
1.59	185.22 ± 25.13	72.1	4.6	9.5	754.0
2.00	226.67 ± 12.56	64.8	2.4	8.4	705.1

[a)] R_q is the redox capacity ratio of PTMA-co-BP to ECP-magenta. [b)] ΔT is the optical contrast of ECDs at 550nm. [c)] t_b (95%) and t_c (95%) the bleaching time and coloration time at 95 % of the optical contrast change, respectively. [d)] $\eta_{95\%}$ is the composite coloration efficiency at 95 % of the optical contrast change.

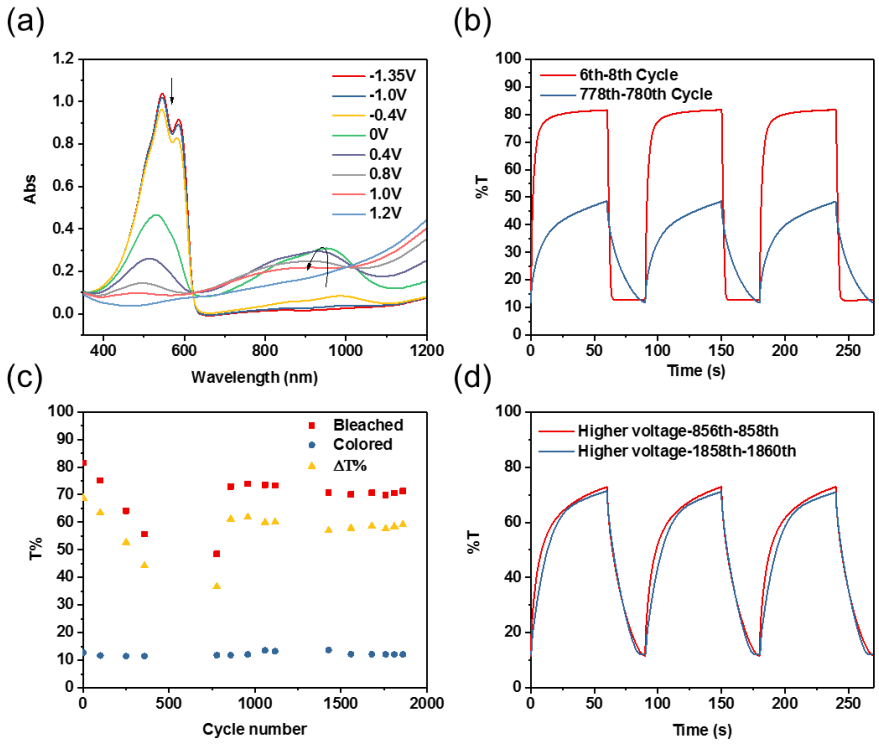

Figure 3.9 (a) The spectroelectrochemical, (b) the double-potential step chronoamperometry cycled between -1.0 V and 1.0 V, (c) the transmittance at bleached and colored state and the change of the transmittance, and (d) the double-potential step chronoamperometry cycled between -1.35 V and 1.2 V of the two-electrode cells with ratios of redox capacity of PTMA-*co*-BP to ECP-magenta at ~ 1.59.

In the spectroelectrochemical study, the two-electrode cell has two strong absorptions at 545 nm and 587 nm originating from the ECP-magenta electrochromic layer. On increasing the applied potential from -1.35 V to 1.2 V, the absorption in the visible region decreased, while the peak in the near-IR region first increased and then decreased (Figure 3.8a). This phenomenon indicated that the neutral ECP-magenta molecules were doped and converted to polarons, and then neutral and polaron molecules were further oxidized to bipolarons, which also suggested that the PTMA-*co*-BP can balance the charges needed in the ECP-magenta layer during the redox reactions. In the cycling test, the potential of the device was first switched between – 1.0 V and + 1.0 V to avoid the possible side reactions such as the water splitting reaction, which occurs at ~ 1.23 V.[87] The DPSC experiments revealed that the bleaching time was longer than the coloring time. Thus, an asymmetric cycle test in which an anodic polarization was applied for 60 s and a cathodic polarization was applied for 30 s was adopted to ensure a thorough color switching.[88] After the break-in, the two-electrode cell can achieve an optical contrast of 68.8 %, and the t_b (95%) and t_c (95%) were 11.8 s and 3.2 s, respectively (Figure 3.8b). After ~ 780 cycles, the optical contrast decreased to 36.7 %, and the t_b (95%) and t_c (95%) increased to 48.5 and 24.2 s, respectively (Figure 3.8b). The lower contrast and slower response time of the ECDs could be due to the drifts of the electrode potential or the ion-trapping within the electrodes during the cycling test.[89–91] A similar phenomenon was also observed in other studies of ECDs of the ECP-magenta and the propylenedioxythiophene/benzothiadiazole copolymer with MCCP as the counter electrode.[88,92,93] Additionally, the thickness of the PTMA-*co*-BP thin film was measured after the cycle test. The thin film that was immersed in the electrolyte and involved in the cycling test had a thickness of 168. ± 18. nm which is comparable to the thickness of the unreacted thin film exposed to air (181.90 ± 25.19 nm.) Thus, dissolution problems of PTMA-*co*-BP were not the dominant reason for the lower contrast and slower switching kinetic of the device after 780 cycles. When the applied potentials were increased to 1.2 V and -1.35 V, the optical contrast of the device can be recovered to 61.1 % and was stable in subsequent 1,000 cycles (Figure 3.8c, d). In total, the cycle test was carried out for ~ 1800 cycles and equal to ~ 45 h under ambient condition, which demonstrated the long cycling stability of the ECD.

Finally, the optical memory of the two-electrode cell was tested by following a previously developed procedure.[94] The time of the applied potential that reset the device back to its colored state has an effect on its self-bleaching behaviors. Thus, applying an (a) anodic/cathodic bias (1.2

V/– 1.35 V) for 300 s was used in this study. When the device was switched to open circuit (V_{off}), the change of transmittance was measured for 30 min. Figure 3.9a,b show that the transmittance of the two-electrode cell changed from 12.8% to 15.5% during the self-bleaching process, and from 82.5% to 80.2% during the self-coloring process, indicating that the device can maintain its both colored and bleached states under open circuit for up to 30 mins with negligible changes of transmission.

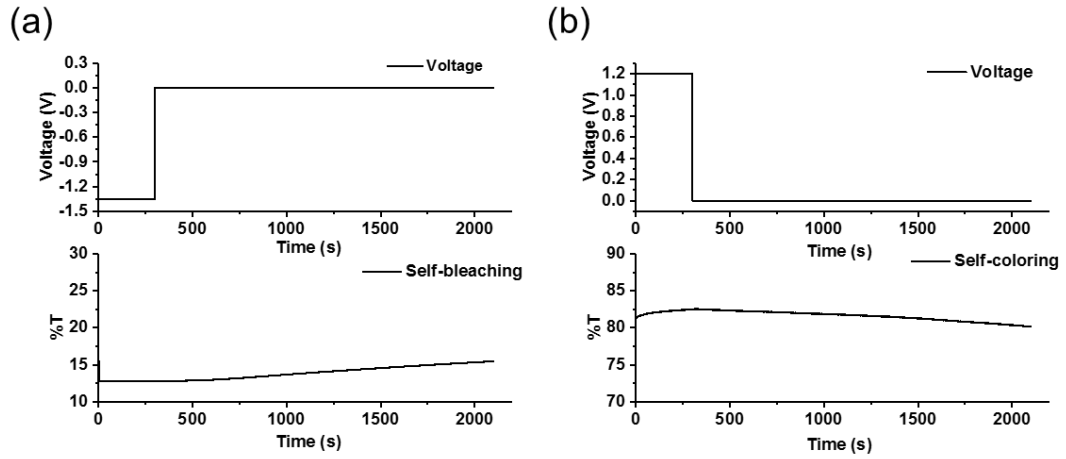

Figure 3.10 Voltage and transmittance vs time during the (a) self-bleaching and (b) self-coloring process of the two-electrode cells with the ratio of the redox capacity of PTMA-*co*-BP to ECP-magenta at ~ 1.59.

3.5 Conclusions

In this work, we demonstrated the potential of the highly transparent crosslinkable open-shell macromolecule copolymer, PTMA-*co*-BP, as the ion storage layer for ECDs. The crosslinked PTMA-*co*-BP thin films showed an improvement of electrochemical stability in the electrolytes. The diffusion coefficient of solvated ions within the radical polymer thin films has a great impact on the redox capacity of radical polymers. By selecting the appropriate electrolytes and optimizing the thickness of the PTMA-*co*-BP, the redox capacity of the PTMA-*co*-BP thin film can be adjusted to match the charge consumption in the electrochromic layer, so that the ECDs can achieve a high contrast, fast switching times, robust cycle stability, and good optical memory at open circuit for both bleached and colored state. The nonconjugated nature makes PTMA-*co*-BP highly transparent in the visible region, and the stable nitroxyl radical sites make it redox-active. Moreover, solution processability and easy synthesis are also advantages in the scaled-up

manufacturing. Hence, the PTMA-*co*-BP has a great potential to be used as the ion storage layer for ECDs.

3.6 Acknowledgements

The authors are grateful for the financial support from Purdue University and the American Chemical Society Petroleum Research Fund (# 57352-DNI7). The radical polymer was provided by S.M. and B.W.B. This work was partially supported by the Air Force Office of Scientific Research (AFOSR) through the Organic Materials Chemistry Program (Grant Number: FA9550-15-1-0449, Program Manager: Dr. Kenneth Caster) to B.W.B, and we thank the AFOSR for their gracious support.

CHAPTER 4. LOW-TEMPERATURE SOLUTION PROCESSED NIOBIUM OXIDE AS THEH ION STORAGE LAYER

This chapter was adapted with permission from the manuscript published in ACS Applied Materials & Interfaces: He, J.; You, L.; Tran, D. T.; Mei, J. Low-Temperature Thermally Annealed Niobium Oxide Thin Films as a Minimally Color Changing Ion Storage Layer in Solution-Processed Polymer Electrochromic Devices. ACS Appl. Mater. Interfaces 2019, 11 (4), 4169–4177.

4.1 Abstract

The limited availability of solution-processable ion storage materials, both inorganic and organic, hinders the adoption of roll-to-roll manufacturing for polymer electrochromic devices (ECDs). The n-type transition metal oxides are known for their ion storage properties. However, the fabrication methods of their amorphous metal oxide thin films typically involve sputtering, thermal deposition, electrical deposition, or sol-gel deposition followed by high-temperature thermal annealing (>300 ^{o}C), thus making them incompatible for low-cost roll-to-roll manufacturing on flexible substrates. In this study, we report the synthesis of amorphous niobium oxide (a-Nb_2O_5) thin films from sol-gel precursors through the combination of photoactivation and low-temperature thermal annealing (150 ^{o}C). Coupled with p-type electrochromic polymers (ECPs), solution-processed a-Nb_2O_5 thin films were evaluated as a minimally color changing counter electrode (MCC-CE) material for electrochromic devices. We found that that ultraviolet ozone (UVO) treated and thermally annealed (UVO-150 °C) a-Nb_2O_5 thin films show excellent electrochemical properties and cycling stability. Notably, a-Nb_2O_5/ ECP-magenta ECD has a high optical contrast of ~ 70 %, a fast switching time (bleaching and coloring time of 1.6 and 0.5 s for reaching 95% of optical contrast). In addition, the ECD demonstrates a high coloration efficiency of ~ 849.5 mC cm^{-2} and a long cycling stability without a noticeable decay up to 3000 cycles.

4.2 Introduction

Electrochromic technology presents a great potential in a wide range of optical applications, ranging from smart windows,[96] self-dimming electrochromic ski goggles, rear mirrors of automobiles, [97,98] to electrochromic irises.[99] In a typical solid-state electrochromic

device (ECD), three major components – an electrochromic layer as the working electrode (WE), a solid-state electrolyte layer for ion transport, and an ion storage layer as the counter electrode (CE) – are critical for high performance and electrochemical cycling stability. Electrochromic polymer (ECP) based solid-state ECDs have been emerging as the competitive technology for smart windows because of their high optical contrast, fast response time, scalability and low-cost.[12,13,100,101] A full-color palette of solution-processable electrochromic polymers has thus been created.[12] These polymers can be switched from colored states to highly transmissive states when they are oxidized. To match these electrochromic polymers, ion storage materials need to be highly transmissive in the reduced states. Currently, the choice for such ion storage materials is rather limited because n-type electrochromic polymers that can switch from colored state to highly transmissive state upon reduction are largely absent.[102] As a compromise solution, p-type electrochromic polymers which are transmissive under both neutral and oxidized states are pre-conditioned to pair with other colored p-type electrochromic polymers. For instance, both non-conjugated nitroxyl based radical polymers and conjugated n-alkyl-substituted poly(3,4-propylenedioxypyrrole) (PProDOP) polymers have been investigated as CEs after the electrochemical or chemical preoxidation.[70,78,79,103–106] The electrochemical preoxidation needs to be performed in an electrochemical cell with electrolyte, reference, and counter electrodes, and the chemically preoxidation is done by immersing the fabricated thin films in a solution of oxidants. Then, the oxidized thin films are subjected to washing and drying steps to remove the chemical residues. These additional pre-conditioning steps bring complexity to roll-to-roll manufacturing and adds up the fabrication cost.[106]

Some transition metal oxides undergo a color change when they are either oxidized or reduced. Such a color change in metal oxide thin films is usually associated with a large amount of charges consumption and generation due to their low coloration efficiency.[18] When metal oxides are paired up with an electrochromic polymer with a high coloration efficiency, they are usually regarded as minimally color changing counter electrodes (MCC-CE). For instance, Hassab *et al* studied tungsten oxide (WO_3) as the CE for ECPs.[107] Because only a small percentage of the total charge was used to balance the charges consumed in a complete switch of ECPs, the color change of WO_3 CE itself was minimum in an ECD. Unfortunately, WO_3 has a relatively high coloration efficiency (> 50 cm^2/C); the doped WO_3 CE thin film showed a strong color residue in

the bleached state of the electrochromic cells.[4] As a result, the electrochromic device made of WO_3 and ECP-magenta only showed a low optical contrast of ~ 52%. Searching for n-type transition metal oxides in literature, we found that amorphous niobium pentoxide (a-Nb_2O_5) appears as an ion storage layer for its large volumetric charge density, high transparency and low coloration efficiency (ca. 20 cm^2/C) in the visible region.[108–110] a-Nb_2O_5 thin films can be prepared by sputtering,[111] chemical vapor deposition[112] and electrodeposition,[113] as well as sol-gel deposition[110]. If the sol-gel method is used, a high-temperature (> 300 °C) thermal annealing will be required to remove residues of organic species and molecular water that are detrimental to their electrochemical properties and cycling performance.[114] In other words, this fabrication process of a-Nb_2O_5 thin films is not compatible with low-cost and high-throughput solution processing on plastic substrates (i.e. PET).[115]

In this work, we report a new synthetic method to prepare a-Nb_2O_5 thin films and use them as MCC-CEs to pair with electrochromic polymers for high-performance ECDs. The newly developed fabrication process involves photoactivation of sol-gel derived Nb_2O_5 thin-films through an UV-Ozone treatment, followed by a low-temperature (150 °C) annealing.[116] We found that the newly prepared a-Nb_2O_5 thin films show a similar charge density as the a-Nb_2O_5 thin films annealed at 300 °C and present an even better cycling performance. When paired with ECP-black and ECP-magenta as the MCC-CE, the ECDs offer a high optical contrast, a high color purity, and a long cycling stability. In addition, flexible thin-film ECDs are fabricated with the solution-processed a-Nb_2O_5 and ECP-magenta on ITO/PET substrates to forecast the potentials of the new synthetic method for a-Nb_2O_5 in future roll-to-roll manufacturing.

4.3 Experiments

Reagents and Materials. The niobium(V) ethoxide (99.95%) and ethanol (99.5%) were purchased from Fisher Scientific. The propylene carbonate (PC), lithium bis(trifluoromethane)sulfonimide (LiTFSI), poly (ethylene glycol) diacrylate (M_n = 575) ($PEGDA_{500}$), 2-hydroxy-2-methylpropiophenone (97%) (HMP), and platinum wire (99%, 0.5 mm) were purchased from Sigma-Aldrich. The leakless miniature Ag/AgCl electrode ET072 was purchased from eDAQ. All chemicals were used as received unless otherwise specified.

Instrumentations. All the spectra were collected using an Agilent Cary 5000 UV/Vis-NIR spectrophotometer. All the electrochemical measurements were performed using a Biologic SP-150 potentiostat. A Laurell spin coater (WS-650Mz-23NPPB) was used to prepare all the thin films. UVO treatment was performed using a HELIOS-500 UV-ozone cleaning system. A Veeco dimension 3100 atomic force microscopy (AFM) and a Gaertner variable angle stokes ellipsometer (L116SF) were used to obtain the thicknesses of a-Nb_2O_5 thin films. A Keithley 2400 sourcemeter was used to monitor the potential distribution on the ECP-black WE during the electrochemistry experiments of a two-electrode cell. A Thermo Nicolet Nexus FTIR was used to study the organic and water residues within a-Nb_2O_5 thin films.

Preparation and Characterization of Thin Films. The niobium ethoxide precursor solution was prepared according to a previously reported method.[110] Under ambient conditions, Nb_2O_5 thin films were prepared by using niobium ethoxide solution via the sol-gel reaction on ITO/glass or ITO/PET substrates followed by annealing at various temperatures (100 , 150 , and 300 °C) for 10 min. The UVO-150 °C a-Nb_2O_5 thin films were UVO treated for 20 min followed by annealing at 150 °C for 10 min. ECP-black and ECP-magenta were also synthesized according to previous work.[117,118] Solutions of ECP-black (40 mg/ml) and ECP-magenta (25mg/ml) were prepared by dissolving the polymers in chloroform and stirred overnight before use. ITO/glass and ITO/PET substrates were cleaned by sonicating in acetone and ethanol for 10 min and blown dry by compressed nitrogen gas. All thin films were prepared by spin-coating at a spin speed of 1500 rpm. The thicknesses of one-layer a-Nb_2O_5 thin films were measured by ellipsometry and confirmed by AFM, and their topology was characterized by AFM. As a control experiment, each a-Nb_2O_5 thin film on ITO/glass substrate was cut in the two pieces. One was subjected to the proposed process and the other was kept untreated. The thicknesses of two- and three-layer a-Nb_2O_5 thin films were measured by ellipsometry.

Electrochemistry. A three-electrode cell was fabricated with ITO/glass substrates coated with ECP-black or a-Nb_2O_5 as the WE, a leakless Ag/AgCl as the reference electrode, 0.2 M LiTFSI in PC as the electrolyte, and a platinum wire as the counter electrode. Cyclic voltammetry experiments were performed using a three-electrode cell, at a scan rate of 40 mV/s, to obtain the charge density of electrodes. The charge density was calculated by the following equation:

$$\text{Charge density} = \int j dV/s$$

Where charge density has a unit of mC cm^{-2}, *j* is current density (mA cm^{-2}), *s* is the scan rate (V s^{-1}), and *V* is the voltage (V).

For two-electrode experiments, ECP-coated ITO/glass WEs together with a-Nb_2O_5-coated ITO/glass CEs were used in 0.2 M LiTFSI in PC electrolyte or PEGDA gel electrolyte with 50 vol% of 0.2 M LiTFSI in PC for liquid- and solid-state devices, respectively. Cyclic voltammetry experiments were performed at a scan rate of 40 mV/s. For in-situ measurements of the potential change of the WE (E_{we}), a Keithley 2400 sourcemeter was used, and the voltage between WE and a leakless Ag/AgCl reference electrode was measured. The E_{we} data obtained during the CV experiments were processed using two points smoothing to remove the electrical noise caused by the vibration.

Device Fabrication. The electrolyte was prepared by mixing $PEGDA_{500}$, 0.2 M LITFSI in PC, and HMP in a volume ratio of 5:5:1 overnight in a nitrogen-filled glove box. All ECP WEs were prepared by spin-coating the solutions on ITO/glass substrates (30 × 50 × 1 mm^3, sheet resistance, 8-12 Ω/sq) at a spin speed of 1500 rpm, and a-Nb_2O_5 CEs were prepared as described previously. Then, they were transferred into the N_2 glove box. 0.2 ml of the mixed electrolyte was titrated on a WE, and a CE was placed on top with the coated sides facing each other. After the electrolyte had spread out by the capillary force, the electrolyte was cross-linked by placing the laminated device under the commercial UV lamps emitting at both 365 and 405 nm for 15 min. The device was taken out from the nitrogen-filled glove box and sealed in the atmosphere by using a General Electric silicone. The flexible device was fabricated by following the same protocol on flexible ITO/PET substrates (sheet resistance, 200 Ω/sq).

4.4 Results and Discussion

An in-situ sol-gel reaction was used to fabricate a-Nb_2O_5 thin films on ITO/glass substrates. The precursor solution was made of niobium (V) ethoxide dissolved in ethanol with a concentration of ~ 0.19 M.[110] XRD measurements suggested that the Nb_2O_5 thin films annealed at both 150 and 300 ºC were amorphous. (Figure 4.1)

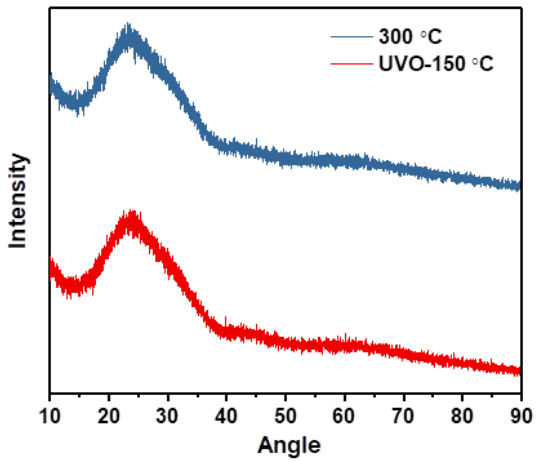

Figure 4.1 X-ray diffraction patterns of UVO-150 °C and 300 °C annealed a-Nb_2O_5 thin films.

Cyclic voltammetry (CV) studies were performed to investigate the effect of the processing conditions on the electrochemical properties of a-Nb_2O_5 thin films. The onset of the reduction potentials of the lithium-ion insertions in a-Nb_2O_5 thin films annealed at 100 ºC and 150 ºC were -1.15 and -1.0 V, respectively, which are more negative than the onset potentials of thin films annealed at 300 ºC (- 0.86 V) (Figure 4.2a). By using UVO treatment followed by annealing at 150 ºC (UVO-150 ºC), the onset potential of the lithium-ion insertion (- 0.84 V) of UVO-150 ºC a-Nb_2O_5 thin films is comparable to the thin films annealed at 300 ºC. A larger potential bias might be required to operate ECDs which use a-Nb_2O_5 thin films annealed at 100 and 150 ºC as the CEs.[78] As a CE material, a high charge density is desired to balance the charges consumed in the electrochromic layer. The charge densities can be calculated from the integration of the cyclic voltammograms (Figure 4.2b). Thin films annealed at 100 ºC and 150 ºC both have a charge density of ~ 4.0 mC cm^{-2}, while UVO-150 ºC a-Nb_2O_5 thin films have a charge density of 7.2 ± 0.9 mC cm^{-2} which is comparable to the charge density of thin films that annealed at 300 ºC (6.8 ± 0.8 mC cm^{-2}). Fourier-transform infrared spectroscopy (FTIR) studies were performed to get insight into the effect of UVO treatment and annealing temperature (Figure 4.2c). A very strong absorption peak from the glass substrate was centered at ~ 900 nm^{-1} and influenced the observation of the other peaks (Figure 4.3). Thus, the spectra are shown from 4500 to 1200 nm^{-1}. The broad absorption peak ~ 3300 nm^{-1} is associated with the -O-H stretching of molecular H_2O and -Nb-OH, and the peak ~ 1630 nm^{-1} can be assigned to the bending of H_2O molecules. The small peaks

around 1400 nm^{-1} can be related to bending and scissoring of the alkane (-C-H) of the organic residues from the precursor solution.[119] The FTIR spectrum of the as-spun a-Nb_2O_5 thin film showed peaks at ~ 3300 nm^{-1} and 1630 nm^{-1} and small peaks around 1400 nm^{-1}, which revealed the existence of both molecular water and organic species. The disappearance of peaks at ~ 1400 nm^{-1} of the UVO treated a-Nb_2O_5 thin film suggests that the organic residues can be completely removed by UVO treatment, while the thin film annealed at 300 ºC still showed traces of organic species. Most of the molecular water in a-Nb_2O_5 thin films can be eliminated by annealing at 150 ºC and can be completely removed by annealing above 300 ºC, as seen by the decrease of both -O-H stretching and scissoring peaks in the FTIR spectrum of a-Nb_2O_5 thin films annealed at 150 ºC and the disappearance of them in the FTIR spectrum of a-Nb_2O_5 thin films annealed at 300 ºC. The FTIR results suggested that UVO treatment was associated with the photoactivation processes of the solution derived a-Nb_2O_5 thin films.

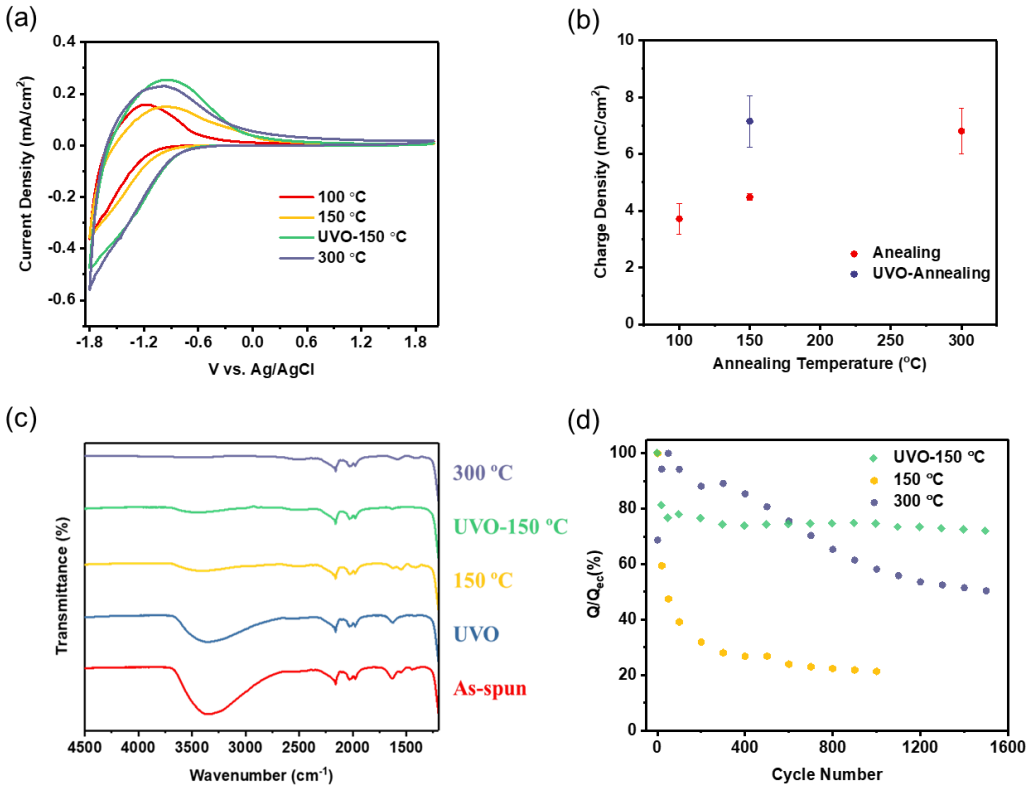

Figure 4.2 (a) Cyclic voltammograms and (b) charge density of UVO-150 °C a-Nb_2O_5 thin films and a-Nb_2O_5 thin films annealed at 100 °C, 150 °C, and 300 °C. (c) FTIR of UVO treated, UVO-150 °C, and as-spun a-Nb_2O_5 thin films and a-Nb_2O_5 thin films annealed at 150 and 300 °C. (d) The percentage of charge density (Q) normalized by the charge density after electrochemical conditioning (Q_{ec}) vs. cycle number of the UVO-150 °C a-Nb_2O_5 thin film and a-Nb_2O_5 thin films annealed at 150 °C and 300 °C.

Under the continuous UV irradiation in an oxygen atmosphere, strong oxidants like ozone or atomic oxygen were generated, and the photolysis of organic residues from ligands and organic solvent led to the formation of free radical species. These highly reactive species promoted the formation of the amorphous metal-oxygen network, resulting in the condensation of the metal oxide thin film.[116,120] As a result, the organic residues-free and densified thin films would have higher homogeneity and reversibility in the redox reactions.[121] AFM studies were performed to investigate the change of the surface morphology and thickness after UVO treatment (Figure 4.4). Compared to the AFM image of the solution-derived a-Nb_2O_5 thin film, the UVO-treated thin film was more granular-like and porous, and thickness decreased from 53.7 ± 5.5 to 39.2 ± 2.7 nm, which confirmed the photoactivation process during the UVO treatment. Following by the low-

temperature (150 ºC) annealing to remove molecular water, UVO-150 ºC a-Nb_2O_5 thin films had a similar reduction onset potential and charge density to the thin films annealed at 300 ºC.

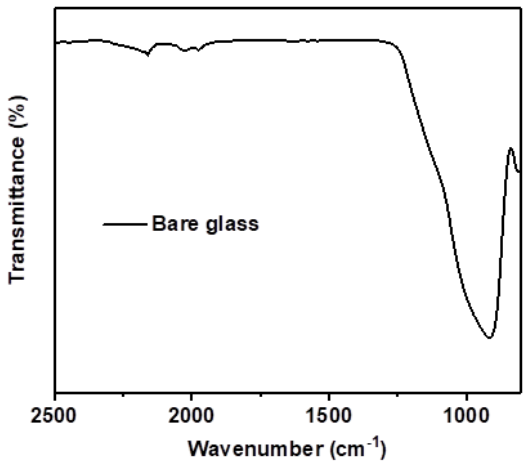

Figure 4.3 FTIR spectrum of a bare glass substrate.

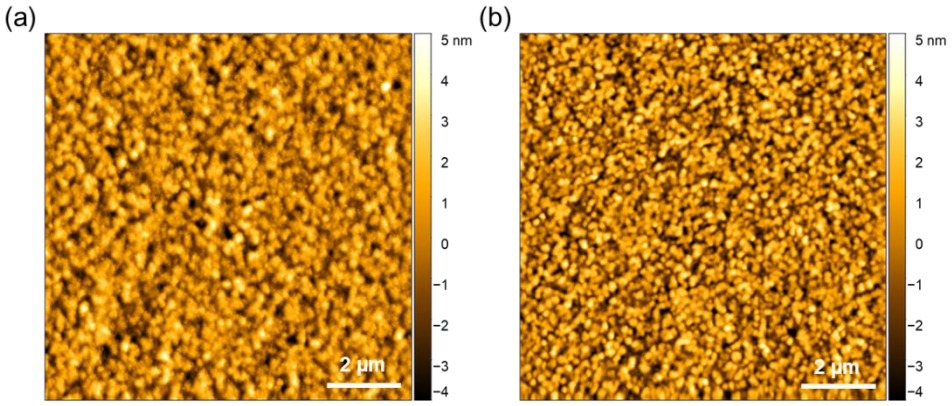

Figure 4.4 AFM images of the a-Nb_2O_5 thin films (a) before and (b) after UVO treatment.

In addition, the effect of organic residues on the electrochemical stability of a-Nb_2O_5 thin films was investigated. a-Nb_2O_5 thin films were cycled by double-potential step chronoamperometry between -1.8 and 2.0 V for a time interval of 20 s. The charge density was calculated using the chronoamperomagram for each cycle and normalized by the charge density after the electrochemical conditioning (Figure 4.2d). The charge density of a-Nb_2O_5 thin film

annealed at 150 ºC lost ~ 80 % after 500 cycles, which suggests that organic residues were detrimental to the electrochemical stability of the a-Nb_2O_5 thin films. In contrast, the UVO-150 ºC a-Nb_2O_5 thin film lost ~ 28 % of its original charge density after 1500 cycles. The remaining charge density was sufficient to balance the charges in the electrochromic layer. Additionally, the a-Nb_2O_5 thin film annealed at 300 ºC showed better cycling stability than the UVO-150 ºC a-Nb_2O_5 thin film during the first 600 cycles but lost ~ 50% of its charge density after 1500 cycles. Therefore, using UVO-150 ºC treatment can induce a more complete formation of metal-oxide bonds resulting in a densified thin-film which has a better electrochemical stability.

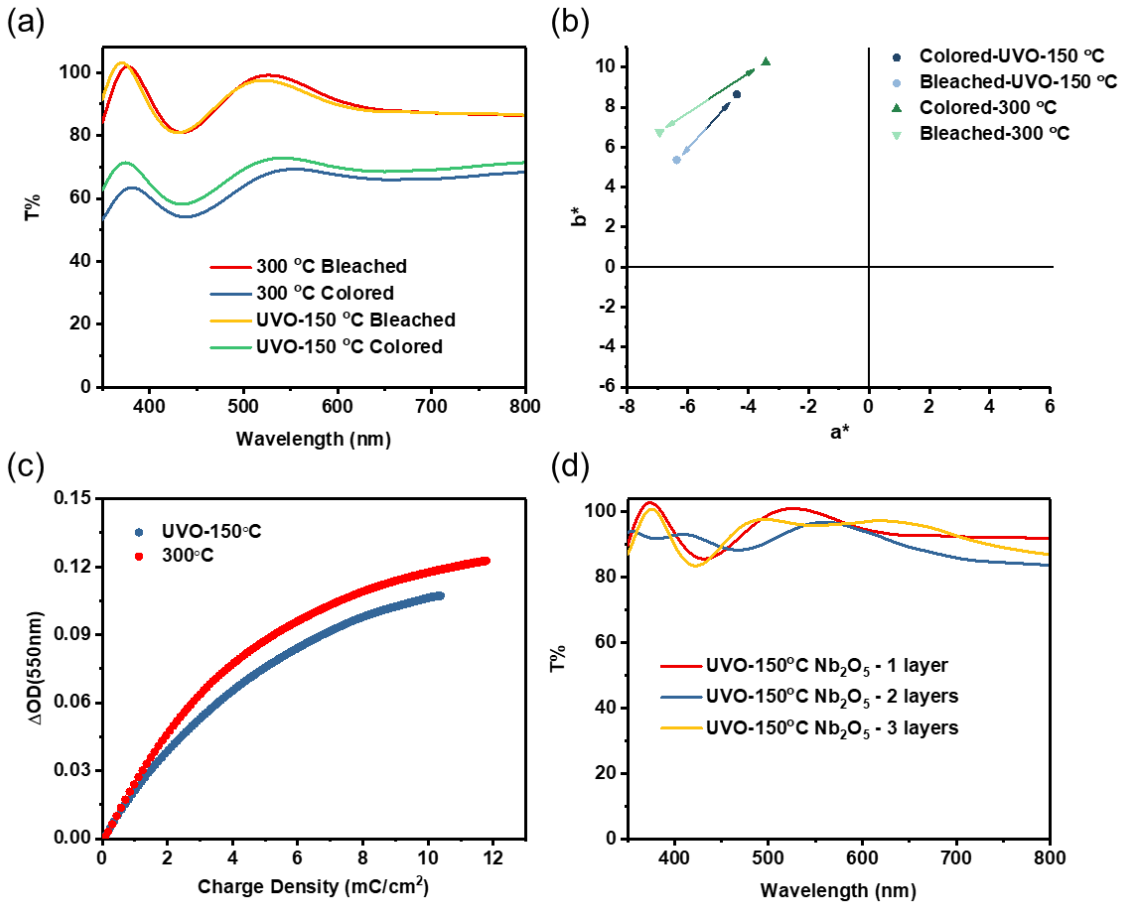

Figure 4.5 (a) UV-visible spectra and (b) colorimetry a*b* (CIE 1976 L*a*b* Color Space) color coordinates of the bleached and colored states a-Nb_2O_5 thin films processed by annealing at 300 °C and UVO-150 °C. (c) Coloration efficiencies of a-Nb_2O_5 thin films processed by annealing at 300 °C and UVO-150 °C. (d) UV-visible spectra of UVO-150 ºC a-Nb_2O_5 thin films with different thickness.

In-situ spectroelectrochemistry was performed to evaluate the hue and transmittance of a-Nb_2O_5 as a MCC-CE material (Figure 4.2a). In the bleached state, the transmittance of both the UVO-150 ºC and 300 ºC-annealed a-Nb_2O_5 thin films are above 85 % for most wavelengths ranging from 350 to 800 nm, except the near-UV region (around 430 nm). Because of the antireflection effect of the a-Nb_2O_5 coating or the smoothing of the ITO/glass substrate, the transmittance is larger than 100 % in wavelengths around 370 nm.[66,122] When a-Nb_2O_5 thin films were reduced at - 1.8 V vs. Ag/AgCl, UVO-150 and 300 ºC-annealed a-Nb_2O_5 thin films presented a light gray color in the colored state while their transmittances remained larger than 60% in most of the visible-light wavelength region. However, because of its charge density being at least 1.4

times higher than p-type ECPs (i.e. ~ 2 - 5 mC cm^{-2}), only part of the capacity will be utilized to balance the charges on the ECPs during color switching.[91] Thus, a-Nb_2O_5 thin films could preserve its high transmission in an ECD. The spectra of a-Nb_2O_5 thin films were used to calculate their L*a*b* color space using the Star-Tek colorimetry software. (Note: the negative and positive a* value correspond to green and red colors, respectively; the negative and positive value of b* are related to blue and yellow colors, respectively; L* represents the lightness (Figure 4.2b). The UVO-150 ºC a-Nb_2O_5 thin film has smaller values of a* and b* than the 300 ºC annealed a-Nb_2O_5 thin film in both colored and bleached states, which suggests that UVO-150 ºC a-Nb_2O_5 thin films have a lower hue. As the CE, UVO-150 ºC a-Nb_2O_5 thin films offer a higher color purity in ECDs. Because only a fraction of the charges would be needed to balance the charge consumption in the ECPs, the coloration efficiency of the a-Nb_2O_5 thin film was calculated from the initial slope of the curve of the change of optical density (ΔOD) versus charge density (Figure 4.2c). The coloration efficiency of UVO-150 ºC a-Nb_2O_5 thin film (16.7 cm^2 C^{-1}) was smaller than that of the a-Nb_2O_5 thin film annealed at 300 ºC (20.7 cm^2 C^{-1}). Compared to a-Nb_2O_5 thin films annealed at 300 °C, UVO-150 ºC a-Nb_2O_5 thin films will have less color change to generate the same amount of charges. The charge density of the UVO-150 ºC a-Nb_2O_5 thin film can be adjusted by changing its thickness (number of coating layers) (Table 4.1). Upon increasing the thickness, the a-Nb_2O_5 thin films remain highly transmissive with a low hue indicated by the high value of L* (> 97.0) and small values of both a* and b* (< 6.0) (Figure 4.2d). Therefore, UVO-150 ºC a-Nb_2O_5 thin films can potentially be paired with a variety of ECPs with different thicknesses in an unbalanced configuration to assemble ECDs that have high optical contrast and color purity. Compared with a-Nb_2O_5 thin films annealed at 300 ºC, UVO-150 ºC a-Nb_2O_5 thin films have a similar charge density, better long-term cycle stability, less color hue, and smaller coloration efficiency. In the following section, UVO-150 ºC a-Nb_2O_5 thin films are demonstrated as MCC-CE material in ECDs.

Table 4.1 Thicknesses, Charge densities and Colorimetry L*a*b* (CIE 1976 L*a*b* Color Space) color coordinates of a-Nb_2O_5 Thin films with Different Thickness Processed by UVO-150 ºC

Number of layers	Thickness/nm	Charge Density/ mC cm^{-2}	L*	a*	b*
1	50.0 ± 9.8	7.2 ± 0.9	99.1	-5.1	5.3
2	82.5 ± 8.4	9.4 ± 0.4	97.8	-1.9	3.3
3	143.2 ± 10.0	13.1 ± 1.7	98.6	-1.3	3.7

Two-electrode liquid cells were assembled to further study the performance of a-Nb_2O_5 thin films as the MCC-CE for ECPs. The WE was an ECP-black coated ITO/glass substrate, the CE was an a-Nb_2O_5-coated ITO/glass substrate, and the electrolyte was 0.2 M LiTFSI in PC. Both WE and CE were electrochemically conditioned by CV cycling prior to the cell assembly. The charge densities of the ECP-black layer and the a-Nb_2O_5 layer were calculated from their CVs to be about 3.0 and 8.0 mC cm^{-2}, respectively. Thus, the two-electrode cell was in an unbalanced electrode configuration (Figure 4.6a). In the spectroelectrochemistry study, the potential of the two-electrode cell was increased from -1.5 V to 2.2 V (Figure 4.6b). The broad absorption in the visible region (350 - 800 nm) was mainly inherited from the ECP-black layer. Broad absorptions in the NIR range ~ 900 nm and beyond 1000 nm are related to polarons and bipolarons, respectively.[25] Upon increasing the potential, the absorption in the visible region decreased; the absorption of polarons first increased and then decreased and the absorption of bipolarons increased dramatically. These results revealed that the a-Nb_2O_5 layer balanced the charges in the ECP-black layer during the color switching in a two-electrode cell. When the cell was oxidized to its bleached state at 2.2 V, the a-Nb_2O_5 CE was taken out to measure transmittance spectrum and compared with its spectroelectrochemistry results (Figure 4.6c). The transmittance spectrum of a-Nb_2O_5 CE in the bleached device was an intermediate between its spectra of the colored and bleached states, which reveals that a-Nb_2O_5 CE was only partially reduced when used as the CE in the two-electrode cell. The partial reduction of the a-Nb_2O_5 thin film was sufficient to balance the charge generated during the oxidation of the ECP-black to a bleached state. Therefore, a-Nb_2O_5 thin films maintained high transmissive and low hue and functioned as the MCC-CE during the switching of the electrochromic cell. Moreover, the composites coloration efficiency of the two-

electrode cell was calculated to be ~ 360.0 mC cm^{-2} at the 95% change in optical contrast (Figure 4.6d).

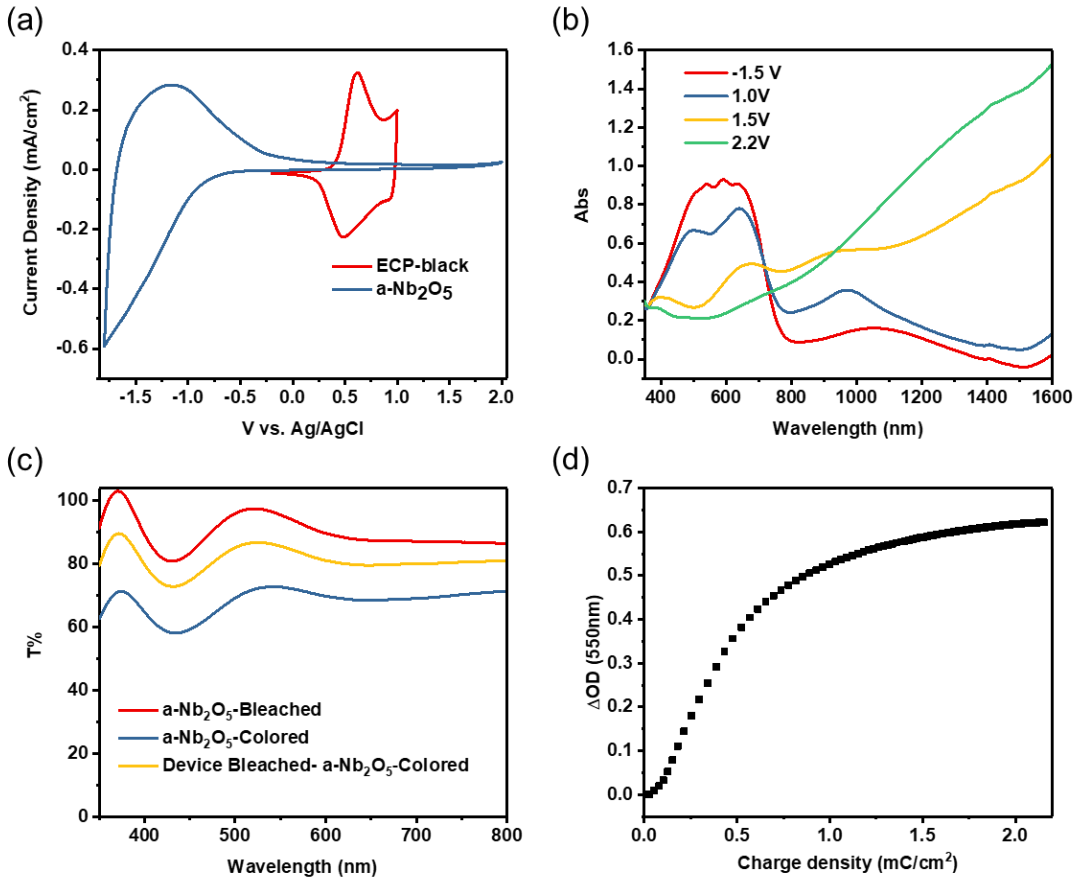

Figure 4.6 (a) Cyclic voltammograms of thin-films of ECP-black and a-Nb_2O_5. (b) Spectroelectrochemistry of the a-Nb_2O_5/ECP-black two-electrode cell. (c) UV-vis spectra of the a-Nb_2O_5 thin film in colored and bleached states and its intermediate state in a bleached a-Nb_2O_5/ECP-black two-electrode cell. (d) Optical density versus charge density of the a-Nb_2O_5/ECP-black two-electrode cell.

In a two-electrode system, the potential distribution on electrodes affects the optical contrast (ΔT%), switching time, coloration efficiency and cycle stability of ECDs.[66] For in-situ measurement of the potential distribution, an Ag/AgCl reference electrode was inserted into the two-electrode cell. When the cell potential (E_{cell}) was applied between the a-Nb_2O_5 CE and ECP-black WE by the potentiostat, the change of the potential distribution on the ECP-black WE (E_{we}) versus Ag/AgCl due to the ions intercalation/de-intercalation was recorded by a Keithley

sourcemeter during the CV and double-potential step chronoabsorptometry (DPSC) experiments (Figure 4.7a). The CV of the two-electrode cell shows a pair of redox peaks at ~ 2.00 and ~ 1.36 V (Figure 4.7b). After electrochemical conditioning of the two-electrode cell, the potential distribution on the E_{we} was measured versus the Ag/AgCl reference electrode during the CV experiments with the E_{cell} at the scan rate of 40 mV s^{-1} (Figure 4.7c). In the forward scan, the E_{we} increased with increasing the E_{cell} from -1.50 to 2.2 V at different rates within different potential windows. In the potential windows (with a red background in Figure 4.7 c) where E_{cell} increased from -1.50 to -0.60 V and from 1.33 to 2.20 V, E_{we} increased at rates of 17.2 and 13.8 mV s^{-1}, respectively. While in the potential window (with a blue background in Figure 4.7c) of E_{cell} from -0.60 to 1.33 V, the E_{we} increased at a relatively slower rate of 4.5 mV s^{-1}. A similar behavior was also observed in the reverse scan of the CV experiments. During the reverse scan, when E_{cell} was scanned from 2.20 to 1.25 V and from -1.00 and 1.50 V, the E_{we} decreased at rates of 12.8 and 34.8 mV s-^{1}, respectively. When the E_{cell} was scanned from 1.20 to -1.00 V, E_{we} reached a plateau at ~ 0.40 V vs. Ag/AgCl. The potential windows where E_{we} responded at a slower rate or reached a plateau suggested that ions cannot intercalate/de-intercalate freely into/from the ECP-black WE. These phenomena could be due to the ion-trapping in the electrochromic layer, which requires an overpotential to overcome the trapping.[90,123–125] In DPSC experiments, the E_{we} was also monitored in-situly using 2.2 and -1.5 V in accordance with the CV and spectroelectrochemistry of the cell (Figure 4.7d). When 2.2 V was applied to the cell, the E_{we} stepped to ~ 0.76 V vs. Ag/AgCl. When the E_{cell} was switched from 2.2 to -1.5 V, the E_{we} quickly changed to -0.68 V vs. Ag/AgCl and gradually increased, stabilizing at -0.15 V vs Ag/AgCl. Both potentials were within the stable electrochromic window of ECP-black (Figure 4.8). Therefore, these conditions were used in the cycling test of solid-state ECDs.

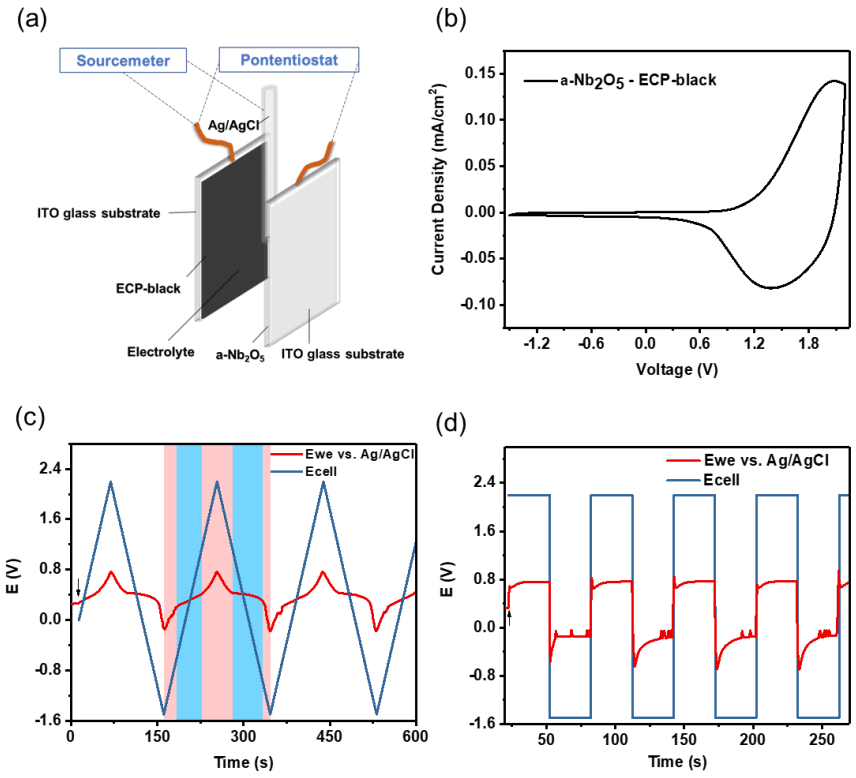

Figure 4.7 (a) The scheme of the a-Nb_2O_5/ECP-black two-electrode cell with a sourcemeter to monitor the potential at the ECP-black WE vs. an Ag/AgCl reference electrode. (b) Cyclic voltammogram of the a-Nb_2O_5/ECP-black two-electrode cell. Change of the potential at the ECP-black WE during the (c) CV experiments and (d) DPSC experiments of the a-Nb_2O_5/ECP-black two-electrode cell. (Note: the potential windows where E_{we} increased quickly have a red background, while the potential windows where E_{we} increased at a slow rate or reached a plateau have a blue background. The black arrows indicated the beginning of the potential measurements)

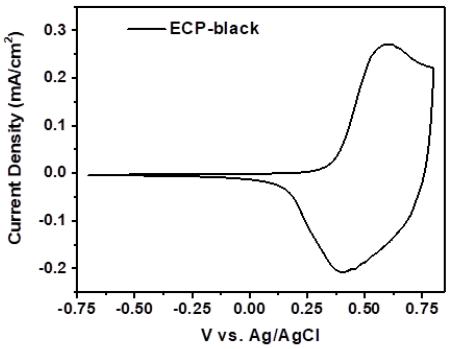

Figure 4.8 Cyclic voltammogram of the ECP-black in 0.2 M LiTFSI PC.

A simple fabrication route is vital to lower the production cost. Thus, the performance of the a-Nb_2O_5 electrode without any pretreatment and electrochemical conditioning was used in the two-electrode solid-state devices. The two-electrode solid state device was assembled by using a-Nb_2O_5-coated ITO/glass as the CE electrode, the ECP-black-coated ITO/glass as the WE, and PEGDA plasticized by 50 % of the 0.2 M LiTFSI in PC as the gel electrolyte. Because reaching E_{we} equilibrium in the coloring process is slower than the bleaching process, the device was kept at a constant potential of 2.2 V for 15 s and -1.5 V for 30 s to achieve complete color change (Figure 4.7d). The device showed a $\Delta T\%$ of ~ 45% and was stable up to 3100 cycles with ~ 1.4 % decreases of $\Delta T\%$ (Figure 4.9a, b). The time to achieve 95 % of its full $\Delta T\%$ is 3.4 and 5.6 s for bleaching and coloring, respectively (Figure 4.9b). The composite coloration efficiency at 95% of the optical contrast ($\eta_{95\%}$) of the solid-state a-Nb_2O_5/ECP-black ECD was ~ 393.3 $cm^2\ C^{-1}$ (Figure 4.10).

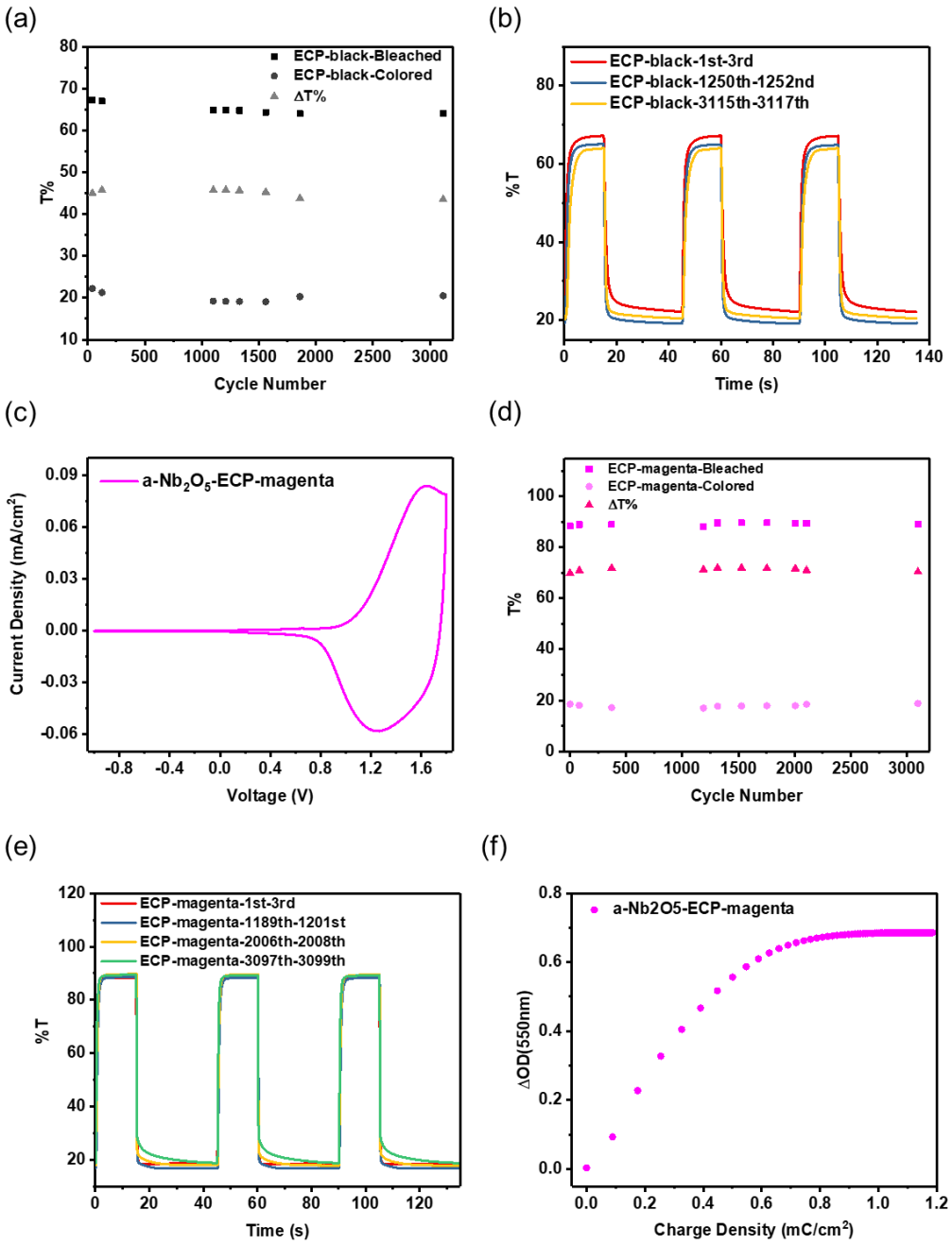

Figure 4.9 (a) Summary of the transmittance at 550 nm in the bleached and colored state and optical contrast of the a-Nb_2O_5/ECP-black ECD at different cycles. (b) DPSC of the a-Nb_2O_5/ECP-black ECD monitored at 550 nm at different cycles. (c) Cyclic voltammogram of the a-Nb_2O_5/ECP-magenta ECD. (d) Summary of the transmittance at 550 nm in the bleached and colored states and optical contrast of the a-Nb_2O_5/ECP-magenta ECD at different cycles. (e) DPSC of the a-Nb_2O_5/ECP-magenta ECD monitored at 550 nm at different cycles. (f) Change of optical density versus the charge density of the a-Nb_2O_5/ECP-magenta ECD.

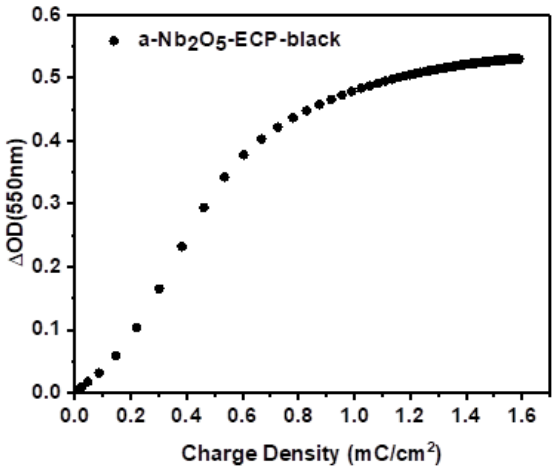

Figure 4.10 The change of optical density versus the charge density of the a-Nb_2O_5/ECP-black ECD.

To extend the scope of this study, the device was also assembled using ECP-magenta as the WE. The ECP-magenta thin film had a charge density of ~ 1.8 mC cm^{-2} and was paired with the a-Nb_2O_5 MCC-CE with a charge density of ~ 7.2 ± 0.9 mC cm^{-2} to construct an ECD in an unbalanced configuration. The CV result of the ECD showed a pair of redox peaks at ~ 1.63 and ~ 1.25 V (Figure 4.9c). Potentials of 1.8 and -1.5 V were used to switch the device during the DPSC cycling test and no side reactions within this electrochemical window were observed from the cyclic voltammogram of the a-Nb_2O_5/ECP-magenta two-electrode cell. (Figure 4.11) The device can achieve ΔT% of 70% in the first cycle and was able to maintain nearly the same contrast in the following 3100 cycles (Figure 4.9d, e). The bleaching and coloring times to achieve 95 % of its ΔT% are 1.6 and 0.5 s, respectively (Figure 4.9e). After 3100 cycles, the coloring time increased to 4.8 s, while the bleaching time (~ 1.0 s) remained similar to the 1st cycle (Figure 4.9e). At last, the $\eta_{95\%}$ of the a-Nb_2O_5/ECP-magenta was calculated to be ~ 849.5 mC cm^{-2} (Figure 4.9f). The high CCE suggests that the ECD can achieve a high contrast by consuming a very small amount of charges. By using a-Nb_2O_5 as the CE materials to balance the charges consumption in electrochromic layers, ECDs of both ECP-black and ECP-magenta showed outstanding cycling stability in double-potential cycling experiments.

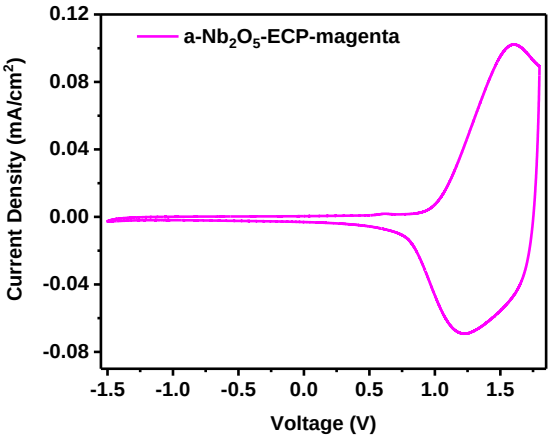

Figure 4.11. Cyclic voltammogram of the a-Nb_2O_5/ECP-magenta two-electrode cell in 0.2 M LiTFSI PC.

Low-temperature (< 150 ºC) solution processing that is compatible with flexible substrates is the key for large-scale, high-throughput roll-to-roll processing. Thus, a UVO-150 ºC a-Nb_2O_5 thin film was fabricated on the ITO/PET substrates with high uniformity and transparency (Figure 4.12a). The as-assembled flexible device had a ΔT% of 62 % at 550nm (Figure 4.12b). The lower contrast of the flexible device could be due to the higher sheet resistance of ITO/PET substrates (~ 200 Ω/sq) than the ITO/glass substrates (~ 8 – 12 Ω/sq). With the demonstration of the flexible ECD, it is evident that the high-performance a-Nb_2O_5 can be fabricated on flexible substrates and serves as the CE for solution-processed low-cost ECDs.

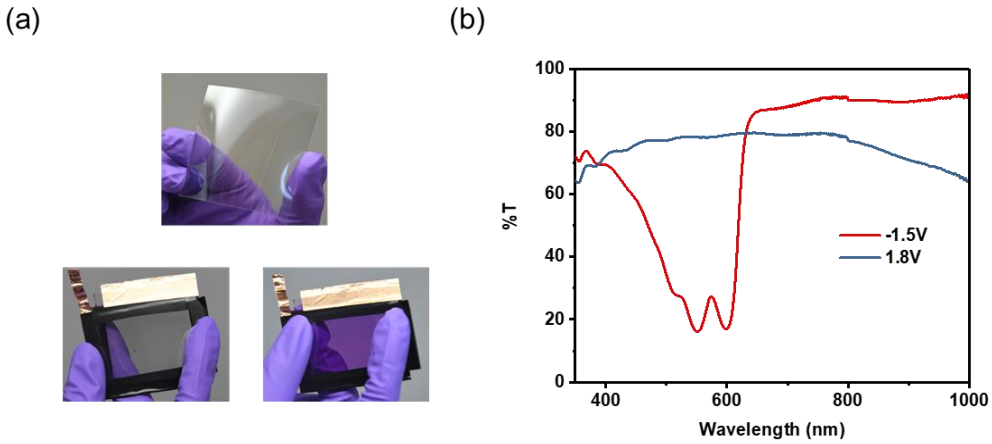

Figure 4.12 (a) Photographs of a UVO-150 ºC a-Nb_2O_5 thin film on ITO/PET substrate and the flexible device of a-Nb_2O_5/ECP-magenta in bleached and colored states. (b) Spectroelectrochemistry of the a-Nb_2O_5/ECP-magenta flexible device.

4.5 Conclusions

In summary, solution-processed UVO-150 ºC a-Nb_2O_5 thin films can achieve a similar charge density as that of a-Nb_2O_5 thin films annealed at 300 ºC, yet with an improved cycling stability. Because UVO-150 ºC a-Nb_2O_5 thin films have a much higher charge density and lower coloration efficiency than ECPs, they were applied as the MCC-CE material to pair with p-type cathodically coloring ECPs. Both a-Nb_2O_5/ECP-black and a-Nb_2O_5/ECP-magenta solid-state ECDs showed a high contrast, fast switching time, high coloration efficiency and stable cycling performance. With the development of reliable highly transparent CE materials that can be solution processed on flexible substrates, we believe it can benefit the development of the future roll-to-roll manufacturing electrochromic technology.

4.6 Acknowledgements

The authors would like to acknowledge Ambilight Inc for the financial support.

CHAPTER 5. CONLUSIONS AND FUTURE PERSPECTIVES OF ELECTROCHROMIC DEVICES

A tremendous effort has been devoted to developing new electrochromic materials while other trivial but vital technique hurdles that are overlooked by researchers. In this section, we summarized our works and a few of the key problems are outlined.

5.1 Conclusions

Our efforts have been devoted to study the low-cost and stable ECDs. First, we have understood ion behaviors in ECPs under the open-circuit condition. Commonly, the small molecules based-electrochromic materials can be re-dissolved in the electrolytes and automatically go through charge transfer with the charge balancing materials in the electrolyte leading to a self-bleaching phenomenon. In our work, we found that self-bleaching behaviors are also existing in the conjugated polymer based-electrochromic materials that have no dissolution issues in electrolytes, whereas the ions tend to re-enter the films driven by the morphology and energy level of ECPs thin films resulting in this phenomenon. The understanding of the self-bleaching behaviors of ECPs gives us a guideline on designing the logic control in the application of smart windows. Instead of applying a constant potential to maintain the transmissive state of EC layer, potential pulses with a certain frequency can be programmed to control the window in a certain transmissive state, so that the energy-saving efficiency can be further increased without compromising the EC functions.

Moreover, we studied solution processable ion storage layers that balance the charges consumed in the EC layer in the ECDs. Many materials are evaluated based on results of either the three-electrode electrochemical cell or ECDs that used the bare ITO as the counter electrode. The stability and performance of ECDs cannot be guaranteed without using the ion storage layer to balance the charges in the electrochromic layer. Developing new ion storage layers that can be solution-processed in a low-temperature are still significant to spur the commercialization of ECDs.

5.2 Thermal and Photostability of organic materials in ECDs

In ECPs based-multilayer ECDs, there are four interfaces namely ITO and EC layer, electrochromic materials and electrolyte, electrolyte and IS layer, and IS layer and ITO. Physical absorption is the domain force for the interface stability at the ITO/EC layer and ITO/IS layer interfaces. The difference of their thermal expansion coefficient cause delamination issues upon heating and cooling cycles test.[14] Moreover, the adhesive properties of the electrolyte used in the ECDs also need to be considered under the thermal stress, which often time needs to comprise the ionic conductivity. When the EC and IS layers are charged, their physical properties are also changed tremendously. As a result, they interact differently with the electrolyte. We envision to perform a systematic study on interfaces and interfaces engineering to investigate these issues, which is critical to fabricate long-term stable ECDs.

Up till now, the commercialized dynamic smart windows are mainly based on the inorganic electrochromic materials. One of the biggest concerns to use organic ECPs is their photostability. With the presence of oxygen and moisture, the α-protons abstraction of alkyl side chains on the ECPs will happen and generate radicals which will further attack the conjugated backbone of ECPs leading to the failure of electrochromic performance.[126] A study showed that by replacing the alkyl side chains with the aromaticoxy-alkyl chains of the conjugated materials can suppress the hydrogen abstraction resulting in improving their photostability.[127] Further understanding on the degradation mechanism of the ECPs under the stimulus of photons will shine line on the design of new ECPs.

5.3 Ion-trapping behaviors in ECDs

In the operation of the ECDs, the electrochemical doping involves the reduction of the cathode materials in the counter electrode and oxidation of the anode materials in the working electrode. When the excess charge carriers are formed, the anions and cations in the electrolyte will intercalate into electrodes to maintain the overall charge neutrality. Thus, the reversibility of ions intercalation/de-intercalation is the key for the long lifespan of the ECDs. Few factors that are related to the reversibility of intercalation/de-intercalation of organic electrochromic materials have been revealed. Ho *et al* studied the effect of the thin-film morphology of the poly(3,4-alkylenedioxythiophene) (PXDOT) derivatives.[125] The bulky substitutions leading to a more

porous macroscopy morphology of the electrodeposited PXDOT thin films resulting in less degree of ion trapping during the cycling. Xu *et al* found that the ion-trapping is related to the interaction between ions and Poly(3,4-(2,2-dimethylpropylenedioxy) thiophene) (PProDot-Me_2).[124] By using less applied voltage, shorter the period of the applied voltage, and lower salt concentration, the lifetime of the PProdot-Me_2 can be improved. However, this also leads to the poor optical contrast of the electrochromic materials. As for the inorganic materials, Wen et al discussed the lithium-ion trapping in amorphous WO_3 and proposed to use constant-current-driven de-trapping to regenerate the electrochromic properties.[90,128,129] Although some insights have been provided, most of these studies are based on the results of a three-electrode set-up which is not practically used. Recently, Barnabé et al[130] and Diao et al[131] proposed the ion-trapping failure mechanism in the monolithic inorganic electrochromic device of WO_3//NiO. The ion-trapping phenomena were observed in both NiO and WO_3 layers by using Raman spectroscopy, XPS, and SIMS. When it comes to the organic-based ECDs, a lot of fundamental questions has remained puzzled.

The reversibility of the ions' intercalation in an ECDs will change dramatically compared to the individual electrode in the three-electrode set-up. Cations and anions intercalation behavior are very different due to their different diffusion rate, intercalation process, and hydrodynamic size. Thus, under the applied potential, the separation and distribution of anions and cations, the degree of their intercalation (the doping state) will lead to the final failure of the electrode which eventually leads to the failure of ECDs. More insights are needed to understand the behaviors of ions in the ECP based-ECDs.

REFERENCES

(1) Cao, X.; Dai, X.; Liu, J. Building Energy-Consumption Status Worldwide and the State-of-the-Art Technologies for Zero-Energy Buildings during the Past Decade. *Energy Build.* **2016**, *128*, 198–213.

(2) Granqvist, C. G.; Arvizu, M. A.; Bayrak Pehlivan, İ.; Qu, H.-Y.; Wen, R.-T.; Niklasson, G. A. Electrochromic Materials and Devices for Energy Efficiency and Human Comfort in Buildings: A Critical Review. *Electrochim. Acta* **2018**, *259*, 1170–1182.

(3) Cannavale, A.; Martellotta, F.; Cossari, P.; Gigli, G.; Ayr, U. Energy Savings Due to Building Integration of Innovative Solid-State Electrochromic Devices. *Appl. Energy* **2018**, *225*, 975–985.

(4) Gillaspie, D. T.; Tenent, R. C.; Dillon, A. C. Metal-Oxide Films for Electrochromic Applications: Present Technology and Future Directions. *J. Mater. Chem.* **2010**, *20* (43), 9585–9592.

(5) Mortimer, R. J. Electrochromic Materials. *Chem. Soc. Rev.* **1997**, *26* (3), 147–156.

(6) Kao, S.-Y.; Lu, H.-C.; Kung, C.-W.; Chen, H.-W.; Chang, T.-H.; Ho, K.-C. Thermally Cured Dual Functional Viologen-Based All-in-One Electrochromic Devices with Panchromatic Modulation. *ACS Appl. Mater. Interfaces* **2016**, *8* (6), 4175–4184.

(7) Moon, H. C.; Lodge, T. P.; Frisbie, C. D. Solution Processable, Electrochromic Ion Gels for Sub-1 V, Flexible Displays on Plastic. *Chem. Mater.* **2015**, *27* (4), 1420–1425.

(8) Cao, X.; Lau, C.; Liu, Y.; Wu, F.; Gui, H.; Liu, Q.; Ma, Y.; Wan, H.; Amer, M. R.; Zhou, C. Fully Screen-Printed, Large-Area, and Flexible Active-Matrix Electrochromic Displays Using Carbon Nanotube Thin-Film Transistors. *ACS Nano* **2016**, *10* (11), 9816–9822.

(9) Argun, A. A.; Reynolds, J. R. Line Patterning for Flexible and Laterally Configured Electrochromic Devices. *J. Mater. Chem.* **2005**, *15* (18), 1793–1800.

(10) Song, X.; Dong, G.; Gao, F.; Xiao, Y.; Liu, Q.; Diao, X. Properties of NiO_x and Its Influence upon All-Thin-Film ITO/NiO_x/$LiTaO_3$/WO_3/ITO Electrochromic Devices Prepared by Magnetron Sputtering. *Vacuum* **2015**, *111*, 48–54.

(11) Widjaja, E. J.; Delporte, G.; Vandevelde, F.; Vanterwyngen, B. Progress toward Roll-to-Roll Processing of Inorganic Monolithic Electrochromic Devices on Polymeric Substrates. *Sol. Energy Mater. Sol. Cells* **2008**, *92* (2), 97–100.

(12) Amb, C. M.; Dyer, A. L.; Reynolds, J. R. Navigating the Color Palette of Solution-Processable Electrochromic Polymers. *Chem. Mater.* **2011**, *23* (3), 397–415.

(13) Beaujuge, P. M.; Reynolds, J. R. Color Control in π-Conjugated Organic Polymers for Use in Electrochromic Devices. *Chem. Rev.* **2010**, *110* (1), 268–320.

(14) Li, X.; Perera, K.; He, J.; Gumyusenge, A.; Mei, J. Solution-Processable Electrochromic Materials and Devices: Roadblocks and Strategies towards Large-Scale Applications. *J. Mater. Chem. C* **2019**.

(15) Ma, D.; Shi, G.; Wang, H.; Zhang, Q.; Li, Y. Hierarchical NiO Microflake Films with High Coloration Efficiency, Cyclic Stability and Low Power Consumption for Applications in a Complementary Electrochromic Device. *Nanoscale* **2013**, *5* (11), 4808–4815.

(16) Wang, S.; Li, F.; Easley, A. D.; Lutkenhaus, J. L. Real-Time Insight into the Doping Mechanism of Redox-Active Organic Radical Polymers. *Nat. Mater.* **2019**, *18* (1), 69–75.

(17) Sönmez, G.; Schwendeman, I.; Schottland, P.; Zong, K.; Reynolds, J. R. N-Substituted Poly(3,4-Propylenedioxypyrrole)s: High Gap and Low Redox Potential Switching Electroactive and Electrochromic Polymers. *Macromolecules* **2003**, *36* (3), 639–647.

(18) Thakur, V. K.; Ding, G.; Ma, J.; Lee, P. S.; Lu, X. Hybrid Materials and Polymer Electrolytes for Electrochromic Device Applications. *Adv. Mater.* **2012**, *24* (30), 4071–4096.

(19) Bange, K.; Gambke, T. Electrochromic Materials for Optical Switching Devices. *Adv. Mater.* **1990**, *2* (1), 10–16.

(20) Mortimer, R. J. Organic Electrochromic Materials. *Electrochim. Acta* **1999**, *44* (18), 2971–2981.

(21) Wang, J.; Zhang, L.; Yu, L.; Jiao, Z.; Xie, H.; Lou, X. W. (David); Wei Sun, X. A Bi-Functional Device for Self-Powered Electrochromic Window and Self-Rechargeable Transparent Battery Applications. *Nat. Commun.* **2014**, *5*, 4921.

(22) Thakur, V. K.; Ding, G.; Ma, J.; Lee, P. S.; Lu, X. Hybrid Materials and Polymer Electrolytes for Electrochromic Device Applications. *Adv. Mater.* **2012**, *24* (30), 4071–4096.

(23) Otley, M. T.; Alamer, F. A.; Zhu, Y.; Singhaviranon, A.; Zhang, X.; Li, M.; Kumar, A.; Sotzing, G. A. Acrylated Poly(3,4-Propylenedioxythiophene) for Enhancement of Lifetime and Optical Properties for Single-Layer Electrochromic Devices. *ACS Appl. Mater. Interfaces* **2014**, *6* (3), 1734–1739.

(24) Lu, Y.; Liu, L.; Foo, W.; Magdassi, S.; Mandler, D.; Lee, P. S. Self-Assembled Polymer Layers of Linear Polyethylenimine for Enhancing Electrochromic Cycling Stability. *J. Mater. Chem. C* **2013**, *1* (23), 3651–3654.

(25) Bulloch, R. H.; Reynolds, J. R. Photostability in Dioxyheterocycle Electrochromic Polymers. *J. Mater. Chem. C* **2016**, *4* (3), 603–610.

(26) Shin, H.; Seo, S.; Park, C.; Na, J.; Han, M.; Kim, E. Energy Saving Electrochromic Windows from Bistable Low-HOMO Level Conjugated Polymers. *Energy Environ. Sci.* **2016**, *9* (1), 117–122.

(27) Dussault, J.-M.; Sourbron, M.; Gosselin, L. Reduced Energy Consumption and Enhanced Comfort with Smart Windows: Comparison between Quasi-Optimal, Predictive and Rule-Based Control Strategies. *Energy Build.* **2016**, *127*, 680–691.

(28) Tavares, P.; Bernardo, H.; Gaspar, A.; Martins, A. Control Criteria of Electrochromic Glasses for Energy Savings in Mediterranean Buildings Refurbishment. *Sol. Energy* **2016**, *134*, 236–250.

(29) Otero, T. F.; Grande, H.; Rodríguez, J. A New Model for Electrochemical Oxidation of Polypyrrole under Conformational Relaxation Control. *J. Electroanal. Chem.* **1995**, *394* (1), 211–216.

(30) Otero, T. F.; Boyano, I. Comparative Study of Conducting Polymers by the ESCR Model. *J. Phys. Chem. B* **2003**, *107* (28), 6730–6738.

(31) Odin, C.; Nechtschein, M. On the Kinetics of Electrochemical Doping in Conducting Polymers: Experimental Characterization. *Synth. Met.* **1993**, *55* (2–3), 1281–1286.

(32) Odin, C.; Nechtschein, M. Slow Relaxation in Conducting Polymers. *Phys. Rev. Lett.* **1991**, *67* (9), 1114–1117.

(33) Grande, H.; Otero, T. F. Conformational Movements Explain Logarithmic Relaxation in Conducting Polymers. *Electrochim. Acta* **1999**, *44* (12), 1893–1900.

(34) Shi, P.; Amb, C. M.; Knott, E. P.; Thompson, E. J.; Liu, D. Y.; Mei, J.; Dyer, A. L.; Reynolds, J. R. Broadly Absorbing Black to Transmissive Switching Electrochromic Polymers. *Adv. Mater.* **2010**, *22* (44), 4949–4953.

(35) Beaujuge, P. M.; Ellinger, S.; Reynolds, J. R. The Donor-Acceptor Approach Allows a Black-to-Transmissive Switching Polymeric Electrochrome. *Nat Mater* **2008**, *7* (10), 795–799.

(36) Amb, C. M.; Beaujuge, P. M.; Reynolds, J. R. Spray-Processable Blue-to-Highly Transmissive Switching Polymer Electrochromes via the Donor–Acceptor Approach. *Adv. Mater.* **2010**, *22* (6), 724–728.

(37) Smela, E.; Gadegaard, N. Surprising Volume Change in PPy(DBS): An Atomic Force Microscopy Study. *Adv. Mater.* **1999**, *11* (11), 953–957.

(38) Wang, X.; Shapiro, B.; Smela, E. Visualizing Ion Currents in Conjugated Polymers. *Adv. Mater.* **2004**, *16* (18), 1605–1609.

(39) Mo, M.; Zhao, W.; Chen, Z.; Yu, Q.; Zeng, Z.; Wu, X.; Xue, Q. Excellent Tribological and Anti-Corrosion Performance of Polyurethane Composite Coatings Reinforced with Functionalized Graphene and Graphene Oxide Nanosheets. *RSC Adv.* **2015**, *5* (70), 56486–56497.

(40) Hernandez, S.; Hidalgo, D.; Sacco, A.; Chiodoni, A.; Lamberti, A.; Cauda, V.; Tresso, E.; Saracco, G. Comparison of Photocatalytic and Transport Properties of TiO_2 and ZnO Nanostructures for Solar-Driven Water Splitting. *Phys. Chem. Chem. Phys.* **2015**, *17* (12), 7775–7786.

(41) Zhang, Z. X. and X. L. and W. W. and C. L. and Z. L. and Z. Enhanced Photoelectrochemical Properties of TiO_2 Nanorod Arrays Decorated with CdS Nanoparticles. *Sci. Technol. Adv. Mater.* **2014**, *15* (5), 55006.

(42) Wang, H.; Wang, B.; Yu, J.; Hu, Y.; Xia, C.; Zhang, J.; Liu, R. Significant Enhancement of Power Conversion Efficiency for Dye Sensitized Solar Cell Using 1D/3D Network Nanostructures as Photoanodes. *Sci. Rep.* **2015**, *5*, 9305.

(43) Wang, J. Z.; Xu, C. H.; Cao, W.; He, Y. Electrochemical Impedance Characterization of Porous Aluminum Oxide after Different Stages of Two-Step Anodization. *Adv. Mater. Res.* **2014**, *953–954*, 1282–1285.

(44) Chidichimo, G.; De Simone, B. C.; Imbardelli, D.; De Benedittis, M.; Barberio, M.; Ricciardi, L.; Beneduci, A. Influence of Oxygen Impurities on the Electrochromic Response of Viologen-Based Plastic Films. *J. Phys. Chem. C* **2014**, *118* (25), 13484–13492.

(45) Lin, Y. Y.; Gundlach, D. J.; Nelson, S. F.; Jackson, T. N. Stacked Pentacene Layer Organic Thin-Film Transistors with Improved Characteristics. *IEEE Electron Device Letters*. 1997, pp 606–608.

(46) Shtein, M.; Mapel, J.; Benziger, J. B.; Forrest, S. R. Effects of Film Morphology and Gate Dielectric Surface Preparation on the Electrical Characteristics of Organic-Vapor-Phase-Deposited Pentacene Thin-Film Transistors. *Appl. Phys. Lett.* **2002**, *81* (2), 268–270.

(47) Yun, D.-J.; Lee, D.-K.; Jeon, H.-K.; Rhee, S.-W. Contact Resistance between Pentacene and Indium–tin Oxide (ITO) Electrode with Surface Treatment. *Org. Electron.* **2007**, *8* (6), 690–694.

(48) Muthurasu, A.; Ganesh, V. Electrochemical Characterization of Self-Assembled Monolayers (SAMs) of Silanes on Indium Tin Oxide (ITO) Electrodes – Tuning Electron Transfer Behaviour across Electrode–electrolyte Interface. *J. Colloid Interface Sci.* **2012**, *374* (1), 241–249.

(49) Uehara, T. M.; de Aguiar, H. B.; Bergamaski, K.; Miranda, P. B. Adsorption of Alkylthiol Self-Assembled Monolayers on Gold and the Effect of Substrate Roughness: A Comparative Study Using Scanning Tunneling Microscopy, Cyclic Voltammetry, Second-Harmonic Generation, and Sum-Frequency Generation. *J. Phys. Chem. C* **2014**, *118* (35), 20374–20382.

(50) Janek, R. P.; Fawcett, W. R.; Ulman, A. Impedance Spectroscopy of Self-Assembled Monolayers on Au(111): Sodium Ferrocyanide Charge Transfer at Modified Electrodes. *Langmuir* **1998**, *14* (11), 3011–3018.

(51) Sugiyama, K.; Ishii, H.; Ouchi, Y.; Seki, K. Dependence of Indium–tin–oxide Work Function on Surface Cleaning Method as Studied by Ultraviolet and X-Ray Photoemission Spectroscopies. *J. Appl. Phys.* **1999**, *87* (1), 295–298.

(52) Herzer, N.; Wienk, M. M.; Schmit, P.; Spoelstra, A. B.; Hendriks, C. E.; Oosterhout, S. D.; Hoeppener, S.; Schubert, U. S. Fabrication of PEDOT-OTS-Patterned ITO Substrates. *J. Mater. Chem.* **2010**, *20* (32), 6618–6621.

(53) Heinze, J.; Frontana-Uribe, B. A.; Ludwigs, S. Electrochemistry of Conducting Polymers—Persistent Models and New Concepts. *Chem. Rev.* **2010**, *110* (8), 4724–4771.

(54) Otero, T. F.; Grande, H.; Rodríguez, J. Reversible Electrochemical Reactions in Conducting Polymers: A Molecular Approach to Artificial Muscles. *J. Phys. Org. Chem.* **1996**, *9* (6), 381–386.

(55) Braun, S.; Salaneck, W. R.; Fahlman, M. Energy-Level Alignment at Organic/Metal and Organic/Organic Interfaces. *Adv. Mater.* **2009**, *21* (14–15), 1450–1472.

(56) Ishii, H.; Sugiyama, K.; Ito, E.; Seki, K. Energy Level Alignment and Interfacial Electronic Structures at Organic/Metal and Organic/Organic Interfaces. *Adv. Mater.* **1999**, *11* (8), 605–625.

(57) Shi, P.; Amb, C. M.; Knott, E. P.; Thompson, E. J.; Liu, D. Y.; Mei, J.; Dyer, A. L.; Reynolds, J. R. Broadly Absorbing Black to Transmissive Switching Electrochromic Polymers. *Adv. Mater.* **2010**, *22* (44), 4949–4953.

(58) Estrada, L. A.; Deininger, J. J.; Kamenov, G. D.; Reynolds, J. R. Direct (Hetero)Arylation Polymerization: An Effective Route to 3,4-Propylenedioxythiophene-Based Polymers with Low Residual Metal Content. *ACS Macro Lett.* **2013**, *2* (10), 869–873.

(59) da Silva, E. T. S. G.; Miserere, S.; Kubota, L. T.; Merkoçi, A. Simple On-Plastic/Paper Inkjet-Printed Solid-State Ag/AgCl Pseudoreference Electrode. *Anal. Chem.* **2014**, *86* (21), 10531–10534.

(60) Lim, J. Y.; Ko, H. C.; Lee, H. Systematic Prediction of Maximum Electrochromic Contrast of an Electrochromic Material. *Synth. Met.* **2005**, *155* (3), 595–598.

(61) Padilla, J.; Seshadri, V.; Sotzing, G. A.; Otero, T. F. Maximum Contrast from an Electrochromic Material. *Electrochem. commun.* **2007**, *9* (8), 1931–1935.

(62) Padilla, J.; Österholm, A. M.; Dyer, A. L.; Reynolds, J. R. Process Controlled Performance for Soluble Electrochromic Polymers. *Sol. Energy Mater. Sol. Cells* **2015**, *140*, 54–60.

(63) Lampert, C. M. Electrochromic Materials and Devices for Energy Efficient Windows. *Sol. Energy Mater.* **1984**, *11* (1), 1–27.

(64) Eric Shen, D.; Osterholm, A. M.; Reynolds, J. R. Out of Sight but Not out of Mind: The Role of Counter Electrodes in Polymer-Based Solid-State Electrochromic Devices. *J. Mater. Chem. C* **2015**, *3* (37), 9715–9725.

(65) Padilla, J.; Seshadri, V.; Sotzing, G. A.; Otero, T. F. Maximum Contrast from an Electrochromic Material. *Electrochem. commun.* **2007**, *9* (8), 1931–1935.

(66) Kim, Y.; Shin, H.; Han, M.; Seo, S.; Lee, W.; Na, J.; Park, C.; Kim, E. Energy Saving Electrochromic Polymer Windows with a Highly Transparent Charge-Balancing Layer. *Adv. Funct. Mater.* **2017**, *27* (31), 1701192.

(67) Reichman, B.; Bard, A. J. The Electrochromic Process at WO_3 Electrodes Prepared by Vacuum Evaporation and Anodic Oxidation of W. *J. Electrochem. Soc.* **1979**, *126* (4), 583–591.

(68) Lee, S.-H.; Deshpande, R.; Parilla, P. A.; Jones, K. M.; To, B.; Mahan, A. H.; Dillon, A. C. Crystalline WO_3 Nanoparticles for Highly Improved Electrochromic Applications. *Adv. Mater.* **2006**, *18* (6), 763–766.

(69) Natarajan, C.; Nogami, G. Cathodic Electrodeposition of Nanocrystalline Titanium Dioxide Thin Films. *J. Electrochem. Soc.* **1996**, *143* (5), 1547–1550.

(70) Knott, E. P.; Craig, M. R.; Liu, D. Y.; Babiarz, J. E.; Dyer, A. L.; Reynolds, J. R. A Minimally Coloured Dioxypyrrole Polymer as a Counter Electrode Material in Polymeric Electrochromic Window Devices. *J. Mater. Chem.* **2012**, *22* (11), 4953–4962.

(71) Suga, T.; Sugita, S.; Ohshiro, H.; Oyaizu, K.; Nishide, H. P- and n-Type Bipolar Redox-Active Radical Polymer: Toward Totally Organic Polymer-Based Rechargeable Devices with Variable Configuration. *Adv. Mater.* **2011**, *23* (6), 751–754.

(72) Suga, T.; Ohshiro, H.; Sugita, S.; Oyaizu, K.; Nishide, H. Emerging N-Type Redox-Active Radical Polymer for a Totally Organic Polymer-Based Rechargeable Battery. *Adv. Mater.* **2009**, *21* (16), 1627–1630.

(73) Janoschka, T.; Hager, M. D.; Schubert, U. S. Powering up the Future: Radical Polymers for Battery Applications. *Adv. Mater.* **2012**, *24* (48), 6397–6409.

(74) Nishide, H.; Iwasa, S.; Pu, Y.-J.; Suga, T.; Nakahara, K.; Satoh, M. Organic Radical Battery: Nitroxide Polymers as a Cathode-Active Material. *Electrochim. Acta* **2004**, *50* (2), 827–831.

(75) Mukherjee, S.; Boudouris, B. W. Applications of Radical Polymers in Solid-State Devices BT - Organic Radical Polymers: New Avenues in Organic Electronics; Mukherjee, S., Boudouris, B. W., Eds.; Springer International Publishing: Cham, 2017; pp 57–71.

(76) Wingate, A. J.; Boudouris, B. W. Recent Advances in the Syntheses of Radical-Containing Macromolecules. *J. Polym. Sci. Part A Polym. Chem.* **2016**, *54* (13), 1875–1894.

(77) Tomlinson, E. P.; Hay, M. E.; Boudouris, B. W. Radical Polymers and Their Application to Organic Electronic Devices. *Macromolecules* **2014**, *47* (18), 6145–6158.

(78) Takahashi, Y.; Hayashi, N.; Oyaizu, K.; Honda, K.; Nishide, H. Totally Organic Polymer-Based Electrochromic Cell Using TEMPO-Substituted Polynorbornene as a Counter Electrode-Active Material. *Polym. J.* **2008**, *40* (8), 763–767.

(79) Vasilyeva, S. V.; Unur, E.; Walczak, R. M.; Donoghue, E. P.; Rinzler, A. G.; Reynolds, J. R. Color Purity in Polymer Electrochromic Window Devices on Indium-Tin Oxide and Single-Walled Carbon Nanotube Electrodes. *ACS Appl. Mater. Interfaces* **2009**, *1* (10), 2288–2297.

(80) Suga, T.; Konishi, H.; Nishide, H. Photocrosslinked Nitroxide Polymer Cathode-Active Materials for Application in an Organic-Based Paper Battery. *Chem. Commun.* **2007**, No. 17, 1730–1732.

(81) Zheng, L.; Mukherjee, S.; Wang, K.; Hay, M. E.; Boudouris, B. W.; Gong, X. Radical Polymers as Interfacial Layers in Inverted Hybrid Perovskite Solar Cells. *J. Mater. Chem. A* **2017**, *5* (45), 23831–23839.

(82) Jensen, J.; Dyer, A. L.; Shen, D. E.; Krebs, F. C.; Reynolds, J. R. Direct Photopatterning of Electrochromic Polymers. *Adv. Funct. Mater.* **2013**, *23* (30), 3728–3737.

(83) Nakahara, K.; Oyaizu, K.; Nishide, H. Electrolyte Anion-Assisted Charge Transportation in Poly(Oxoammonium Cation/Nitroxyl Radical) Redox Gels. *J. Mater. Chem.* **2012**, *22* (27), 13669–13673.

(84) Iwasa, S.; Nishi, T.; Nakamura, S. Effect of Charge Transportation on High-Rate Discharge Properties of Organic Radical Batteries with Gel-State Cathode. *J. Electroanal. Chem.* **2017**, *805* (Supplement C), 171–176.

(85) Heinze, J.; Frontana-Uribe, B. A.; Ludwigs, S. Electrochemistry of Conducting Polymers-Persistent Models and New Concepts. *Chem. Rev.* **2010**, *110* (8), 4724–4771.

(86) Gaupp, C. L.; Welsh, D. M.; Rauh, R. D.; Reynolds, J. R. Composite Coloration Efficiency Measurements of Electrochromic Polymers Based on 3,4-Alkylenedioxythiophenes. *Chem. Mater.* **2002**, *14* (9), 3964–3970.

(87) Khan, S. U. M.; Al-Shahry, M.; Ingler, W. B. Efficient Photochemical Water Splitting by a Chemically Modified N-TiO_2. *Science (80-.).* **2002**, *297* (5590), 2243–2245.

(88) Remmele, J.; Shen, D. E.; Mustonen, T.; Fruehauf, N. High Performance and Long-Term Stability in Ambiently Fabricated Segmented Solid-State Polymer Electrochromic Displays. *ACS Appl. Mater. Interfaces* **2015**, *7* (22), 12001–12008.

(89) Wen, R.-T.; Arvizu, M. A.; Morales-Luna, M.; Granqvist, C. G.; Niklasson, G. A. Ion Trapping and Detrapping in Amorphous Tungsten Oxide Thin Films Observed by Real-Time Electro-Optical Monitoring. *Chem. Mater.* **2016**, *28* (13), 4670–4676.

(90) Wen, R. T.; Granqvist, C. G.; Niklasson, G. A. Eliminating Degradation and Uncovering Ion-Trapping Dynamics in Electrochromic WO_3 Thin Films. *Nat. Mater.* **2015**, *14* (10), 996–1001.

(91) Hassab, S.; Shen, D. E.; Österholm, A. M.; Reynolds, J. R.; Padilla, J. Exploring Unbalanced Electrode Configurations for Electrochromic Devices. *J. Mater. Chem. C* **2018**, *6* (2), 393–400.

(92) Jensen, J.; Krebs, F. C. From the Bottom Up – Flexible Solid State Electrochromic Devices. *Adv. Mater.* **2014**, *26* (42), 7231–7234.

(93) Padilla, J.; Seshadri, V.; Otero, T. F.; Sotzing, G. A. Electrochemical Study of Dual Conjugated Polymer Electrochromic Devices. *J. Electroanal. Chem.* **2007**, *609* (2), 75–84.

(94) He, J.; You, L.; Mei, J. Self-Bleaching Behaviors in Black-to-Transmissive Electrochromic Polymer Thin Films. *ACS Appl. Mater. Interfaces* **2017**, *9* (39), 34122–34130.

(95) Bobacka, J.; Lewenstam, A.; Ivaska, A. Electrochemical Impedance Spectroscopy of Oxidized Poly(3,4-Ethylenedioxythiophene) Film Electrodes in Aqueous Solutions. *J. Electroanal. Chem.* **2000**, *489* (1), 17–27.

(96) Rauh, R. D. Electrochromic Windows: An Overview. *Electrochim. Acta* **1999**, *44* (18), 3165–3176.

(97) Ma, C.; Taya, M.; Xu, C. Smart Sunglasses Based on Electrochromic Polymers. *Polym. Eng. Sci.* **2008**, *48* (11), 2224–2228.

(98) Baucke, F. G. K. Electrochromic Mirrors with Variable Reflectance. *Sol. Energy Mater.* **1987**, *16* (1–3), 67–77.

(99) Deutschmann, T.; Kortz, C.; Walder, L.; Oesterschulze, E. High Contrast Electrochromic Iris. *Opt. Express* **2015**, *23* (24), 31544.

(100) Jensen, J.; Krebs, F. C. From the Bottom Up - Flexible Solid State Electrochromic Devices. *Adv. Mater.* **2014**, *26* (42), 7231–7234.

(101) Jensen, J.; Dam, H. F.; Reynolds, J. R.; Dyer, A. L.; Krebs, F. C. Manufacture and Demonstration of Organic Photovoltaic-Powered Electrochromic Displays Using Roll Coating Methods and Printable Electrolytes. *J. Polym. Sci. Part B Polym. Phys.* **2012**, *50* (8), 536–545.

(102) Dyer, A. L.; Österholm, A. M.; Shen, D. E.; Johnson, K. E.; Reynolds, J. R. Conjugated Electrochromic Polymers: Structure-Driven Colour and Processing Control. *Electrochromic Materials and Devices*. July 24, 2015, pp 113–184.

(103) Vasilyeva, S. V.; Beaujuge, P. M.; Wang, S.; Babiarz, J. E.; Ballarotto, V. W.; Reynolds, J. R. Material Strategies for Black-to-Transmissive Window-Type Polymer Electrochromic Devices. *ACS Appl. Mater. Interfaces* **2011**, *3* (4), 1022–1032.

(104) He, J.; Mukherjee, S.; Zhu, X.; You, L.; Boudouris, B. W.; Mei, J. A Highly Transparent Crosslinkable Radical Copolymer Thin Film as the Ion Storage Layer in Organic Electrochromic Devices. *ACS Appl. Mater. Interfaces* **2018**, *10* (22), 18956–18963.

(105) Takahashi, Y.; Oyaizu, K.; Honda, K.; Nishide, H. Low-Energy Driven Electrochromic Devices Using Radical Polymer as Transparent Counter Electroactive Material. *J. Photopolym. Sci. Technol.* **2007**, *20* (1), 29–34.

(106) Pittelli, S. L.; Shen, D. E.; Österholm, A. M.; Reynolds, J. R. Chemical Oxidation of Polymer Electrodes for Redox Active Devices: Stabilization through Interfacial Interactions. *ACS Appl. Mater. Interfaces* **2018**, *10* (1), 970–978.

(107) Hassab, S.; Padilla, J. Using WO_3 as a Transparent, Optically-Passive Counter Electrode in an Unbalanced Electrochromic Configuration. *Electrochem. commun.* **2016**, *72*, 87–90.

(108) Schmitt, M.; Heusing, S.; Aegerter, M. A.; Pawlicka, A.; Avellaneda, C. Electrochromic Properties of Nb_2O_5 Sol–gel Coatings. *Sol. Energy Mater. Sol. Cells* **1998**, *54* (1–4), 9–17.

(109) Pawlicka, A.; Atik, M.; Aegerter, M. . Synthesis of Multicolor Nb_2O_5 Coatings for Electrochromic Devices. *Thin Solid Films* **1997**, *301* (1–2), 236–241.

(110) Özer, N.; Chen, D. G.; Lampert, C. M. Preparation and Properties of Spin-Coated Nb_2O_5 films by the Sol-Gel Process for Electrochromic Applications. *Thin Solid Films* **1996**, *277* (1–2), 162–168.

(111) Chen, K.-N.; Hsu, C.-M.; Liu, J.; Liou, Y.-C.; Yang, C.-F. Investigation of Antireflection Nb_2O_5 Thin Films by the Sputtering Method under Different Deposition Parameters. *Micromachines*. 2016, p 151.

(112) Maruyama, T. Electrochromic Properries of Manganese Oxide Thin Films Prepared by Chemical Vapor Deposition. *J. Electrochem. Soc.* **1995**, *142* (9), 3137–3141.

(113) Lee, G. R.; Crayston, J. A. Studies on the Electrochemical Deposition of Niobium Oxide. *J. Mater. Chem.* **1996**, *6* (2), 187–192.

(114) Llordés, A.; Wang, Y.; Fernandez-Martinez, A.; Xiao, P.; Lee, T.; Poulain, A.; Zandi, O.; Saez Cabezas, C. A.; Henkelman, G.; Milliron, D. J. Linear Topology in Amorphous Metal Oxide Electrochromic Networks Obtained via Low-Temperature Solution Processing. *Nat. Mater.* **2016**, *15* (12), 1267–1273.

(115) Zardetto, V.; Brown, T. M.; Reale, A.; Di Carlo, A. Substrates for Flexible Electronics: A Practical Investigation on the Electrical, Film Flexibility, Optical, Temperature, and Solvent Resistance Properties. *J. Polym. Sci. Part B Polym. Phys.* **2011**, *49* (9), 638–648.

(116) Bretos, I.; Jiménez, R.; Ricote, J.; Calzada, M. L. Low-Temperature Crystallization of Solution-Derived Metal Oxide Thin Films Assisted by Chemical Processes. *Chem. Soc. Rev.* **2018**, *47* (2), 291–308.

(117) Reeves, B. D.; Grenier, C. R. G.; Argun, A. A.; Cirpan, A.; McCarley, T. D.; Reynolds, J. R. Spray Coatable Electrochromic Dioxythiophene Polymers with High Coloration Efficiencies. *Macromolecules* **2004**, *37* (20), 7559–7569.

(118) Shi, P.; Amb, C. M.; Knott, E. P.; Thompson, E. J.; Liu, D. Y.; Mei, J.; Dyer, A. L.; Reynolds, J. R. Broadly Absorbing Black to Transmissive Switching Electrochromic Polymers. *Adv. Mater.* **2010**, *22* (44), 4949–4953.

(119) Verma, A.; Basu, A.; Bakhshi, A. K.; Agnihotry, S. A. Structural, Optical and Electrochemical Properties of Sol-Gel Derived TiO_2 Films: Annealing Effects. *Solid State Ionics* **2005**, *176* (29–30), 2285–2295.

(120) Park, S.; Kim, K.-H.; Jo, J.-W.; Sung, S.; Kim, K.-T.; Lee, W.-J.; Kim, J.; Kim, H. J.; Yi, G.-R.; Kim, Y.-H.; Yoon, M.-H.; Park, S. K. In-Depth Studies on Rapid Photochemical Activation of Various Sol–Gel Metal Oxide Films for Flexible Transparent Electronics. *Adv. Funct. Mater.* **2015**, *25* (19), 2807–2815.

(121) Spinolo, G.; Ardizzone, S.; Trasatti, S. Surface Characterization of Co_3O_4 Electrodes Prepared by the Sol-Gel Method. *J. Electroanal. Chem.* **1997**, *423* (1), 49–57.

(122) Kwon, Y.-H.; Jang, G.-E. Effect of SiO_2 and Nb_2O_5 Buffer Layer on Optical Characteristics of ITO Thin Film. *Trans. Electr. Electron. Mater.* **2015**, *16* (1), 29–33.

(123) Plieth, W.; Bund, A.; Rammelt, U.; Neudeck, S.; Duc, L. M. The Role of Ion and Solvent Transport during the Redox Process of Conducting Polymers. *Electrochim. Acta* **2006**, *51* (11), 2366–2372.

(124) Guan, S.; Elmezayyen, A. S.; Zhang, F.; Zheng, J.; Xu, C. Deterioration Mechanism of Electrochromic Poly(3,4-(2,2-Dimethylpropylenedioxy)Thiophene) Thin Films. *J. Mater. Chem. C* **2016**, *4* (20), 4584–4591.

(125) Huang, J. H.; Hsu, C. Y.; Hu, C. W.; Chu, C. W.; Ho, K. C. The Influence of Charge Trapping on the Electrochromic Performance of Poly(3,4-Alkylenedioxythiophene) Derivatives. *ACS Appl. Mater. Interfaces* **2010**, *2* (2), 351–359.

(126) Rivaton, A.; Tournebize, A.; Gaume, J.; Bussière, P.-O.; Gardette, J.-L.; Therias, S. Photostability of Organic Materials Used in Polymer Solar Cells. *Polym. Int.* **2014**, *63* (8), 1335–1345.

(127) Silva, H. S.; Tournebize, A.; Bégué, D.; Peisert, H.; Chassé, T.; Gardette, J.-L.; Therias, S.; Rivaton, A.; Hiorns, R. C. A Universal Route to Improving Conjugated Macromolecule Photostability. *RSC Adv.* **2014**, *4* (97), 54919–54923.

(128) Wen, R.-T.; Niklasson, G. A.; Granqvist, C. G. Sustainable Rejuvenation of Electrochromic WO_3 Films. *ACS Appl. Mater. Interfaces* **2015**, *7* (51), 28100–28104.

(129) Baloukas, B.; Arvizu, M. A.; Wen, R.-T.; Niklasson, G. A.; Granqvist, C. G.; Vernhes, R.; Klemberg-Sapieha, J. E.; Martinu, L. Galvanostatic Rejuvenation of Electrochromic WO_3 Thin Films: Ion Trapping and Detrapping Observed by Optical Measurements and by Time-of-Flight Secondary Ion Mass Spectrometry. *ACS Appl. Mater. Interfaces* **2017**, *9* (20), 16995–17001.

(130) Dong, D.; Wang, W.; Rougier, A.; Dong, G.; Da Rocha, M.; Presmanes, L.; Zrikem, K.; Song, G.; Diao, X.; Barnabé, A. Life-Cycling and Uncovering Cation-Trapping Evidence of a Monolithic Inorganic Electrochromic Device: Glass/ITO/WO_3/$LiTaO_3$/NiO/ITO. *Nanoscale* **2018**, *10* (35), 16521–16530.

(131) Dong, D.; Wang, W.; Rougier, A.; Barnabé, A.; Dong, G.; Zhang, F.; Diao, X. Lithium Trapping as a Degradation Mechanism of the Electrochromic Properties of All-Solid-State WO_3//NiO Devices. *J. Mater. Chem. C* **2018**, *6* (37), 9875–9889.

VITA

Education

South China University of Technology	B.S., 2014
The University of Akron	M.S., 2015
Purdue University	Ph.D. 2019

Appointments

2015-2019	Graduate Teaching/Researching Assistant, Purdue University
06-09/2015	Undergraduate and Master Research Assistant, The University of Akron
06-09/2014	Student Research Project, South China University of Technology

Awards

2013 The scholarship of YOKOHAMA (2%), South China University of Technology

2012 The scholarship of TANOTO FOUNDATION (7%), South China University of Technology

2011 The third prize of scholarship in university (10%), South China University of Technology

Publications

1. Solution Behaviour of a Polymer with Polyoxometalate Inorganic Molecular Clusters in Its Main Chain, Fadi Haso, Ruixin Wang, **Jiazhi He,** Jiancheng Luo, Seyed Ali Eghtesadi, Zhonghua Peng* and Tianbo Liu*, New J. Chem. 2016, 40, 910-913.

2. Direct Arylation Polymerization of Asymmetric Push-Pull Aryl Halides, Liyan You, Saadia T Chaudhry, Yan Zhao, Junchen Liu, Xikang Zhao, **Jiazhi He** and Jianguo Mei*, Polym. Chem., 2017, 8, 2438-2441.

3. Self-bleaching Behaviors in Black-to-Transmissive Electrochromic Polymer Thin Films, **Jiazhi He**, Liyan You, Jianguo Mei*, ACS Appl. Mater. & Interfaces, 2017, 9, 34122

4. Continuous Melt-Drawing of Highly Aligned Flexible and Stretchable Semiconducting Microfibers for Organic Electronics, Yan Zhao, Aristide Gumyusenge, **Jiazhi He**, Ge Qu, William McNutt, Yuan Long, Hongyi Zhang, Libai Huang, Ying Diao, Jianguo Mei*, Adv. Funct. Mater., 2018, 28, 1705584

5. Tuning of Polyoxopalladate Macroanionic Hydration Shell via Countercation Interaction, **Jiazhi He**, Hui Li, Peng Yang, Fadi Haso, Jiayingzi Wu, Tao Li, Ulrich Kortz, and Tianbo Liu*, Chemistry–A European Journal, 2018,24, 3052-3057.
6. A Highly Transparent Crosslinkable Radical Copolymer Thin Film as the Ion Storage Layer in Organic Electrochromic Devices, **Jiazhi He**, Sanjoy Mukherjee, Xingrui Zhu, Liyan You, Bryan W. Boudouris, Jianguo Mei*, ACS Appl Mater. & Interfaces, 2018,10, 18956-18963.

7. Tunable green electrochromic polymers via direct arylation polymerization, Liyan You,† **Jiazhi He**,† Jianguo Mei*, Polym. Chem., 2018, 9, 5262-5267

8. Low-temperature, Solution-Processed Niobium Oxide Thin Film as a Minimally Color Changing Ion Storage Layer in Electrochromic Devices, **Jiazhi He**, Liyan You, Dung T. Tran, Jianguo Mei*, ACS Appl Mater. & Interfaces, 2019, 11, 4169-4177

9. Electrochromic polymer and synthesis and uses thereof, Jianguo Mei, **Jiazhi He**, and Yan Zhou. US Patent App. 16/033,012, 2019

10. Solution-Processable Electrochromic Materials and Devices: Roadblocks and Strategies towards Large-Scale Applications, Xuefei Li,† Kuluni Perera,† **Jiazhi He**, Aristide Gumyusenge, Jianguo Mei*, J. Mater. Chem., 2019

11. Electrochromic polymer thin films having reduced self-bleaching behavior and enhanced cycling stability, Jianguo Mei, **Jiazhi He**, Yan Zhou. US Patent App. 16/032,980, 2019

ACS APPLIED MATERIALS & INTERFACES

Research Article

www.acsami.org

Self-Bleaching Behaviors in Black-to-Transmissive Electrochromic Polymer Thin Films

Jiazhi He, Liyan You, and Jianguo Mei*

Department of Chemistry, Purdue University, 560 Oval Drive, West Lafayette, Indiana 47907, United States

Supporting Information

ABSTRACT: Polymer-based electrochromic smart windows are an emerging energy-saving technology. There are several technological hurdles in the development of organic electrochromics. In this article, the self-bleaching behaviors of a black electrochromic polymer (ECP-black) thin film were investigated. We found that the electrochemical break-in process led to a less dense morphology and the increased free volume facilitated ion permeation in the ECP-black thin films. The polarized interface between the polymer thin film and transparent indium-tin-oxide (ITO) electrode made charge transfer accessible, which caused the self-bleaching behaviors. Herein, we proposed two approaches to study and mitigate the self-bleaching phenomenon. First, a densely packed morphology was regenerated by increasing the cathodic polarization time under open-circuit conditions (V_{off}). The second involved the modification of the electrode (ITO) surface with a partial coverage of the octadecyltrichlorosilane layer. The combination of the two approaches rendered the ECP-black thin film capable of maintaining the colored state for up to 900 s. To extend the scope of our studies, self-bleaching of ECP-magenta and ECP-blue thin films were also tested and suppressed by using these two methods. Additionally, the cycling stability of the ECP-black has been improved from ~600 cycles to up to 2300 cycles without a noticeable decay of optical contrast.

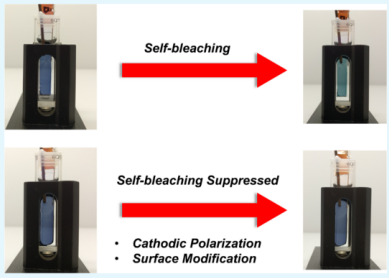

KEYWORDS: *self-bleaching, optical memory, organic electrochromic thin film, surface modification, cycle stability*

INTRODUCTION

Electrochromic thin films whose light transmission can be manipulated by switching a small voltage bias to oxidize/reduce the active materials have been developed for decades. Various types of active materials, including inorganic materials (e.g., WO_3, MoO_3, V_2O_5, Nb_2O_5, etc.),[1] small molecules (e.g., viologens,[2] Prussian blue,[3] etc.), conjugated polymers,[2,4,5] and inorganic−organic hybrids,[6] have been explored. Among them, conjugated polymers present many attractive properties, such as fast coloring-bleaching time, low cost, and flexibility.[4] However, there are a few obstacles in the commercialization of polymer electrochromics, including cycle stability,[7,8] photostability,[9] optical memory,[3,10] etc.

The optical memory is the ability of an electrochromic material to maintain its colored/bleached state under V_{off}. Although conjugated polymer thin films generally have good adhesion on device electrodes,[4] the self-bleaching behaviors of conjugated polymers are often observed[10] thus limiting the applications of electrochromic windows. For instance, the transmissivity of smart windows is required to be precisely controlled on the basis of the variation of solar radiation.[11,12] Because of the self-bleaching behaviors, the automatic control becomes more challenging. Therefore, it is important to understand and inhibit the self-bleaching behaviors of electrochromic polymer thin films.

Shin et al.[10] suggested that in the case of conjugated polymers with a highest occupied molecular orbital (HOMO) level higher than −5 eV, the electrons spontaneously transferred from conjugated polymers to the electrode indium-tin-oxide (ITO) at the interfaces, leading to the self-bleaching of electrochromic windows under V_{off}.[10] By redesigning the side chain of poly(3,4-ethylenedioxythiophene), the HOMO of the conjugated polymer was lowered down to −5.15 eV. Subsequently, the degree of self-bleaching was dramatically mitigated. However, changing the side chains of conjugated polymers also led to the change of their absorption spectra and higher oxidation potentials were required to oxidize the polymers.[10]

As it is shown in eq 1 below, self-bleaching also involves ion motion. During the self-bleaching process, positive charges (polarons and bipolarons) are generated on the polymer backbone. To maintain the overall electroneutrality of the electrochromic polymer (ECP) thin film, the permeation of counterions is a necessity and can be controlled by the compactness of conjugated polymer thin films.[13,14] If a compact polymer thin film was regenerated after electrochemical processes, the self-bleaching behaviors could be suppressed.

Received: June 25, 2017
Accepted: September 9, 2017
Published: September 9, 2017

DOI: 10.1021/acsami.7b09140
ACS Appl. Mater. Interfaces 2017, 9, 34122−34130

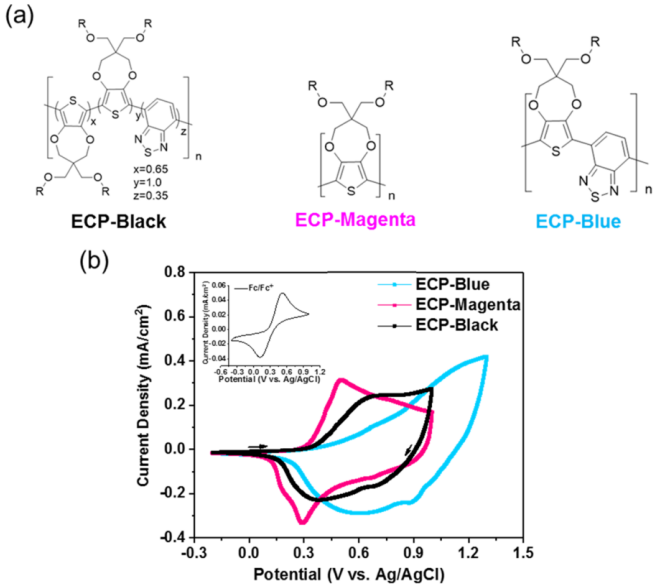

Figure 1. (a) Chemical structures and (b) cyclic voltammograms of ECP-black, ECP-magenta, and ECP-blue. R = 2-ethylhexyl. (Inset: the cyclic voltammogram of ferrocene).

$$\text{ECP} + \text{M}^+\cdot\text{A}^- \rightleftharpoons \text{ECP}^+\cdot\text{A}^- + \text{M}^+ + \text{e}^- \quad (1)$$

where ECP represents electrochromic polymer thin film, $M^+ \cdot A^-$ represents the electrolyte, M^+ is for metal or organic cation, and A^- is for the counter anion of the electrolyte, $ECP^+ \cdot A^-$ represents the oxidized conjugated polymer thin film whose charges are compensated by the endosmotic anions.

In previous works, Otero et al. and Odin et al. showed that the compactness of conjugated polymers under V_{off} was related to the cathodic polarization time in a logarithmic relationship, reflected by the retardant observations in both anodic[13,15,16] The work proposed the electrochemically stimulated conformational relaxation (ESCR) model to describe this relationship. In the ESCR model, the electrochemical behavior of conjugated polymers is treated as the conformation relaxation.[13] In the oxidation process, electrons are taken away from polymer chains, and polarons and bipolarons are formed consequently. The electrostatic repulsions between the positive charges result in opening channels for the swelling of counterions and electrolyte into the polymer thin film. In the reverse process, when the polymer is reduced back to the neutral state, the counterions and electrolyte are expelled. A closed and compact polymer network is regenerated. These conformation relaxations, opening and closing of the ion channels, are essentially related to the latter electrochemical response of the conjugated polymers.[17] Thus, the compact polymer thin film generated by the cathodic polarization can be used to inhibit the self-bleaching behaviors of ECP thin film under V_{off}.

Herein, we studied the electrochemical processes of ECP-black[18,19] thin films in association with self-bleaching behaviors. First, the impact of the break-in process was probed. Then, we investigated the effect of cathodic polarization time on the self-bleaching behaviors of ECP-black thin films. Additionally, we modified ITO with a partial coverage of octadecyltrichlorosilane (POTS) to impede the spontaneous charge transfer at interfaces. Finally, combing a long cathodic polarization (300 s) and POTS-modified surface, we demonstrated that self-bleaching of ECP-black can be suppressed to a large degree. These approaches are general and applicable to ECP-magenta and ECP-blue[20] thin films as well. We also found that the cycling stability of the ECP-black thin film on surface-modified ITO was significantly improved.

RESULTS AND DISCUSSION

The HOMO energy level of the ECP-black (Figure 1b) was estimated to be −4.8 eV by using the empirical formula (eq 2). Thus, the self-bleaching of ECP-black polymer could occur under V_{off} due to the interface electron transfer (IET), according to the previous work.[10]

$$E_{HOMO} = -[4.8 + (E_{ox} - E_{1/2(ferrocene)})] \text{ eV} \quad (2)$$

where E_{HOMO} is the HOMO energy level of the conjugated polymer; E_{ox} is the onset oxidation potential of the conjugated polymer obtained from the cyclic voltammetry (CV) (Figure 1b) of the ECP-black thin film, which is comparable to the E_{ox} in the differential pulse voltammetry (DPV) (Figure S5); $E_{1/2(ferrocene)}$ is the half-wave potential of ferrocene.

The optical memory of the pristine ECP-black thin film was evaluated by recording the optical density at $\sim\lambda_{max}$ (640 nm) for 900 s under V_{off} (Figure 2a). It was found that the absorption of the pristine film remained unchanged, suggesting that the pristine thin film did not undergo self-bleaching within the observation period. This observation does not follow the early report that conjugated polymers with HOMO levels higher than −5 eV will undergo self-bleaching on the ITO

DOI: 10.1021/acsami.7b09140
ACS Appl. Mater. Interfaces 2017, 9, 34122−34130

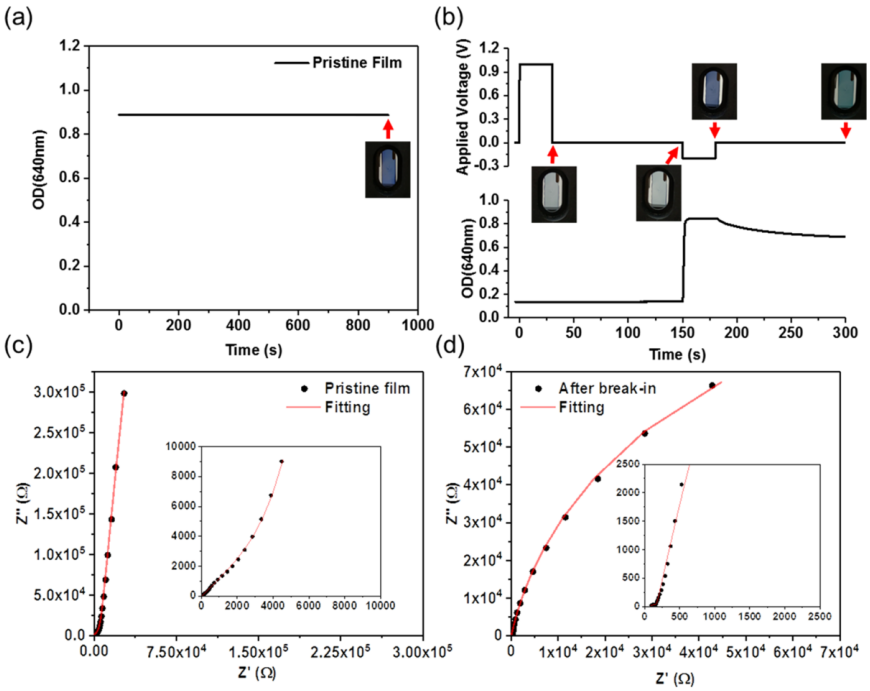

Figure 2. In situ optical density (OD) (640 nm) measurements of the ECP-black thin film: (a) at the pristine state (inset: a photograph of the pristine film) and (b) after break-in and at different potentials (inset: photographs of the ECP-black film at different states). Electrochemical impedance spectroscopy (EIS) measurements from 1 Hz to 1 MHz of the ECP-black thin film (c) at the pristine state (inset: the enlarged EIS spectrum), and (d) after break-in and with 300 s cathodic polarization (inset: the enlarged EIS spectrum).

substrate.[10] We then applied 15 cycles of break-in to the ECP-black thin film by cycling from −0.2 to 1.0 V at 40 mV/s (Figure S6). Thereafter, the ECP-black thin film was first oxidized to its bleached state. The preoxidized thin film was then subjected to 1.0 V for 30 s, and the potential was switched off from the 30th to the 150th second. The optical density of the bleached ECP-black thin film had little change, indicating that the self-coloring was absent. Subsequently, the ECP-black thin film was reduced back to its colored state by applying a reverse bias at −0.2 V for 30 s. When the cathodic voltage bias was removed, we immediately observed that the optical density of the colored thin film started to decay (Figure 2b). The ECP-black thin film can be reversely switched from the transmissive state to its original black-blue state, suggesting that the polymer thin film did not decompose during the break-in process. Therefore, we hypothesized that the activation of the self-bleaching behaviors can be ascribed to the conformational changes of the ECP-black thin film during the redox processes.

To validate our hypothesis, atomic-force microscopy (AFM) and electrochemical impedance spectroscopy (EIS) experiments were conducted to probe the structural changes of the ECP-black thin film after the break-in. Indeed, looser surface morphologies were observed for ECP-black thin films after the break-in process from the AFM images (Figure S7). The resulting loose surface morphologies would facilitate the diffusion of solvated ions to compensate the positive charges generated on the polymer backbone during the self-bleaching process. Dramatic structural changes for the pristine film were also observed in a previous report on the volume changes of polypyrrole (dodecylbenzenesulfonate) (PPy (DBS)) during redox cycles by using in situ AFM experiments.[21] The volume changes of the first cycle were between 60 and 100%, whereas only 30−40% volume changes were obtained in the following cycles. The differences of volume changes indicated that the pristine compactness of the PPy (DBS) thin films cannot be recovered. Wang et al. also observed the slow ion diffusion in the first reduction of PPy (DBS) due to exceptional compactness of the as-deposited film.[22] Our results are in good agreement with previous studies which state that initial electrochemical processes can cause the conformational changes of the pristine conjugated polymer thin films to facilitate ion diffusion.

The conformational changes of the ECP-black caused by the break-in were further confirmed by EIS measurements. First, the EIS of the ECP-black film was obtained before break-in (Figure 2c). Then, the break-in process was carried out, followed by a 300 s cathodic polarization potential (−0.2 V) that was applied to reset the ECP-black thin film back to its color state. Right after the cathodic polarization, the EIS of the broken-in thin film was taken (Figure 2d). In the EIS experiment, because the electrode was coated with the neutral semiconducting polymer thin film, the counterions needed to

DOI: 10.1021/acsami.7b09140
ACS Appl. Mater. Interfaces 2017, 9, 34122−34130

penetrate through the polymer thin film to reach the interfaces where the charge transfer occurs.[13,23] The EIS results can hence be fitted by the $R_s(Q_{film}R_{film})(Q_{dl}R_{ct})$,[23−27] where R_s is the solution resistance, Q_{film} and R_{film} are the capacitance and resistance of the thin film, and Q_{dl} and R_{ct} are double-layer capacitance and charge transfer resistance at the ECP-black film/ITO interfaces. The fitted results were summarized in the Supporting Information (Table S1). Both the R_{film} and R_{ct} decreased dramatically for the broken-in thin film, even after applying 300 s cathodic prepolarization to reset the film. This implied that the ECP-black thin film became looser, which would make it easier for the counterions to permeate through and facilitate the self-bleaching reactions (eq 1).

Next, the relationship between the cathodic polarization and the degree of self-bleaching of the ECP-black thin film was explored. The degree of self-bleaching is quantified as the percentage change of the optical density (ΔOD/OD (%)) under V_{off}. It is shown in Figure 3 that the degree of self-bleaching within 120 s decreased on increasing the cathodic polarization time. The result matches that of the ESCR model. The longer the cathodic polarization, the more counterions/electrolyte were expelled out from the polymer matrix, and the polymer matrix became more condensed due to the electro-osmotic processes.[14−16] After the voltage was turned off, the degree of self-bleaching became lower because it was more difficult for ions to penetrate into the thin-film matrix to compensate the positive charges generated in the self-bleaching process. These results suggest that the permeation of the counterions is necessary for the self-bleaching processes and can be potentially used to mediate the degree of the self-bleaching. Also, it is consistent with the previous observation (Figure 2) that the self-bleaching behaviors only occur when the ECP-black thin film presents a loose structure that has resulted from the break-in process.

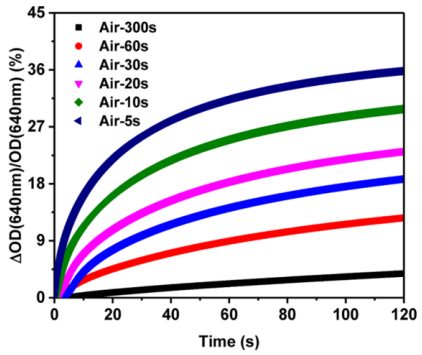

Figure 3. Short-term percentage change of optical density after different durations of reverse bias (−0.2 V vs Ag/AgCl) in ambient environment.

A more rigorous procedure was adopted to rule out the effect of oxidants (e.g., molecular oxygen in the air) that might cause the self-bleaching of ECP-black (Figure S8). The freeze pump treatment was applied to get rid of the oxygen residue inside the propylene carbonate electrolyte. The cuvette was sealed by Teflon tape and parafilm inside the N_2 glovebox. The spectral measurement was conducted under the N_2 protection. The result (Figure S8) suggested that cathodic polarization still played a role in controlling the degree of self-bleaching, similar to the results obtained under the ambient conditions. The degree of self-bleaching decreased when increasing the duration of cathodic polarization. In addition, if the existence of the oxidant was the dominant factor that caused the self-bleaching of the ECP-black thin film, then the self-bleaching would be observed for the pristine film before any electrochemical experiments (Figure 2a).[28] Thus, we believe that the self-bleaching of the broken-in ECP-black thin films is due to the spontaneous electron transfer from the ECP-black thin film to the ITO electrode, instead of the effect of oxidants.

To mitigate the self-bleaching problem, interfacial engineering was proposed to evade the need for redesigning the polymer structure. Octadecyltrichlorosilane (OTS) modification has been widely used in the field of organic field effect transistor to increase the adhesion of the organic layer (e.g., pentacene) to the substrate (Si wafer/ITO).[29−31] For electrochromic devices, the insulated nature of OTS could be used to impede the spontaneous electron transfer associated with the self-bleaching of ECP thin films.[32] However, the electrochemical processes of ECP thin films could be hampered at the same time. Therefore, we chose to make ITO partially covered by OTS (POTS) to mitigate the self-bleaching of the ECP thin film. To generate a partial coverage of OTS on ITO, both the roughness and the immersion time of the ITO in OTS solution are critical.[33] For unpolished ITO substrates, it generally takes longer time (~15 hrs) to form a densely packed self-assembled monolayer (SAM).[32] Kept under 1 vol % OTS hexane solution for a short time (80 min), ITO substrates were expected to be partially modified by OTS.

To evaluate the coverage of the as-formed SAM layer, cyclic voltammetry experiments of 0.1 M ferrocene in 0.1 M $TBAPF_6$ propylene carbonate solution were conducted by using a bare ITO and an OTS-modified ITO, respectively. For OTS-modified ITO, the voltammogram of ferrocene showed a lower peak current density and a larger distance between cathodic and anodic peaks, as compared to the bare ITO (Figure 4a). The surface coverage (θ) of the POTS-ITO was estimated to be 0.22 by using eq 3.[32,34] By extending the absorption time to 15 h, a more densely packed OTS (DOTS) layer formed on ITO, which was indicated by the extremely small current from the CV of ferrocene. The θ of DOTS-ITO was estimated to be 0.99. The CV studies demonstrated that the ITO was partially covered by OTS at which electron transfer was interfered but could proceed with the aid of an external potential.

$$\theta = 1 - (I_{p'}/I_p) \quad (3)$$

where I_p and $I_{p'}$ are the peak current densities of the CVs of ferrocene using bare ITO and OTS-modified ITO electrodes, respectively.

To further study the formation of the POTS layer on the ITO, the contact angle and AFM measurements were performed. In the contact angle measurements, 5 μL of deionized water was titrated on top of each substrate and images were taken immediately. The substrates were cleaned by UV-ozone treatment ahead of OTS modification. The surface wettability of bare ITO, UV-ozone cleaned ITO, and partially OTS-modified ITO (POTS-ITO) were determined by their contact angles, respectively. The typical images of contact angle measurements of bare ITO, UV-ozone treated ITO, and POTS-ITO are shown in Figure 4c. The average contact angle values were obtained from measurements at four different positions

DOI: 10.1021/acsami.7b09140
ACS Appl. Mater. Interfaces 2017, 9, 34122−34130

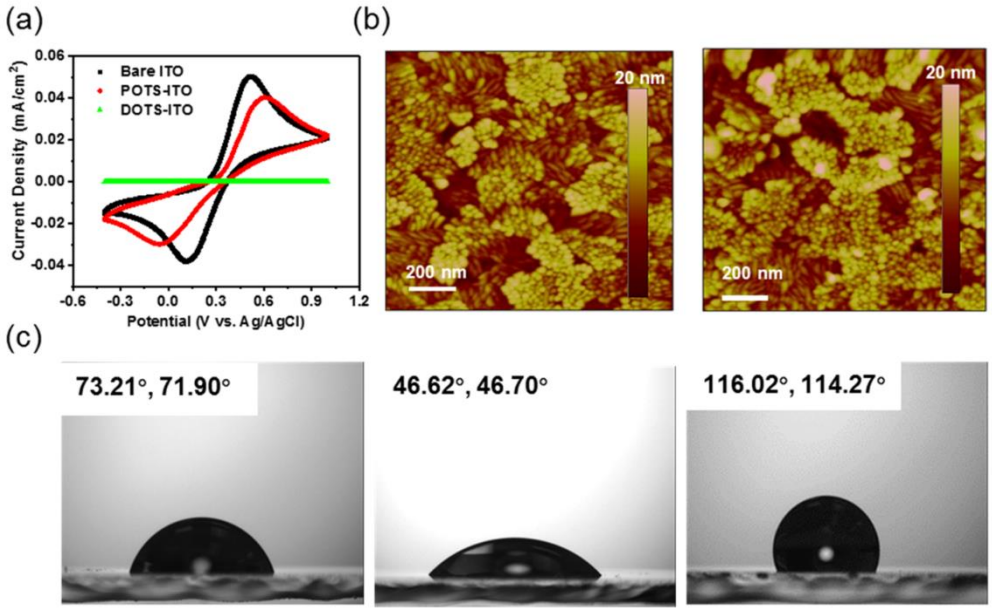

Figure 4. (a) Cyclic voltammograms of 0.1 M ferrocene in 0.1 M $TBAPF_6$ propylene carbonate solution using POTS-ITO, DOTS-ITO, and bare ITO as the working electrodes. (b) AFM images of the bare ITO (left) and POTS-ITO (right). (c) Contact angle images of bare ITO, UV-ozone treated ITO, and POTS-ITO.

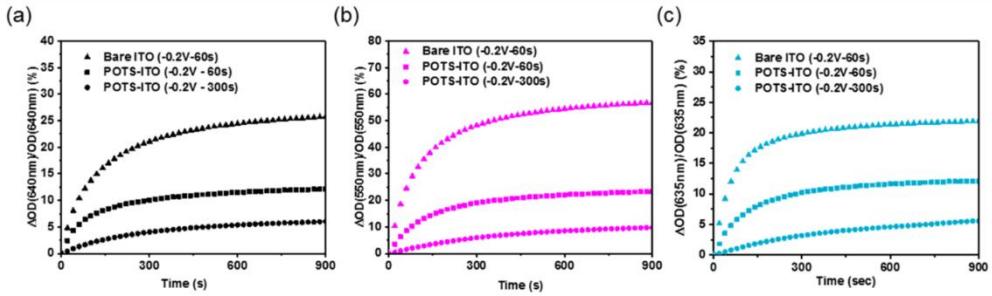

Figure 5. Long-term percentage change of optical density of (a) ECP-black on bare ITO after 60 s of cathodic polarization and on POTS-ITO after 60 and 300 s of cathodic polarization, (b) ECP-magenta on bare ITO after 60 s of cathodic polarization and on POTS-ITO after 60 and 300 s of cathodic polarization, and (c) ECP-blue on bare ITO after 60 s of cathodic polarization and on POTS-ITO after 60 and 300 s of cathodic polarization.

(Table S2). After the UV-ozone treatment, the ITO surface became more hydrophilic, with a small average contact angle ~49°.[35] Compared with the UV-ozone treated ITO, the OTS-modified ITO has a larger average contact angle of 116°, indicating the formation of the hydrophobic OTS layer on the ITO surface. From the AFM measurements, the average R_q increased slightly from 2.93 to 3.38 nm, which suggested that a self-assembled monolayer was formed on most of the surfaces (Figure 4b).

To test the effect of the POTS layer on the self-bleaching behaviors of the broken-in ECP-black thin films, the percentage change of optical density was measured for ECP-black thin films on both bare ITO and POTS-ITO. From the first derivative of OD (640 nm) of ECP-black with respect to time during the self-bleaching process, the change of the OD (640 nm) is negligible after ~500 s indicated by a small value of the decay rate (dOD/dt) (Figure S9). Thus, 900 s was sufficient to monitor the degree of self-bleaching. In Figure 5a, the degree of self-bleaching was observed to decrease from 27.6 ± 4.6% to 15.5 ± 2.98% (the average and standard deviation were calculated on the basis of three individual experiments (Figure S10)) after using the POTS-ITO and 60 s cathodic polarization. This is because the spontaneous electron transfer was disturbed by the insulated POTS layer.[36] By extending the

DOI: 10.1021/acsami.7b09140
ACS Appl. Mater. Interfaces 2017, 9, 34122−34130

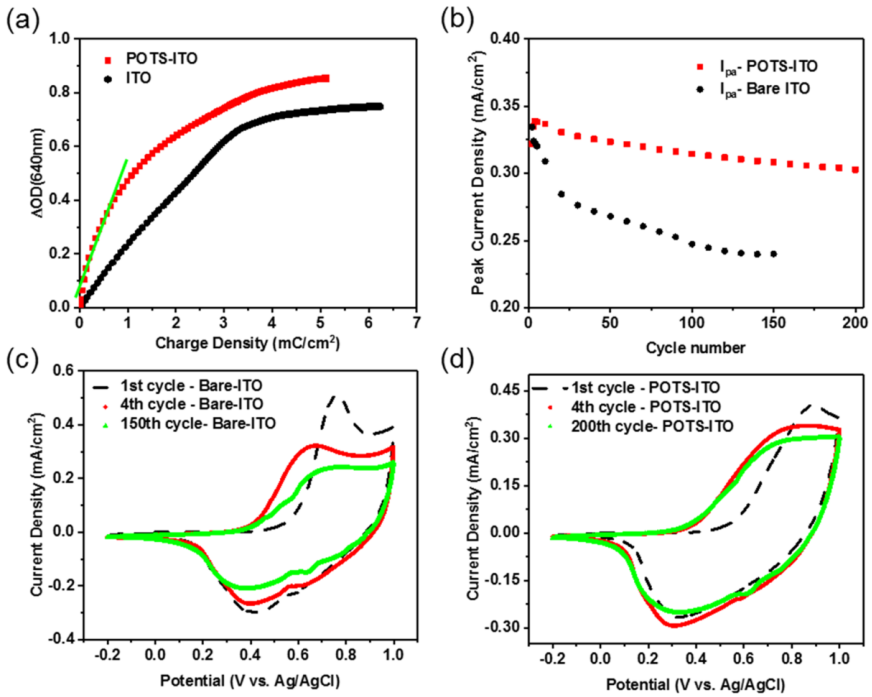

Figure 6. (a) Coloration efficiency of ECP-black thin films on bare ITO and POTS-ITO. (b) The development of anodic peak current density of ECP-black thin films on POTS-ITO and bare ITO vs number of cycles (the first cycle is not included). Selected cyclic voltammograms of ECP-black thin films on (c) bare ITO and (d) POTS-ITO.

cathodic polarization time to 300 s, the degree of self-bleaching can be further reduced to 7.6 ± 1.4%. This phenomenon also supports that the self-bleaching behaviors of the ECP-black thin film are primarily caused by the IET at the organic/ITO interfaces.

To demonstrate the universality of the POTS layer and cathodic polarization on the suppression of self-bleaching, ECP-magenta and ECP-blue polymers were also selected to measure the degree of self-bleaching after the break-in on both bare ITO and POTS-ITO. Both ECP-magenta and ECP-blue underwent self-bleaching because of their high HOMO levels, which were calculated to be −4.79 and −4.95 eV, respectively (Figure 1b). By using POTS-ITO and applying long cathodic polarization, the degree of self-bleaching can be reduced from 56.78 to 9.75% for the broken-in ECP-magenta thin film, and from 21.92 to 5.56% for the broken-in ECP-blue thin film (Figure 5b,c). Therefore, POTS modification and cathodic polarization are able to suppress the self-bleaching behaviors of ECPs. Additionally, the spectro-electrochemical behaviors and electrochromic switching of the ECP-black thin film on POTS-ITO were studied (Figure S11). There is no obvious difference compared with the ECP-black thin film on bare ITO (Table S3). Because the ITO surface is partially covered by OTS, electrochemical oxidation/reduction can still progress when driven by an external potential. From the energy point of view, the coloration efficiency measurements were carried out for broken-in thin films of ECP-black on both substrates. The coloration efficiency (CE) of the bleaching process can be calculated from the slope of the curve made by ΔOD versus ejected charge density. Compared with the ECP-black on bare ITO (203.23 cm^2/C), the slope of the ECP-black on POTS-ITO (473.4 cm^2/C) is more inclined at the beginning but starts to gradually decrease till the end (Figure 6a). The initial larger values of the CE might be due to the better contact between the polymer thin film and ITO electrode, so the electron transfer driven by an externally applied voltage was more efficient at the beginning. However, due to the existence of insulated POTS on the surfaces of ITO, it consumed more charges to completely oxidize the whole ECP-black thin film.

Finally, the cycling stability of the ECP-black on POTS-ITO was tested by cyclic voltammetry (CV) and double potential step chronoamperometry (DPSC). The CV cycling test can assess the adhesion of the ECP-black thin film on the substrate by monitoring the development of the voltammogram and peak current density of each cycle. On the other hand, DPSC cycling experiments can provide in situ transmittance change at the on−off switching mode. However, the transmittance measurement is based on one spot where the light penetrates through, so the results might not represent the conditions of the entire film. Therefore, we combined these two methods to evaluate the effect of POTS on the cycling stability. The CV cycling experiments were scanned between −0.2 and 1.0 V at a scan rate of 40 mV/s. The development of the anodic peak current density (I_{pa}) of CV was summarized in Figure 6b. The

DOI: 10.1021/acsami.7b09140
ACS Appl. Mater. Interfaces 2017, 9, 34122−34130

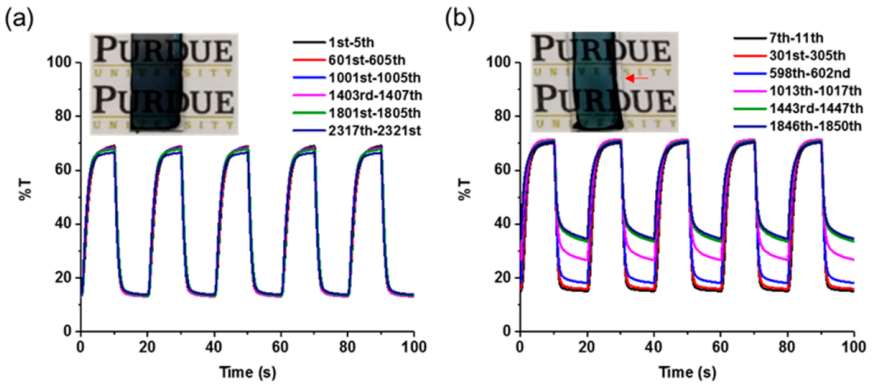

Figure 7. Transmittance at 640 nm of ECP-black thin films on (a) POTS-ITO (the inset is the photography of the thin film after 4300 cycles) and (b) bare ITO (the inset is the photography of the thin film after 3300 cycles) under double potential step chronoamperometric experiments, switching between 1.0 and −0.2 V vs Ag/AgCl.

voltammogram of initial cycle, fourth cycle, and the last cycle were shown in Figure 6c,d for ECP-black on POTS-ITO and bare ITO, respectively. The I_{pa} of the first scan (dash line) was excluded due to the first scan effect, as shown in Figure 6c,d.[37] For the ECP-black on bare ITO, the I_{pa} of CV decreased rapidly and the shape of CV changed dramatically with more and more cycles, indicated by the delamination of ECP-black from bare ITO. During the redox cycles, electrochromic thin films on ITO are expanded/contracted due to the incorporation and extraction of solvated ions.[21,38] The hydrophilic surface of the ITO cannot provide enough adhesion to hydrophobic conjugated polymer thin films to overcome the volume change. It led to the delamination of the thin film, indicated by the 28% decrease (from 2nd cycle to 150th cycle) of the value of I_{pa}. For the CV of the ECP-black on POTS-ITO, the position of the anodic peak slightly moved toward higher potential, whereas the oxidation onset was comparable, which supports our hypothesis that electron transfer is partially impeded. The I_{pa} for the ECP-black on POTS-ITO increased slightly from the 1st to the 4th cycle because the thin film became looser for solvated ions to permeate into and more materials could get involved in the reaction. Then, the I_{pa} decreased by 10% from the 4th cycle to 200th cycle (Figure 6b). The overall shape of CV only changed slightly for 200 cycles, which indicated that the ECP-black on POTS-ITO can maintain its adhesion via the hydrophobic interaction (Figure 6d) resulting in the improvement of cycling stability. In the DPSC measurement, the potential was switched between −0.2 and 1.0 V, with a 10 s time interval. The optical contrast of the ECP-black thin film on POTS-ITO can be maintained up to 2300 cycles while losing only 5% of its original contrast. After ∼4300 cycles, most of the part of the ECP-black thin film can remain well adhered on POTS-ITO (Figure 7a). As a comparison, the losses of optical contrast can be observed for the ECP-black thin film on bare ITO at ∼600 cycles and increased to ∼35% of its original contrast after ∼1800 cycles, which indicated the delamination of the thin film. After 3300 cycles, the ECP-black thin film delaminated from the bare ITO and was not capable of being fully reduced back to black-blue, as shown in the photograph (Figure 7b).

CONCLUSIONS

We adopted two approaches, partial OTS surface modification and cathodic polarization, to probe and study the self-bleaching behaviors of ECP-black. Taking advantage of these two approaches, we have successfully mitigated the self-bleaching problem of ECP thin films. Moreover, compared with the bare ITO, the POTS-ITO has a more hydrophobic surface that provides stronger adhesion to conjugated polymer thin films. As a result, the cycling stability of the ECP-black thin film on POTS-ITO can be enhanced dramatically.

In the future work, we envisage to investigate an appropriate SAM layer that can induce an interfacial dipole to increase the work function of ITO so that the electron transfer at the ITO/ECP interfaces can be prevented under V_{off}.[39,40] Meanwhile, it is important to improve the adhesion of thin film on the ITO surface to enhance the cycling stability. By introducing the SAM-modified ITO, other properties, including switching time, coloration efficiency, and color contrast, should also be taken into consideration. This work provides more insight into the self-bleaching behaviors of electrochromic polymers and offers solutions toward reliable automation control of electrochromic windows. For instance, the colored state of the electrochromic windows can be maintained by refreshing cathodic bias at a low frequency and with minimum energy consumption.

ASSOCIATED CONTENT

Supporting Information

The Supporting Information is available free of charge on the ACS Publications website at DOI: 10.1021/acsami.7b09140.

Experimental details of characterizations and synthesis of ECP-black, ECP-magenta, and ECP-blue: materials used in this work, ^{1}H NMR of ECP-black, ECP-magenta, and ECP-blue, instrumentation used in this work, CV, DPV, the degree of self-bleaching, OTS surface modification, EIS, and AFM; short-term percentage change of optical density after different durations of reverse bias under nitrogen flow; thickness optimization of ECP-black; DPV of ECP-black; CVs of the break-in process; additional characterization (AFM and EIS) on ECP-black before and after break-in; the procedure for obtaining the

DOI: 10.1021/acsami.7b09140
ACS Appl. Mater. Interfaces 2017, 9, 34122−34130

degree of self-bleaching from UV/vis optical density measurement; EIS equivalent circuit and fitting results for ECP-black before and after break-in; average contact angles of bare ITO, UV-ozone treated ITO, POTS-ITO; the first derivative of OD (640 nm) of ECP-black with respect to time during the self-bleaching process; three individual measurements of the long-term percentage change of optical density of ECP-black on bare ITO and OTS partially modified ITO; spectro-electrochromic behaviors and double potential step chronoamperometric experiments of ECP-black on bare ITO and POTS-ITO (PDF)

AUTHOR INFORMATION

Corresponding Author

*E-mail: jgmei@purdue.edu.

ORCID

Jianguo Mei: 0000-0002-5743-2715

Notes

The authors declare the following competing financial interest(s): This study has been financially supported in part by the Furcifer Inc. J.M. was a scientific advisor and co-founder.

ACKNOWLEDGMENTS

The authors would like to thank Prof. Ritural Borgohain for the use of the contact angle goniometer and Dr. Yan Zhao for the assistance on the OTS modification.

REFERENCES

(1) Bange, K.; Gambke, T. Electrochromic Materials for Optical Switching Devices. *Adv. Mater.* **1990**, *2*, 10−16.

(2) Mortimer, R. J. Organic Electrochromic Materials. *Electrochim. Acta* **1999**, *44*, 2971−2981.

(3) Wang, J.; Zhang, L.; Yu, L.; Jiao, Z.; Xie, H.; Lou, X. W. D.; Sun, X. W. A Bi-Functional Device for Self-Powered Electrochromic Window and Self-Rechargeable Transparent Battery Applications. *Nat. Commun.* **2014**, *5*, No. 4921.

(4) Beaujuge, P. M.; Reynolds, J. R. Color Control in π-Conjugated Organic Polymers for Use in Electrochromic Devices. *Chem. Rev.* **2010**, *110*, 268−320.

(5) Amb, C. M.; Dyer, A. L.; Reynolds, J. R. Navigating the Color Palette of Solution-Processable Electrochromic Polymers. *Chem. Mater.* **2011**, *23*, 397−415.

(6) Thakur, V. K.; Ding, G.; Ma, J.; Lee, P. S.; Lu, X. Hybrid Materials and Polymer Electrolytes for Electrochromic Device Applications. *Adv. Mater.* **2012**, *24*, 4071−4096.

(7) Otley, M. T.; Alamer, F. A.; Zhu, Y.; Singhaviranon, A.; Zhang, X.; Li, M.; Kumar, A.; Sotzing, G. A. Acrylated Poly(3,4-Propylenedioxythiophene) for Enhancement of Lifetime and Optical Properties for Single-Layer Electrochromic Devices. *ACS Appl. Mater. Interfaces* **2014**, *6*, 1734−1739.

(8) Lu, Y.; Liu, L.; Foo, W.; Magdassi, S.; Mandler, D.; Lee, P. S. Self-Assembled Polymer Layers of Linear Polyethylenimine for Enhancing Electrochromic Cycling Stability. *J. Mater. Chem. C* **2013**, *1*, 3651−3654.

(9) Bulloch, R. H.; Reynolds, J. R. Photostability in Dioxyheterocycle Electrochromic Polymers. *J. Mater. Chem. C* **2016**, *4*, 603−610.

(10) Shin, H.; Seo, S.; Park, C.; Na, J.; Han, M.; Kim, E. Energy Saving Electrochromic Windows from Bistable Low-HOMO Level Conjugated Polymers. *Energy Environ. Sci.* **2016**, *9*, 117−122.

(11) Dussault, J.-M.; Sourbron, M.; Gosselin, L. Reduced Energy Consumption and Enhanced Comfort with Smart Windows: Comparison between Quasi-Optimal, Predictive and Rule-Based Control Strategies. *Energy Build.* **2016**, *127*, 680−691.

(12) Tavares, P.; Bernardo, H.; Gaspar, A.; Martins, A. Control Criteria of Electrochromic Glasses for Energy Savings in Mediterranean Buildings Refurbishment. *Sol. Energy* **2016**, *134*, 236−250.

(13) Otero, T. F.; Grande, H.; Rodríguez, J. A New Model for Electrochemical Oxidation of Polypyrrole under Conformational Relaxation Control. *J. Electroanal. Chem.* **1995**, *394*, 211−216.

(14) Otero, T. F.; Boyano, I. Comparative Study of Conducting Polymers by the ESCR Model. *J. Phys. Chem. B* **2003**, *107*, 6730−6738.

(15) Odin, C.; Nechtschein, M. On the Kinetics of Electrochemical Doping in Conducting Polymers: Experimental Characterization. *Synth. Met.* **1993**, *55*, 1281−1286.

(16) Odin, C.; Nechtschein, M. Slow Relaxation in Conducting Polymers. *Phys. Rev. Lett.* **1991**, *67*, 1114−1117.

(17) Grande, H.; Otero, T. F. Conformational Movements Explain Logarithmic Relaxation in Conducting Polymers. *Electrochim. Acta* **1999**, *44*, 1893−1900.

(18) Shi, P.; Amb, C. M.; Knott, E. P.; Thompson, E. J.; Liu, D. Y.; Mei, J.; Dyer, A. L.; Reynolds, J. R. Broadly Absorbing Black to Transmissive Switching Electrochromic Polymers. *Adv. Mater.* **2010**, *22*, 4949−4953.

(19) Beaujuge, P. M.; Ellinger, S.; Reynolds, J. R. The Donor-Acceptor Approach Allows a Black-to-Transmissive Switching Polymeric Electrochrome. *Nat. Mater.* **2008**, *7*, 795−799.

(20) Amb, C. M.; Beaujuge, P. M.; Reynolds, J. R. Spray-Processable Blue-to-Highly Transmissive Switching Polymer Electrochromes via the Donor−Acceptor Approach. *Adv. Mater.* **2010**, *22*, 724−728.

(21) Smela, E.; Gadegaard, N. Surprising Volume Change in PPy(DBS): An Atomic Force Microscopy Study. *Adv. Mater.* **1999**, *11*, 953−957.

(22) Wang, X.; Shapiro, B.; Smela, E. Visualizing Ion Currents in Conjugated Polymers. *Adv. Mater.* **2004**, *16*, 1605−1609.

(23) Mo, M.; Zhao, W.; Chen, Z.; Yu, Q.; Zeng, Z.; Wu, X.; Xue, Q. Excellent Tribological and Anti-Corrosion Performance of Polyurethane Composite Coatings Reinforced with Functionalized Graphene and Graphene Oxide Nanosheets. *RSC Adv.* **2015**, *5*, 56486−56497.

(24) Hernández, S.; Hidalgo, D.; Sacco, A.; Chiodoni, A.; Lamberti, A.; Cauda, V.; Tresso, E.; Saracco, G. Comparison of Photocatalytic and Transport Properties of TiO2 and ZnO Nanostructures for Solar-Driven Water Splitting. *Phys. Chem. Chem. Phys.* **2015**, *17*, 7775−7786.

(25) Xie, Z.; Liu, X.; Wang, W.; Liu, C.; Li, Z.; Zhang, Z. Enhanced Photoelectrochemical Properties of TiO2 Nanorod Arrays Decorated with CdS Nanoparticles. *Sci. Technol. Adv. Mater.* **2014**, *15*, 55006.

(26) Wang, H.; Wang, B.; Yu, J.; Hu, Y.; Xia, C.; Zhang, J.; Liu, R. Significant Enhancement of Power Conversion Efficiency for Dye Sensitized Solar Cell Using 1D/3D Network Nanostructures as Photoanodes. *Sci. Rep.* **2015**, *5*, No. 9305.

(27) Wang, J. Z.; Xu, C. H.; Cao, W.; He, Y. Electrochemical Impedance Characterization of Porous Aluminum Oxide after Different Stages of Two-Step Anodization. *Adv. Mater. Res.* **2014**, *953*−*954*, 1282−1285.

(28) Chidichimo, G.; De Simone, B. C.; Imbardelli, D.; De Benedittis, M.; Barberio, M.; Ricciardi, L.; Beneduci, A. Influence of Oxygen Impurities on the Electrochromic Response of Viologen-Based Plastic Films. *J. Phys. Chem. C* **2014**, *118*, 13484−13492.

(29) Lin, Y. Y.; Gundlach, D. J.; Nelson, S. F.; Jackson, T. N. Stacked Pentacene Layer Organic Thin-Film Transistors with Improved Characteristics. *IEEE Electron Device Lett.* **1997**, *18*, 606−608.

(30) Shtein, M.; Mapel, J.; Benziger, J. B.; Forrest, S. R. Effects of Film Morphology and Gate Dielectric Surface Preparation on the Electrical Characteristics of Organic-Vapor-Phase-Deposited Pentacene Thin-Film Transistors. *Appl. Phys. Lett.* **2002**, *81*, 268−270.

(31) Yun, D.-J.; Lee, D.-K.; Jeon, H.-K.; Rhee, S.-W. Contact Resistance between Pentacene and Indium−tin Oxide (ITO) Electrode with Surface Treatment. *Org. Electron.* **2007**, *8*, 690−694.

(32) Muthurasu, A.; Ganesh, V. Electrochemical Characterization of Self-Assembled Monolayers (SAMs) of Silanes on Indium Tin Oxide (ITO) Electrodes − Tuning Electron Transfer Behaviour across

DOI: 10.1021/acsami.7b09140
ACS Appl. Mater. Interfaces 2017, 9, 34122−34130

Electrode−electrolyte Interface. *J. Colloid Interface Sci.* **2012**, *374*, 241−249.
(33) Uehara, T. M.; de Aguiar, H. B.; Bergamaski, K.; Miranda, P. B. Adsorption of Alkylthiol Self-Assembled Monolayers on Gold and the Effect of Substrate Roughness: A Comparative Study Using Scanning Tunneling Microscopy, Cyclic Voltammetry, Second-Harmonic Generation, and Sum-Frequency Generation. *J. Phys. Chem. C* **2014**, *118*, 20374−20382.
(34) Janek, R. P.; Fawcett, W. R.; Ulman, A. Impedance Spectroscopy of Self-Assembled Monolayers on Au(111): Sodium Ferrocyanide Charge Transfer at Modified Electrodes. *Langmuir* **1998**, *14*, 3011−3018.
(35) Sugiyama, K.; Ishii, H.; Ouchi, Y.; Seki, K. Dependence of Indium−tin−oxide Work Function on Surface Cleaning Method as Studied by Ultraviolet and X-Ray Photoemission Spectroscopies. *J. Appl. Phys.* **2000**, *87*, 295−298.
(36) Herzer, N.; Wienk, M. M.; Schmit, P.; Spoelstra, A. B.; Hendriks, C. E.; Oosterhout, S. D.; Hoeppener, S.; Schubert, U. S. Fabrication of PEDOT-OTS-Patterned ITO Substrates. *J. Mater. Chem.* **2010**, *20*, 6618−6621.
(37) Heinze, J.; Frontana-Uribe, B. A.; Ludwigs, S. Electrochemistry of Conducting Polymers−Persistent Models and New Concepts. *Chem. Rev.* **2010**, *110*, 4724−4771.
(38) Otero, T. F.; Grande, H.; Rodríguez, J. Reversible Electrochemical Reactions in Conducting Polymers: A Molecular Approach to Artificial Muscles. *J. Phys. Org. Chem.* **1996**, *9*, 381−386.
(39) Braun, S.; Salaneck, W. R.; Fahlman, M. Energy-Level Alignment at Organic/Metal and Organic/Organic Interfaces. *Adv. Mater.* **2009**, *21*, 1450−1472.
(40) Ishii, H.; Sugiyama, K.; Ito, E.; Seki, K. Energy Level Alignment and Interfacial Electronic Structures at Organic/Metal and Organic/Organic Interfaces. *Adv. Mater.* **1999**, *11*, 605−625.

DOI: 10.1021/acsami.7b09140
ACS Appl. Mater. Interfaces 2017, 9, 34122−34130

ACS APPLIED MATERIALS & INTERFACES

Research Article

Cite This: ACS Appl. Mater. Interfaces 2018, 10, 18956−18963

www.acsami.org

Highly Transparent Crosslinkable Radical Copolymer Thin Film as the Ion Storage Layer in Organic Electrochromic Devices

Jiazhi He,[†] Sanjoy Mukherjee,[‡] Xingrui Zhu,[‡] Liyan You,[†] Bryan W. Boudouris,[†,‡] and Jianguo Mei*[,†]

[†]Department of Chemistry, Purdue University, 560 Oval Drive, West Lafayette, Indiana 47907, United States

[‡]Charles D. Davidson School of Chemical Engineering, Purdue University, West Lafayette, Indiana 47907, United States

Supporting Information

ABSTRACT: A highly transparent crosslinkable thin film made of the radical polymer poly(2,2,6,6-tetramethyl-4-piperidinyloxy methacrylate)-*co*-(4-benzoylphenyl methacrylate) (PTMA-*co*-BP) has been developed as the ion storage layer in electrochromic devices (ECDs). After photo-crosslinking, the dissolution of PTMA-*co*-BP in electrolytes was mitigated, which results in an enhanced electrochemical stability compared with the homopolymer PTMA thin film. Moreover, the redox capacity of PTMA-*co*-BP increased because of the formation of a crosslinked network. By matching the redox capacity of the PTMA-*co*-BP thin film and bis(alkoxy)-substituted poly(propylenedioxythiophene), the ECD achieved an optical contrast of 72% in a small potential window of 2.55 V (i.e., switching between +1.2 and −1.35 V), and it was cycled up to 1800 cycles. The ECD showed an excellent optical memory as its transmittance decayed by less than 3% in both the colored and bleached states while operating for over 30 min under open-circuit conditions. Use of crosslinkable radical polymers as the transparent ion storage layer opens up a new venue for the fabrication of transmissive-mode organic ECDs.

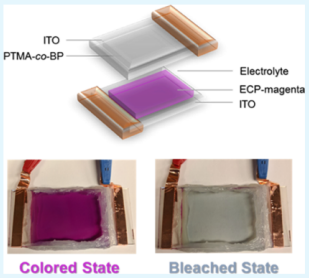

KEYWORDS: *Crosslinkable radical polymer, high transparency, electrochemical stability, ion storage layer, organic electrochromic devices*

INTRODUCTION

Polymer-based electrochromic devices (ECDs) have a great potential in a number of applications that range from smart windows to transmissive-mode displays.[1] A great deal of effort has been devoted to electrochromic materials and resulted in a vast library of redox polymers with various color states that span the whole color wheel.[2,3] Typically, a full ECD has minimally three layers, namely, the electrochromic layer, the electrolyte, and the counter electrode (i.e., the ion storage layer). In stark contrast to the electrochromic layer, the ion storage layer has rarely been systematically studied.[2] A bare transparent metal oxide conductor [e.g., tin-doped indium oxide (ITO)] is often directly used as the ion storage layer.[4] To balance the charge generated in the electrochromic layer, an overpotential (>−1.5 V vs Ag/Ag^+) needs to be applied to reduce the ITO electrode, and this is an irreversible process.[4] The irreversible reduction of the ITO electrode leads to a severe decay of the optical contrast of ECDs during the cycling test. Thus, it is crucial to develop a robust ion storage layer for ECDs. A few electrode materials have been utilized in this fashion, and they include metal oxides (e.g., NiO, TiO_2, and WO_3); conjugated polymers [e.g., poly(3,4-ethylenedioxythiophene) polystyrene sulfonate (PEDOT:PSS) and N−C_{18}-substituted poly(3,4-propylenedioxypyrrole) (PProDOP)]; and radical polymers [e.g., poly(2,2,6,6-tetramethyl-4-piperidinyloxy methacrylate) (PTMA) and poly(2,3-bis(2′,2′,6′,6′-tetramethylpiperidinyl-*N*-oxyl-4′-oxycarbonyl)-5-norbornene) (PTNB)]. Among these materials, WO_3 and PEDOT:PSS have absorption in the visible light region after being reduced, which affects the color purity of ECDs. Moreover, Padilla et al. suggested that the contrast of a dual electrochromic system was lower than either of the optical contrasts that can be achieved by the individual material, based on the mathematical calculation of the electrochromic system that obeys the Lambert−Beer law.[5] Therefore, a highly transparent and nonelectrochromic ion storage material is desired to achieve a high optical contrast. Kim et al. recently used a highly transparent TiO_2 film as the counter electrode and obtained a high contrast.[6] However, the processing of metal oxide-based thin-film counter electrodes is rather sophisticated and costly. It often involves high vacuum or high-temperature annealing (>500 °C) when solution processing is adopted.[6−9]

Polymers with highly transmissive neutral and doped states are attractive as counter electrodes in ECDs, including both semiconducting polymers and radical polymers. For instance, PProDOP has an absorbance in the near-ultraviolet (UV) region in its neutral state, and this absorption band directly shifts to the near-infrared (NIR) region upon oxidation. Reynolds et al. studied such a minimal color-changing polymer (MCCP)—PProDOP—as a counter electrode and obtained a

Received: February 27, 2018
Accepted: May 10, 2018
Published: May 10, 2018

DOI: 10.1021/acsami.8b03235
ACS Appl. Mater. Interfaces 2018, 10, 18956−18963

high optical contrast.[10] It is noted that the synthesis of PProDOP is nontrivial and multiple reactions are involved. Radical polymers attract a lot of attention as the active materials for energy storage devices and organic electronics.[11−17] Few attempts have also been made to use radical polymers as active materials of the counter electrode for ECDs, as they have negligible absorption in the visible region. However, they present significant disadvantages. For instance, when Nishide et al. used PTNB as the counter electrode to couple with Prussian blue and poly(decylviologen)−poly(styrenesulfonate) (PV10−PSS) and constructed ECDs, the devices did not achieve a high contrast and were not robust during the cycling test.[18] One possible explanation is the dissolution of radical polymers, which results in an unmatched redox capacity between PTNB and PV10−PSS. To mitigate the dissolution of radical polymers, Vasilyeva et al. reported that the PTMA/poly(methyl methacrylate) (PMMA) (1:3 molar ratio) polymer blend can increase the redox stability of the radical polymer, and the ECP-magenta device can achieve a contrast of over 70% with a fast switching rate and a high cycle stability.[19] Nevertheless, 75% of the PTMA/PMMA blend was PMMA, which is not a redox-active material. To compensate for the charge involved in the color switching of the electrochromic active layer, a thick PTMA/PMMA layer was used, which led to a large ohmic resistance of the ECDs.[6] As a result, a high anodic potential (2.35 V) was adopted to achieve a large optical contrast. Moreover, a long annealing time was required to obtain a homogeneous polymer blend that has a good electrochemical stability. Therefore, an alternative strategy is needed to address the dissolution of radical polymers in electrolytes without sacrificing the ion storage capacity of radical polymers.

A crosslinking strategy has been applied to make stable radical polymers as the cathode-active materials in energy storage devices.[20] Here, we turned to using a radical polymer-based material that includes a small number of copolymerized repeat units that are capable of undergoing photo-crosslinking. Specifically, we used the photo-crosslinkable radical random copolymer PTMA-*co*-(4-benzoylphenyl methacrylate) (PTMA-*co*-BP) as the counter electrode for ECDs. The effects of crosslinking and the associated electrolytes on the electrochemical behavior of PTMA-*co*-BP were established. By using the optimized thicknesses of each layer and using 0.2 M 1-ethyl-3-methylimidazolium bis(trifluoromethylsulfonyl)imide (EMI-TFSI) in propylene carbonate (PC) as electrolytes, the bis(alkoxy)-substituted poly(propylenedioxythiophene) (ECP-magenta)/PTMA-*co*-BP device had a high optical contrast of ∼72% at a wavelength of 550 nm, and the composite coloration efficiency was calculated to be ∼754.0 cm^2 C^{-1}. The high composite coloration efficiency suggests that the device can achieve a high optical contrast by consuming a small amount of charge. Moreover, the device can be switched using a small potential bias of 2.55 V and cycled for more than 1800 cycles in a reversible manner. Last but not the least, the device maintained its colored/bleached state for 30 min at open circuit with a minimum color change.

EXPERIMENTAL SECTION

Reagents and Materials. All reagents were purchased from Sigma-Aldrich, and they were used as received unless otherwise specified. The synthetic procedure for the preparation of PTMA-*co*-BP has been published earlier elsewhere.[21] ITO/glass substrates (CG-501N-CUV) were purchased from Delta Technologies, Ltd. The leakless miniature Ag/AgCl electrode ET072 was purchased from eDAQ. EMI-TFSI was purchased from Millipore Sigma.

UV Crosslinking. PTMA-*co*-BP thin films were spin-coated onto ITO substrates at a spin speed of 1500 rpm. Then, the thin films were transferred into the N_2 glovebox and crosslinked by Thermo Scientific Pierce UVP UV lamps (8 W) that emit at 254 nm for 30 min. A longer exposure time causes the formation of a highly crosslinking network, which could impede the ion diffusion.

Instrumentation. Electrochemical experiments were performed using a BioLogic SP-150 potentiostat. The UV−vis spectra and the optical memory measurements were obtained from an Agilent Cary 5000 UV−vis−NIR spectrophotometer. The thickness of thin films was measured by a Veeco dimension 3100 atomic force microscope.

Thin-Film Characterization. The three-electrode cyclic voltammetry (CV) experiments were carried out to calculate the redox capacity of ECP-magenta and PTMA-*co*-BP thin films with different thicknesses. The working electrode is an ITO substrate coated by the ECP-magenta/PTMA-*co*-BP thin film; the reference electrode is an ET072 leakless miniature Ag/AgCl electrode; the counter electrode is a platinum wire; and the electrolytes used are 0.2 M tetrabutylammonium hexafluorophosphate ($TBAPF_6$) in PC or acetonitrile (ACN) or 0.2 M EMI-TFSI in PC. The voltage was scanned from −0.2 to 1.0 V at a scan rate of 40 mV/s for ECP-magenta. For PTMA-*co*-BP, the voltage was scanned from −0.2 to 1.0, 1.4, 1.5, or 1.6 V at a scan rate of 40 mV/s. The anodic voltage was adjusted when different electrolytes and film thicknesses were used. The same setup was also used for the CV cycling stability test. The anodic and cathodic peak current densities in the voltammogram were used to indicate the cycling stability of the polymer thin film. Moreover, all the thin films were preconditioned by the CV cycling before characterizations of the polymer thin films unless otherwise mentioned. The two-electrode CV experiments were carried out to study the appropriate ratio of the redox capacity of the PTMA-*co*-BP thin film to the ECP-magenta. All the thin films were made by spin-coating of the solutions on ITO substrates at a spin speed of 1500 rpm. The thickness of PTMA-*co*-BP can be controlled by varying the concentrations of the solutions in the range of 5−26.7 mg/mL. ECP-magenta solutions (30 mg/mL) were used for spin-coating, resulting in a thin film with a thickness of ∼240 nm. To assemble a two-electrode cell, a PTMA-*co*-BP-coated ITO substrate and an ECP-magenta-coated ITO substrate were inserted into a precut plastic cap parallelly, and then they were immersed in the electrolyte housed in a UV cuvette. The two-electrode CV experiments were carried out between −1.35 and 1.2 V at a scan rate of 40 mV/s. Chronoabsorptiometry experiments were performed between −1.35 and 1.2 V, and the absorbance spectra were recorded between 350 and 1200 nm after each potential was applied. The background absorbance was corrected by a reference cell that has two bare ITO substrates immersed in the same electrolyte. Atomic force microscopy (AFM) images were obtained in a tapping mode at a 0.3 Hz scan rate. The thickness was measured by scanning across a scratch in the samples. The average step height was calculated from four different measurements.

RESULTS AND DISCUSSION

A crosslinkable radical polymer PTMA-*co*-BP was synthesized via radical polymerization using a previously reported procedure (Figure 1a).[21] From the ^1H NMR, the ratio between the radical and the benzophenone moieties was approximately about 85:15. By incorporating the benzophenone moieties, PTMA-*co*-BP can undergo photo-crosslinking reaction by proton subtraction under UV irradiation, leading to the formation of a crosslinked network which prevents the dissolution of PTMA-*co*-BP thin films. The CV of the crosslinked PTMA-*co*-BP thin film in 0.2 M $TBAPF_6$ ACN shows a pair of redox peaks at +0.93 and +0.49 V (Figure 1a). These signals are associated with the reversible redox property of the conversion of the nitroxide radical to the oxoammonium cation (and vice versa on the reverse sweep). The UV−vis light

DOI: 10.1021/acsami.8b03235
ACS Appl. Mater. Interfaces 2018, 10, 18956−18963

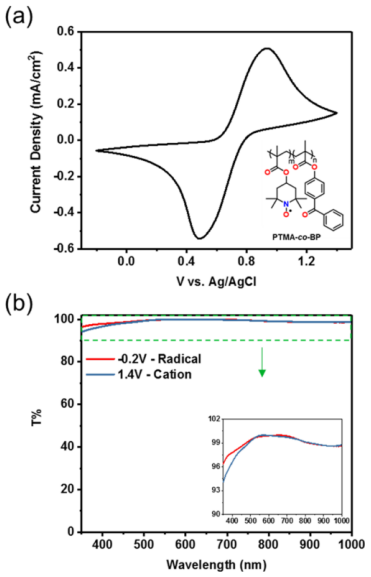

Figure 1. (a) Cyclic voltammogram of PTMA-*co*-BP (inset: molecular structure of PTMA-*co*-BP). (b) UV−vis transmittance spectra of PTMA-*co*-BP in the radical and cation forms (inset: the enlarged plot).

absorption measurements show that the spectra of the PTMA-*co*-BP thin film with a thickness of ∼180 nm are similar in both radical and cation states (Figure 1b). Moreover, transmittances of both are above ∼94% from 350 to 1000 nm. Therefore, PTMA-*co*-BP can be an excellent candidate as a noncolor change ion storage layer for ECDs.

UV−vis and CV measurements were performed to determine the effect of the crosslinking on the optical and electrochemical properties of the PTMA-*co*-BP thin films. From the UV−vis measurements, the peak at ∼250 nm is associated with the BP moieties in the PTMA-*co*-BP thin film (Figure 2a). The intensity decreases after UV light irradiation and remains the same with longer exposure, indicating that the consumption of the benzoylphenyl group was complete within 60 min of exposure. The CV results show an increase in the current density after crosslinking, resulting in a higher redox capacity (Figure 2b). The increase of redox capacity is believed to be due to two factors. First, the electrochemical stability of PTMA-*co*-BP was improved after crosslinking. Second, the polymer chains formed a semi-locked conformation after crosslinking, which resulted in an increase of current generated from a diffusional-dependent double-layer charging process.[22]

CV cycle tests were performed to confirm the electrochemical stability of PTMA-*co*-BP after photo-crosslinking. A thin layer of PTMA and PTMA-*co*-BP was coated on two different ITO substrates. Then, CV cycle tests were scanned at a rate of 40 mV s^{-1} in a 0.2 M $TBAPF_6$ in ACN. The thin film of PTMA-*co*-BP went through a break-in process during which the I_{pa} increased from the 1st to the 50th cycle (Figure 3a). Relative to the CV profile of the homopolymer PTMA thin film, a broad plateau around 0.7 V can be observed in the CV of PTMA-*co*-BP, which became sharper with extended cycles (Figure 3a,b). The broader redox processes also suggested that the PTMA-*co*-BP thin film was indeed crosslinked.[22] The I_{pa} of PTMA-*co*-BP lost 9.3% upon the 250th cycle after the break-in process, while the I_{pa} of the PTMA thin film lost 84% after 150 cycles (Figure 3c). Therefore, the crosslinking strategy can effectively prevent the dissolution of PTMA-*co*-BP thin films.

Next, we investigated the effect of electrolytes on the electrochemical behaviors of PTMA-*co*-BP as electrolyte anions were found to assist the charge transportation in the PTMA gel previously.[23] Moreover, different electrolyte anions have different diffusion coefficients in the charge transportation that occurs within the PTMA matrix, and this affects the discharging rate characteristics of the organic radical battery.[24] When radical polymers were used as the ion storage layer in ECDs, the diffusion coefficient of solvated anions within the electrodes determined the accessibility of redox sites of electrodes. As a result, the redox capacity of radical polymers might have a variation in different electrolytes. Selecting the appropriate electrolytes could be the key factor to enhancing the performance of radical polymer-based ECDs. The redox capacity of PTMA-*co*-BP thin films was calculated from the CV at a scan rate of 40 mV s^{-1} in a three-electrode setup with a platinum wire serving as the counter electrode and Ag/AgCl serving as the reference electrode. The CV experiments of PTMA-*co*-BP thin films with similar thicknesses were carried out in 0.2 M $TBAPF_6$ PC and ACN. The thickness of the thin films was controlled by spin-coating of the same solution at the same spin speed. The redox capacity of the PTMA-*co*-BP thin

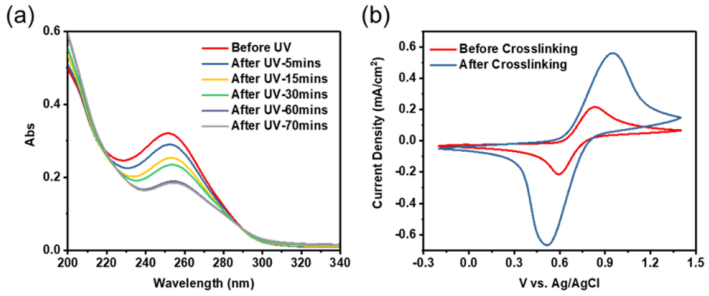

Figure 2. (a) UV−vis absorption spectra of PTMA-*co*-BP thin films with a thickness of ∼180 nm before and after UV irradiation for different time intervals. (b) Cyclic voltammograms of the PTMA-*co*-BP thin film before and after UV crosslinking.

DOI: 10.1021/acsami.8b03235
ACS Appl. Mater. Interfaces 2018, 10, 18956−18963

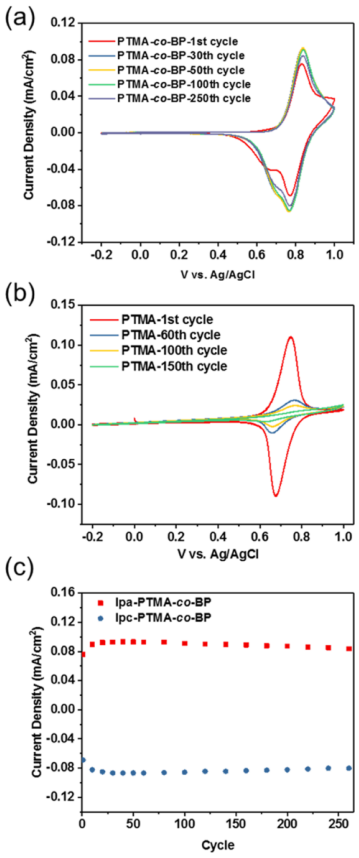

Figure 3. Cyclic voltammograms of (a) PTMA-*co*-BP and (b) PTMA. (c) I_{pa} and I_{pc} of the cyclic voltammograms of the PTMA-*co*-BP thin film vs the number of cycles.

film was smaller in PC (~0.8 mC/cm^2) compared to the thin film with a similar thickness in ACN (~5.6 mC/cm^2) (Figure 4a). CV experiments at different scan rates ranging from 10 to 200 mV/s were performed in both electrolytes. The square root of the scan rate has a linear correlation with the anodic peak current of the CVs of PTMA-*co*-BP thin films in both PC and ACN, which indicated a diffusion-controlled process (Figure 4b). The diffusion coefficients of the solvated PF_6^- can be calculated from the slope of the anodic peak current versus the square root of scan rates, which were 7.18×10^{-9} and 2.41×10^{-6} cm^2/s for the PTMA-*co*-BP thin film in PC and ACN, respectively (Figure 4b). The diffusion coefficient of the solvated PF_6^- in the PTMA-*co*-BP thin film was about 3 orders of magnitude larger in ACN than in PC. Therefore, the smaller redox capacity of PTMA-*co*-BP in PC was due to the slow diffusion of the solvated counterions. The low redox capacity of PTMA-*co*-BP in 0.2 M $TBAPF_6$ PC made it insufficient to balance the redox capacity of the electrochromic layer, resulting in a low optical contrast of the ECD (Figure S1). Although PTMA-*co*-BP thin films have a larger redox capacity in ACN, ACN is highly volatile and not suitable for device fabrications. We investigated the nonvolatile electrolyte 0.2 M EMI-TFSI in PC. After the break-in, the PTMA-*co*-BP thin film in 0.2 M EMI-TFSI PC had a redox capacity of ~3.9 mC cm^{-2}, and the diffusion coefficient of the solvated $TFSI^-$ was calculated to be $\sim 8.29 \times 10^{-7}$ cm^2 s^{-1} (Figure 4b). We believed that the increased redox capacity of PTMA-*co*-BP thin films in PC was due to the higher diffusion coefficient of the solvated $TFSI^-$ counterions.[24] Thus, 0.2 M EMI-TFSI PC was used in the following studies.

Two-electrode cells were assembled to further evaluate PTMA-*co*-BP as the ion storage layer of electrochromic materials (Figure 5a). ECP-magenta that can be switched between magenta (neutral state) and a highly transmissive state (oxidized state) was used as the electrochromic layer (Figure 5a). The two electrodes were inserted into the plastic cap such that they were parallel, and they were then immersed in a 0.2 M EMI-TFSI PC electrolyte, which was housed in a UV cuvette cell (Figure 5a). Because both PTMA-*co*-BP and ECP-magenta are P-type materials and will only undergo reversible oxidation reactions, the PTMA-*co*-BP layer was oxidized first before being assembled into two-electrode cells. In an ECD, the redox capacity of the counter electrode determined whether the charges generated in the electrochromic layer can be balanced to accomplish a color switching. Hence, by changing the

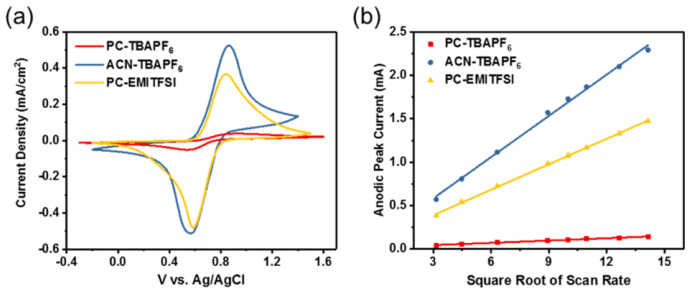

Figure 4. (a) Cyclic voltammograms of PTMA-*co*-BP thin films in 0.2 M $TBAPF_6$ PC, 0.2 M $TBAPF_6$ ACN, and 0.2 M EMI-TFSI PC. (b) Anodic peak current of PTMA-*co*-BP thin films obtained from the cyclic voltammograms in 0.2 M $TBAPF_6$ PC, 0.2 M $TBAPF_6$ ACN, and 0.2 M EMI-TFSI PC vs square root of the scan rate.

DOI: 10.1021/acsami.8b03235
ACS Appl. Mater. Interfaces 2018, 10, 18956−18963

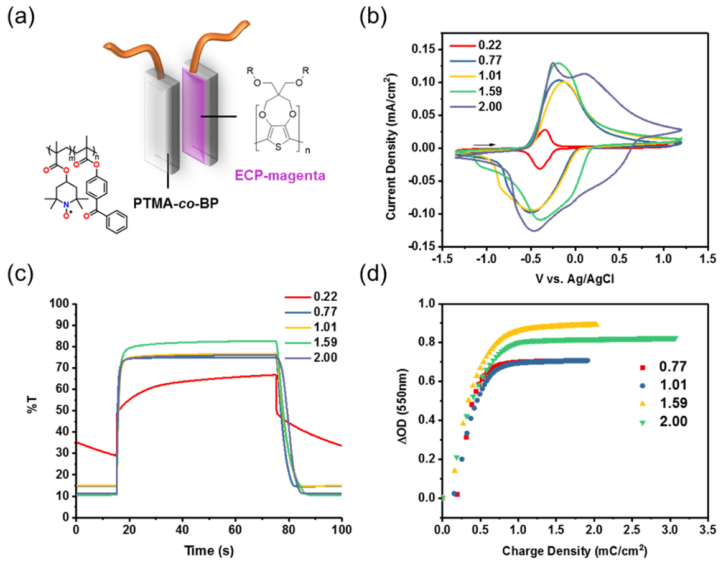

Figure 5. (a) Schematic demonstration of two-electrode cells and the structures of PTMA-*co*-BP and ECP-magenta. (b) Cyclic voltammograms, (c) DPSC, and (d) plots of change of the optical density at 550 nm vs charge density of two-electrode cells with different ratios of redox capacity of PTMA-*co*-BP to ECP-magenta.

thickness of the counter electrode, the redox capacity of the counter electrode can be varied to optimize the performance of the electrochromic layer. The redox capacity of each layer was estimated from the CV at a scan rate of 40 mV s^{-1} in a three-electrode setup before assembling the materials into a two-electrode cell. The thickness of the ECP-magenta layer was fixed at ~240 nm with a redox capacity of ~2.56 mC/cm^2. The thicknesses of PTMA-*co*-BP layers were varied from ~40 to ~220 nm by spin-coating of solutions with different concentrations (Table 1). The redox capacity of the PTMA-*co*-BP layer increased with the increase of thickness. In addition, the ratio of the redox capacity of the PTMA-*co*-BP layer to the ECP-magenta layer (R_q) can be adjusted from 0.22 to 2.00 (Table 1). Figure 5b shows the CVs of two-electrode cells of PTMA-*co*-BP/ECP-magenta with different R_q. The CVs show a pair of broad peaks around ~−0.5 and ~−0.2 V, suggesting that the reversible electrochemical reactions occurred within this electrochemical window (−1.35−1.2 V). When R_q is smaller than 1.0, the shape of the CVs is more like the CV of PTMA-*co*-BP. On increasing the R_q of PTMA-*co*-BP to ECP-magenta to over 1.0, CVs show more obvious capacitive-like plateaus appearing at both forward and backward scans, which are similar to the CV of the ECP-magenta (Figure S2). These capacitive-like plateaus were believed to be the faradaic redox processes during the charging/discharging of redox-active polymer thin films.[25] Then, −1.35 and 1.2 V were selected as the potentials in the double potential-step chronoamperometry (DPSC) experiments during which the transmittance was measured at 550 nm (Figure 5c). The results are summarized in Table 1. When the R_q was ~0.22, the charge capacity of the PTMA-*co*-BP layer could not balance the charge consumed in the ECP-magenta layer during the color switching. As a result, the two-electrode cell could only have an optical contrast (ΔT) of 37.8%. On increasing the R_q to ~1.59, the ΔT of the two-electrode cells reached a maximum value of 72.1% and decreased to 64.8% at the R_q of 2.00. Although the switching time at the R_q of 1.59 is the longest, the two-electrode cell can still reach 95% of its colored/bleached state within 10 s. Additionally, composite coloration efficiencies at 95% change of optical contrast ($\eta_{95\%}$) during the bleaching process were calculated based on a previously reported method (Figure 5d).[26] The composite coloration efficiency reached a maximum at the R_q of 0.77. This is because the thinner films generate less capacitive current during the redox processes, and thus, most of the charge injection/extraction is due to the color switching of the electrochromic layer. However, the charge consumed in the ECP-magenta layer had not been balanced completely, and the

Table 1. Thickness of PTMA-*co*-BP, Optical Contrast, and Switching Time That Achieved 95% of Optical Contrast and Composite Coloration Efficiencies of Two-Electrode Cells with Different Ratios of Redox Capacity of PTMA-*co*-BP to ECP-Magenta

R_q[a]	PTMA-*co*-BP thickness/nm	ΔT[b]	t_b (95%)[c]/s	t_c (95%)[c]/s	$\eta_{95\%}$[d]/cm^2 C^{-1}
0.22	42.61 ± 4.90	37.8			
0.77	85.69 ± 3.76	60.1	1.8	5.6	880.5
1.00	159.19 ± 10.77	61.7	3.4	7.7	713.5
1.59	185.22 ± 25.13	72.1	4.6	9.5	754.0
2.00	226.67 ± 12.56	64.8	2.4	8.4	705.1

[a] R_q is the redox capacity ratio of PTMA-*co*-BP to ECP-magenta. [b] ΔT is the optical contrast of ECDs at 550 nm. [c] t_b (95%) and t_c (95%) are the bleaching time and coloration time at 95% of the optical contrast change, respectively. [d] $\eta_{95\%}$ is the composite coloration efficiency at 95% of the optical contrast change.

DOI: 10.1021/acsami.8b03235
ACS Appl. Mater. Interfaces 2018, 10, 18956−18963

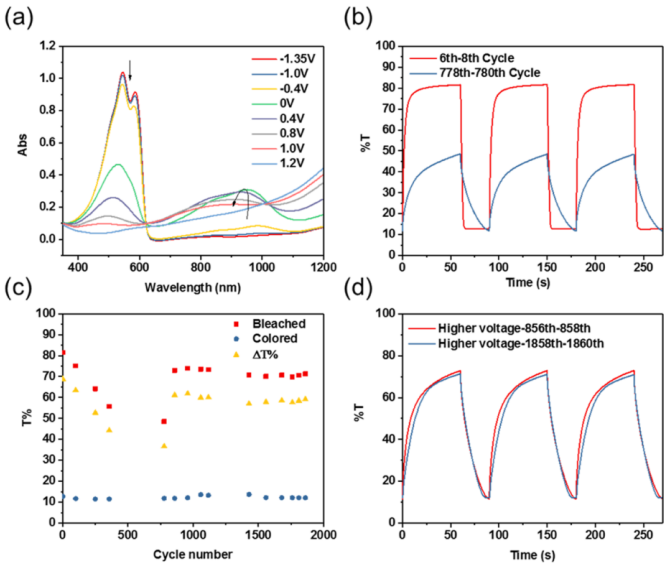

Figure 6. (a) Spectroelectrochemical study, (b) DPSC cycled between −1.0 and 1.0 V, (c) transmittance in the bleached and colored states and the change of the transmittance, and (d) DPSC cycled between −1.35 and 1.2 V of the two-electrode cells with the ratios of the redox capacity of PTMA-*co*-BP to ECP-magenta at ∼1.59.

optical contrast was not optimized. With the increase of the R_q to 1.00, the ΔT did not have an obvious change and more charge generated from the capacitive charging, resulting in a lower value of the composite coloration efficiency. At the R_q of 1.59, the doping level of ECP-magenta was further increased, which was indicated by the higher transmissive at 550 nm. The sufficient doping of the ECP-magenta layer led to a higher composite coloration efficiency of 754.0 cm^2 C^{-1}. The further increase of the R_q caused the decrease of ΔT and coloration efficiency. The thicker layer of PTMA-*co*-BP might lead to an increase of resistance and capacitive charge, resulting in an inefficient charge consumption of the ECD.[6] Therefore, the R_q of PTMA-*co*-BP to ECP-magenta was kept at ∼1.59 in the spectroelectrochemical study and the cycling test. The optimized ECD has an optical contrast of 72%, which is higher than the previously reported value of 66% for the ECD made by ECP-magenta and PMMA/PTMA, and their coloration efficiencies are comparable.[19] The slower switching time in this work could be due to the smaller working potential.

In the spectroelectrochemical study, the two-electrode cell has two strong absorptions at 545 and 587 nm originating from the ECP-magenta electrochromic layer. On increasing the applied potential from −1.35 to 1.2 V, the absorption in the visible region decreased, while the peak in the NIR region first increased and then decreased (Figure 6a). This phenomenon indicated that the neutral ECP-magenta molecules were doped and converted to polarons, and then neutral and polaron molecules were further oxidized to bipolarons, which also suggested that PTMA-*co*-BP can balance the charges needed in the ECP-magenta layer during the redox reactions. In the cycling test, the potential of the device was first switched between −1.0 and +1.0 V to avoid the possible side reactions such as the water-splitting reaction, which occurs at ∼1.23 V.[27] The DPSC experiments revealed that the bleaching time was longer than the coloring time. Thus, an asymmetric cycle test in which an anodic polarization was applied for 60 s and a cathodic polarization was applied for 30 s was adopted to ensure a thorough color switching.[28] After the break-in, the two-electrode cell can achieve an optical contrast of 68.8%, and the t_b (95%) and t_c (95%) were 11.8 and 3.2 s, respectively (Figure 6b). After ∼780 cycles, the optical contrast decreased to 36.7%, and the t_b (95%) and t_c (95%) increased to 48.5 and 24.2 s, respectively (Figure 6b). The lower contrast and slower response time of the ECDs could be due to the drifts of the electrode potential or the ion trapping within the electrodes during the cycling test.[29−31] A similar phenomenon was also observed in other studies of ECDs of the ECP-magenta and the propylenedioxythiophene/benzothiadiazole copolymer with MCCP as the counter electrode.[28,32,33] Additionally, the thickness of the PTMA-*co*-BP thin film was measured after the cycle test. The thin film that was immersed in the electrolyte and involved in the cycling test had a thickness of 168. ± 18. nm which is comparable to the thickness of the unreacted thin film exposed to air (182 ± 25 nm). Thus, dissolution problems of PTMA-*co*-BP were not the dominant reason for the lower contrast and slower switching kinetic of the device after 780 cycles. When the applied potentials were increased to 1.2 and −1.35 V, the optical contrast of the device could be recovered to 61.1% and was stable in the subsequent 1000 cycles (Figure 6c,d). In total, the cycle test was carried out for ∼1800 cycles and equal to ∼45 h under ambient condition, which demonstrated the long cycling stability of the ECD.

Finally, the optical memory of the two-electrode cell was tested by following a previously developed procedure.[34] The time of the applied potential that reset the device back to its colored state has an effect on its self-bleaching behaviors. Thus,

DOI: 10.1021/acsami.8b03235
ACS Appl. Mater. Interfaces 2018, 10, 18956−18963

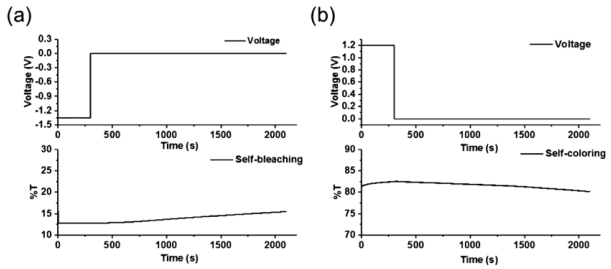

Figure 7. Voltage and transmittance vs time during the (a) self-bleaching and (b) self-coloring processes of the two-electrode cells with the ratio of the redox capacity of PTMA-*co*-BP to ECP-magenta at ∼1.59.

applying an (a) anodic/cathodic bias (1.2 V/−1.35 V) for 300 s was used in this study. When the device was switched to open circuit (V_{off}), the change of transmittance was measured for 30 min. Figure 7a,b shows that the transmittance of the two-electrode cell changed from 12.8 to 15.5% during the self-bleaching process and from 82.5 to 80.2% during the self-coloring process, indicating that the device can maintain its both colored and bleached states under open circuit for up to 30 min with negligible changes of transmission.

■ CONCLUSIONS

In this work, we demonstrated the potential of the highly transparent crosslinkable open-shell macromolecule copolymer, PTMA-*co*-BP, as the ion storage layer for ECDs. The crosslinked PTMA-*co*-BP thin films showed an improvement of electrochemical stability in the electrolytes. The diffusion coefficient of solvated ions within the radical polymer thin films has a great impact on the redox capacity of radical polymers. By selecting the appropriate electrolytes and optimizing the thickness of PTMA-*co*-BP, the redox capacity of the PTMA-*co*-BP thin film can be adjusted to match the charge consumption in the electrochromic layer so that the ECDs can achieve a high contrast, fast switching times, robust cycle stability, and good optical memory at open circuit for both bleached and colored states. The nonconjugated nature makes PTMA-*co*-BP highly transparent in the visible region, and the stable nitroxyl radical sites make it redox-active. Moreover, solution processability and easy synthesis are also advantages in the scaled-up manufacturing. Hence, PTMA-*co*-BP has a great potential to be used as the ion storage layer for ECDs.

■ ASSOCIATED CONTENT

Supporting Information

The Supporting Information is available free of charge on the ACS Publications website at DOI: 10.1021/acsami.8b03235.

DPSC of a two-electrode cell of PTMA-*co*-BP and preoxidized ECP-magenta; cyclic voltammogram of ECP-magenta; electrochemical impedance spectroscopy measurements of the PTMA and PTMA-*co*-BP thin films; and R(Q(RM)) equivalent circuit (PDF)

■ AUTHOR INFORMATION

Corresponding Author

*E-mail: jgmei@purdue.edu.

ORCID

Bryan W. Boudouris: 0000-0003-0428-631X

Jianguo Mei: 0000-0002-5743-2715

Notes

The authors declare no competing financial interest.

■ ACKNOWLEDGMENTS

The authors are grateful for the financial support from Purdue University and the American Chemical Society Petroleum Research Fund (# 57352-DNI7). The radical polymer was provided by S.M. and B.W.B. This work was partially supported by the Air Force Office of Scientific Research (AFOSR) through the Organic Materials Chemistry Program (grant number: FA9550-15-1-0449, Program Manager: Dr. Kenneth Caster) to B.W.B., and the authors thank the AFOSR for their gracious support.

■ REFERENCES

(1) Lampert, C. M. Electrochromic Materials and Devices for Energy Efficient Windows. *Sol. Energy Mater.* **1984**, *11*, 1−27.

(2) Beaujuge, P. M.; Reynolds, J. R. Color Control in π-Conjugated Organic Polymers for Use in Electrochromic Devices. *Chem. Rev.* **2010**, *110*, 268−320.

(3) Mortimer, R. J. Electrochromic Materials. *Chem. Soc. Rev.* **1997**, *26*, 147−156.

(4) Shen, D. E.; Österholm, A. M.; Reynolds, J. R. Out of Sight but Not out of Mind: The Role of Counter Electrodes in Polymer-Based Solid-State Electrochromic Devices. *J. Mater. Chem. C* **2015**, *3*, 9715−9725.

(5) Padilla, J.; Seshadri, V.; Sotzing, G.; Otero, T. Maximum Contrast from an Electrochromic Material. *Electrochem. Commun.* **2007**, *9*, 1931−1935.

(6) Kim, Y.; Shin, H.; Han, M.; Seo, S.; Lee, W.; Na, J.; Park, C.; Kim, E. Energy Saving Electrochromic Polymer Windows with a Highly Transparent Charge-Balancing Layer. *Adv. Funct. Mater.* **2017**, *27*, 1701192.

(7) Reichman, B.; Bard, A. J. The Electrochromic Process at WO_3 Electrodes Prepared by Vacuum Evaporation and Anodic Oxidation of W. *J. Electrochem. Soc.* **1979**, *126*, 583−591.

(8) Lee, S.-H.; Deshpande, R.; Parilla, P. A.; Jones, K. M.; To, B.; Mahan, A. H.; Dillon, A. C. Crystalline WO_3 Nanoparticles for Highly Improved Electrochromic Applications. *Adv. Mater.* **2006**, *18*, 763−766.

(9) Natarajan, C.; Nogami, G. Cathodic Electrodeposition of Nanocrystalline Titanium Dioxide Thin Films. *J. Electrochem. Soc.* **1996**, *143*, 1547−1550.

(10) Knott, E. P.; Craig, M. R.; Liu, D. Y.; Babiarz, J. E.; Dyer, A. L.; Reynolds, J. R. A Minimally Coloured Dioxypyrrole Polymer as a Counter Electrode Material in Polymeric Electrochromic Window Devices. *J. Mater. Chem.* **2012**, *22*, 4953−4962.

(11) Suga, T.; Sugita, S.; Ohshiro, H.; Oyaizu, K.; Nishide, H. P- and N-Type Bipolar Redox-Active Radical Polymer: Toward Totally

Organic Polymer-Based Rechargeable Devices with Variable Configuration. *Adv. Mater.* **2011**, *23*, 751−754.
(12) Suga, T.; Ohshiro, H.; Sugita, S.; Oyaizu, K.; Nishide, H. Emerging N-Type Redox-Active Radical Polymer for a Totally Organic Polymer-Based Rechargeable Battery. *Adv. Mater.* **2009**, *21*, 1627−1630.
(13) Janoschka, T.; Hager, M. D.; Schubert, U. S. Powering up the Future: Radical Polymers for Battery Applications. *Adv. Mater.* **2012**, *24*, 6397−6409.
(14) Nishide, H.; Iwasa, S.; Pu, Y.-J.; Suga, T.; Nakahara, K.; Satoh, M. Organic Radical Battery: Nitroxide Polymers as a Cathode-Active Material. *Electrochim. Acta* **2004**, *50*, 827−831.
(15) Mukherjee, S.; Boudouris, B. W. Applications of Radical Polymers in Solid-State Devices BT. *Organic Radical Polymers: New Avenues in Organic Electronics*; Mukherjee, S., Boudouris, B. W., Eds.; Springer International Publishing: Cham, 2017; pp 57−71.
(16) Wingate, A. J.; Boudouris, B. W. Recent Advances in the Syntheses of Radical-Containing Macromolecules. *J. Polym. Sci., Part A: Polym. Chem.* **2016**, *54*, 1875−1894.
(17) Tomlinson, E. P.; Hay, M. E.; Boudouris, B. W. Radical Polymers and Their Application to Organic Electronic Devices. *Macromolecules* **2014**, *47*, 6145−6158.
(18) Takahashi, Y.; Hayashi, N.; Oyaizu, K.; Honda, K.; Nishide, H. Totally Organic Polymer-Based Electrochromic Cell Using TEMPO-Substituted Polynorbornene as a Counter Electrode-Active Material. *Polym. J.* **2008**, *40*, 763.
(19) Vasilyeva, S. V.; Unur, E.; Walczak, R. M.; Donoghue, E. P.; Rinzler, A. G.; Reynolds, J. R. Color Purity in Polymer Electrochromic Window Devices on Indium−Tin Oxide and Single-Walled Carbon Nanotube Electrodes. *ACS Appl. Mater. Interfaces* **2009**, *1*, 2288−2297.
(20) Suga, T.; Konishi, H.; Nishide, H. Photocrosslinked Nitroxide Polymer Cathode-Active Materials for Application in an Organic-Based Paper Battery. *Chem. Commun.* **2007**, *17*, 1730−1732.
(21) Zheng, L.; Mukherjee, S.; Wang, K.; Hay, M. E.; Boudouris, B. W.; Gong, X. Radical Polymers as Interfacial Layers in Inverted Hybrid Perovskite Solar Cells. *J. Mater. Chem. A* **2017**, *5*, 23831−23839.
(22) Jensen, J.; Dyer, A. L.; Shen, D. E.; Krebs, F. C.; Reynolds, J. R. Direct Photopatterning of Electrochromic Polymers. *Adv. Funct. Mater.* **2013**, *23*, 3728−3737.
(23) Nakahara, K.; Oyaizu, K.; Nishide, H. Electrolyte Anion-Assisted Charge Transportation in Poly(oxoammonium Cation/nitroxyl Radical) Redox Gels. *J. Mater. Chem.* **2012**, *22*, 13669−13673.
(24) Iwasa, S.; Nishi, T.; Nakamura, S. Effect of Charge Transportation on High-Rate Discharge Properties of Organic Radical Batteries with Gel-State Cathode. *J. Electroanal. Chem.* **2017**, *805*, 171−176.
(25) Heinze, J.; Frontana-Uribe, B. A.; Ludwigs, S. Electrochemistry of Conducting Polymers-Persistent Models and New Concepts. *Chem. Rev.* **2010**, *110*, 4724−4771.
(26) Gaupp, C. L.; Welsh, D. M.; Rauh, R. D.; Reynolds, J. R. Composite Coloration Efficiency Measurements of Electrochromic Polymers Based on 3,4-Alkylenedioxythiophenes. *Chem. Mater.* **2002**, *14*, 3964−3970.
(27) Khan, S. U. M.; Al-Shahry, M.; Ingler, W. B. Efficient Photochemical Water Splitting by a Chemically Modified N-TiO_2. *Science* **2002**, *297*, 2243−2245.
(28) Remmele, J.; Shen, D. E.; Mustonen, T.; Fruehauf, N. High Performance and Long-Term Stability in Ambiently Fabricated Segmented Solid-State Polymer Electrochromic Displays. *ACS Appl. Mater. Interfaces* **2015**, *7*, 12001−12008.
(29) Wen, R.-T.; Arvizu, M. A.; Morales-Luna, M.; Granqvist, C. G.; Niklasson, G. A. Ion Trapping and Detrapping in Amorphous Tungsten Oxide Thin Films Observed by Real-Time Electro-Optical Monitoring. *Chem. Mater.* **2016**, *28*, 4670−4676.
(30) Wen, R.-T.; Granqvist, C. G.; Niklasson, G. A. Eliminating Degradation and Uncovering Ion-Trapping Dynamics in Electrochromic WO_3 Thin Films. *Nat. Mater.* **2015**, *14*, 996.
(31) Hassab, S.; Shen, D. E.; Österholm, A. M.; Reynolds, J. R.; Padilla, J. Exploring Unbalanced Electrode Configurations for Electrochromic Devices. *J. Mater. Chem. C* **2018**, *6*, 393−400.
(32) Jensen, J.; Krebs, F. C. From the Bottom Up − Flexible Solid State Electrochromic Devices. *Adv. Mater.* **2014**, *26*, 7231−7234.
(33) Padilla, J.; Seshadri, V.; Otero, T. F.; Sotzing, G. A. Electrochemical Study of Dual Conjugated Polymer Electrochromic Devices. *J. Electroanal. Chem.* **2007**, *609*, 75−84.
(34) He, J.; You, L.; Mei, J. Self-Bleaching Behaviors in Black-to-Transmissive Electrochromic Polymer Thin Films. *ACS Appl. Mater. Interfaces* **2017**, *9*, 34122−34130.

DOI: 10.1021/acsami.8b03235
ACS Appl. Mater. Interfaces 2018, 10, 18956−18963

ACS APPLIED MATERIALS & INTERFACES

Research Article

Cite This: ACS Appl. Mater. Interfaces 2019, 11, 4169−4177

www.acsami.org

Low-Temperature Thermally Annealed Niobium Oxide Thin Films as a Minimally Color Changing Ion Storage Layer in Solution-Processed Polymer Electrochromic Devices

Jiazhi He, Liyan You, Dung T. Tran, and Jianguo Mei*

Department of Chemistry, Purdue University, 560 Oval Drive, West Lafayette, Indiana 47907, United States

Supporting Information

ABSTRACT: The limited availability of solution-processable ion storage materials, both inorganic and organic, hinders the adoption of roll-to-roll manufacturing for polymer electrochromic devices (ECDs). The n-type transition metal oxides are known for their ion storage properties. However, the fabrication methods of their amorphous metal oxide thin films typically involve sputtering, thermal deposition, electrical deposition, or sol−gel deposition followed by high-temperature thermal annealing (>300 °C), thus making them incompatible for low-cost roll-to-roll manufacturing on flexible substrates. In this study, we report the synthesis of amorphous niobium oxide(a-Nb_2O_5) thin films from sol−gel precursors through the combination of photoactivation and low-temperature thermal annealing (150 °C). Coupled with p-type electrochromic polymers (ECPs), solution-processed a-Nb_2O_5 thin films were evaluated as a minimally color changing counter electrode (MCC-CE) material for electrochromic devices. We found that ultraviolet ozone (UVO) treated and 150 °C thermally annealed (UVO-150 °C) a-Nb_2O_5 thin films show excellent electrochemical properties and cycling stability. Notably, a-Nb_2O_5/ECP-magenta ECD has a high optical contrast of ∼70% and a fast switching time (bleaching and coloring time of 1.6 and 0.5 s for reaching 95% of optical contrast). In addition, the ECD demonstrates a high coloration efficiency of ∼849.5 mC cm^{-2} and a long cycling stability without a noticeable decay up to 3000 cycles.

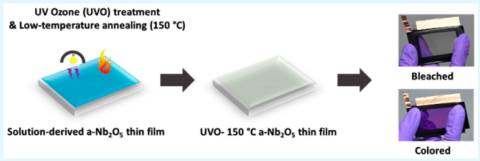

KEYWORDS: *low-temperature, solution-processed, niobium oxide, ion storage layer, counter electrode, electrochromic device*

INTRODUCTION

Electrochromic technology presents a great potential in a wide range of optical applications, ranging from smart windows,[1] self-dimming electrochromic ski goggles, and rear mirrors of automobiles[2,3] to electrochromic irises.[4] In a typical solid-state electrochromic device (ECD), three major components—an electrochromic layer as the working electrode (WE), a solid-state electrolyte layer for ion transport, and an ion storage layer as the counter electrode (CE)—are critical for high performance and electrochemical cycling stability. Electrochromic polymer (ECP) based solid-state ECDs have been emerging as the competitive technology for smart windows because of their high optical contrast, fast response time, scalability, and low cost.[5−8] A full-color palette of solution-processable electrochromic polymers has thus been created.[5] These polymers can be switched from colored states to highly transmissive states when they are oxidized. To match these electrochromic polymers, ion storage materials need to be highly transmissive in the reduced states. Currently, the choice for such ion storage materials is rather limited because n-type electrochromic polymers that can switch from a colored state to a highly transmissive state upon reduction are largely absent.[9] As a compromise solution, p-type electrochromic polymers which are transmissive under both neutral and oxidized states are preconditioned to pair with other colored p-type electrochromic polymers. For instance, both nonconjugated nitroxyl-based radical polymers and conjugated *n*-alkyl-substituted poly(3,4-propylenedioxypyrrole) (PProDOP) polymers have been investigated as CEs after the electrochemical or chemical preoxidation.[10−16] The electrochemical preoxidation needs to be performed in an electrochemical cell with electrolyte, reference, and counter electrodes, and the chemical preoxidation is done by immersing the fabricated thin films in a solution of oxidants. Then, the oxidized thin films are subjected to washing and drying steps to remove the chemical residues. These additional preconditioning steps bring complexity to roll-to-roll manufacturing and adds up to the fabrication cost.[15]

Some transition metal oxides undergo a color change when they are either oxidized or reduced. Such a color change in metal oxide thin films is usually associated with a large amount of charges consumption and generation due to their low coloration efficiency.[17] When metal oxides are paired up with an electrochromic polymer with a high coloration efficiency, they are usually regarded as minimally color changing counter electrodes (MCC-CE). For instance, Hassab et al. studied

Received: September 16, 2018
Accepted: December 31, 2018
Published: January 4, 2019

DOI: 10.1021/acsami.8b16154
ACS Appl. Mater. Interfaces 2019, 11, 4169−4177

tungsten oxide (WO_3) as the CE for ECPs.[18] Because only a small percentage of the total charges was used to balance the charges consumed in a complete switch of ECPs, the color change of WO_3 CE itself was minimum in an ECD. Unfortunately, WO_3 has a relatively high coloration efficiency (>50 cm^2/C); the doped WO_3 CE thin film showed a strong color residue in the bleached state of the electrochromic cells.[19] As a result, the electrochromic device made of WO_3 and ECP-magenta only showed a low optical contrast of ~52%. Searching for n-type transition metal oxides in the literature, we found that amorphous niobium pentoxide (a-Nb_2O_5) appears as an ion storage layer for its large volumetric charge density, high transparency, and low coloration efficiency (ca. 20 cm^2/C) in the visible region.[20−22] a-Nb_2O_5 thin films can be prepared by sputtering,[23] chemical vapor deposition,[24] electrodeposition[25] as well as sol−gel deposition.[22] If the sol−gel method is used, a high-temperature (>300 °C) thermal annealing will be required to remove residues of organic species and molecular water that are detrimental to their electrochemical properties and cycling performance.[26] In other words, this fabrication process of a-Nb_2O_5 thin films is not compatible with low-cost and high-throughput solution processing on plastic substrates (i.e., PET).[27]

In this work, we report a new synthetic method to prepare a-Nb_2O_5 thin films and use them as MCC-CEs to pair with electrochromic polymers for high-performance ECDs. The newly developed fabrication process involves photoactivation of sol−gel derived Nb_2O_5 thin films through an UV-ozone treatment, followed by a low-temperature (150 °C) annealing.[28] We found that the newly prepared a-Nb_2O_5 thin films show a similar charge density as the a-Nb_2O_5 thin films annealed at 300 °C and present an even better cycling performance. When paired with ECP-black and ECP-magenta as the MCC-CE, the ECDs offer a high optical contrast, a high color purity, and a long cycling stability. In addition, flexible thin-film ECDs are fabricated with the solution-processed a-Nb_2O_5 and ECP-magenta on ITO/PET substrates to forecast the potentials of the new synthetic method for a-Nb_2O_5 in future roll-to-roll manufacturing.

EXPERIMENTAL SECTION

Reagents and Materials. The niobium(V) ethoxide (99.95%) and ethanol (99.5%) were purchased from Fisher Scientific. The propylene carbonate (PC), lithium bis(trifluoromethane)sulfonimide (LiTFSI), poly(ethylene glycol) diacrylate (M_n = 575) ($PEGDA_{500}$), 2-hydroxy-2-methylpropiophenone (97%) (HMP), and platinum wire (99%, 0.5 mm) were purchased from Sigma-Aldrich. The leakless miniature Ag/AgCl electrode ET072 was purchased from eDAQ. All chemicals were used as received unless otherwise specified.

Instrumentations. All the spectra were collected using an Agilent Cary 5000 UV/vis−NIR spectrophotometer. All the electrochemical measurements were performed using a Biologic SP-150 potentiostat. A Laurell spin-coater (WS-650Mz-23NPPB) was used to prepare all the thin films. UVO treatment was performed using a HELIOS-500 UV-ozone cleaning system. A Veeco dimension 3100 atomic force microscopy (AFM) and a Gaertner variable angle Stokes ellipsometer (L116SF) were used to obtain the thicknesses of a-Nb_2O_5 thin films. A Keithley 2400 sourcemeter was used to monitor the potential distribution on the ECP-black WE during the electrochemistry experiments of a two-electrode cell. A Thermo Nicolet Nexus FTIR was used to study the organic and water residues within a-Nb_2O_5 thin films.

Preparation and Characterization of Thin Films. The niobium ethoxide precursor solution was prepared according to a previously reported method.[22] Under ambient conditions, Nb_2O_5 thin films were prepared using niobium ethoxide solution via the sol−gel reaction on ITO/glass or ITO/PET substrates followed by annealing at various temperatures (100, 150, and 300 °C) for 10 min. The UVO-150 °C a-Nb_2O_5 thin films were UVO treated for 20 min followed by annealing at 150 °C for 10 min. ECP-black and ECP-magenta were also synthesized according to previous work.[29,30] Solutions of ECP-black (40 mg/mL) and ECP-magenta (25 mg/mL) were prepared by dissolving the polymers in chloroform and stirred overnight before use. ITO/glass and ITO/PET substrates were cleaned by sonicating in acetone and ethanol for 10 min and blown dry by compressed nitrogen gas. All thin films were prepared by spin-coating at a spin speed of 1500 rpm. The thicknesses of one-layer a-Nb_2O_5 thin films were measured by ellipsometry and confirmed by AFM, and their topology was characterized by AFM. As a control experiment, each a-Nb_2O_5 thin film on ITO/glass substrate was cut into two pieces. One was subjected to the proposed process, and the other was kept untreated. The thicknesses of two- and three-layer a-Nb_2O_5 thin films were measured by ellipsometry.

Electrochemistry. A three-electrode cell was fabricated with ITO/glass substrates coated with ECP-black or a-Nb_2O_5 as the WE, a leakless Ag/AgCl as the reference electrode, 0.2 M LiTFSI in PC as the electrolyte, and a platinum wire as the counter electrode. Cyclic voltammetry experiments were performed using a three-electrode cell, at a scan rate of 40 mV/s, to obtain the charge density of electrodes. The charge density was calculated by the equation

$$\text{charge density} = \int j \, dV/s$$

where charge density has units of mC cm^{-2}, j is current density (mA cm^{-2}), s is the scan rate (V s^{-1}), and V is the voltage (V).

For two-electrode experiments, ECP-coated ITO/glass WEs and a-Nb_2O_5-coated ITO/glass CEs were used in 0.2 M LiTFSI in PC electrolyte or PEGDA gel electrolyte with 50 vol % of 0.2 M LiTFSI in PC for liquid- and solid-state devices, respectively. Cyclic voltammetry experiments were performed at a scan rate of 40 mV/s. For *in-situ* measurements of the potential change of the WE (E_{we}), a Keithley 2400 sourcemeter was used, and the voltage between WE and a leakless Ag/AgCl reference electrode was measured. The E_{we} data obtained during the CV experiments were processed using two points smoothing to remove the electrical noise caused by the vibration.

Device Fabrication. The electrolyte was prepared by mixing $PEGDA_{500}$, 0.2 M LITFSI in PC, and HMP in a volume ratio of 5:5:1 overnight in a nitrogen-filled glovebox. All ECP WEs were prepared by spin-coating the solutions on ITO/glass substrates (30 × 50 × 1 mm^3, sheet resistance, 8−12 Ω/sq) at a spin speed of 1500 rpm, and a-Nb_2O_5 CEs were prepared as described previously. Then, they were transferred into the N_2 glovebox. 0.2 mL of the mixed electrolyte was titrated on a WE, and a CE was placed on top with the coated sides facing each other. After the electrolyte had spread out by the capillary force, the electrolyte was cross-linked by placing the laminated device under the commercial UV lamps emitting at both 365 and 405 nm for 15 min. The device was taken out from the nitrogen-filled glovebox and sealed in the atmosphere by using a General Electric silicone. The flexible device was fabricated by following the same protocol on flexible ITO/PET substrates (sheet resistance 200 Ω/sq).

RESULTS AND DISCUSSION

An *in-situ* sol−gel reaction was used to fabricate a-Nb_2O_5 thin films on ITO/glass substrates. The precursor solution was made of niobium(V) ethoxide dissolved in ethanol with a concentration of ~0.19 M.[22] XRD measurements suggested that the Nb_2O_5 thin films annealed at both 150 and 300 °C were amorphous (Figure S1). Cyclic voltammetry (CV) studies were performed to investigate the effect of the processing conditions on the electrochemical properties of a-Nb_2O_5 thin films. The onset of the reduction potentials of the lithium-ion insertions in a-Nb_2O_5 thin films annealed at 100

DOI: 10.1021/acsami.8b16154
ACS Appl. Mater. Interfaces 2019, 11, 4169−4177

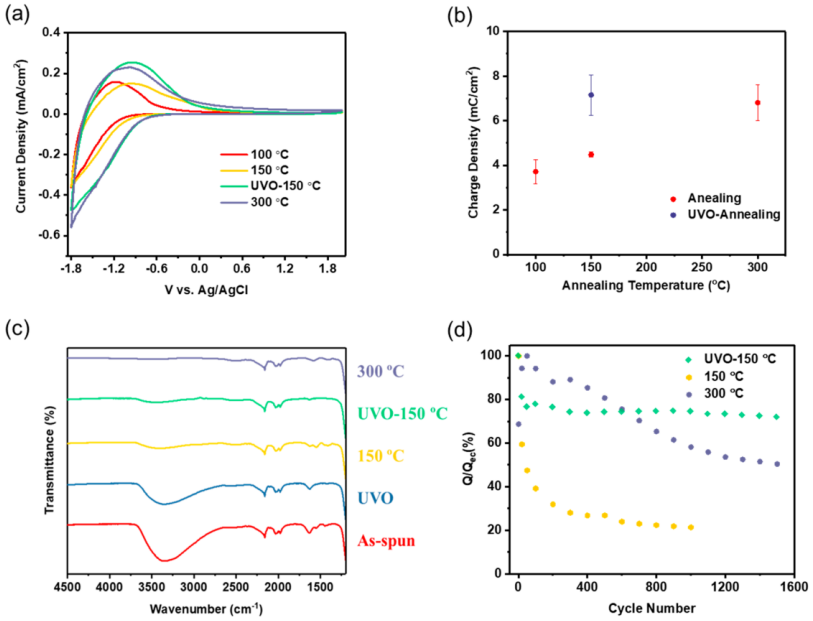

Figure 1. (a) Cyclic voltammograms and (b) charge density of UVO-150 °C a-Nb_2O_5 thin films and a-Nb_2O_5 thin films annealed at 100, 150, and 300 °C. (c) FTIR of UVO-treated, UVO-150 °C, and as-spun a-Nb_2O_5 thin films and a-Nb_2O_5 thin films annealed at 150 and 300 °C. (d) Percentage of charge density (Q) normalized by the charge density after electrochemical conditioning (Q_{cc}) versus cycle number of the UVO-150 °C a-Nb_2O_5 thin film and a-Nb_2O_5 thin films annealed at 150 and 300 °C.

and 150 °C was −1.15 and −1.0 V, respectively, which are more negative than the onset potentials of thin films annealed at 300 °C (−0.86 V) (Figure 1a). By using UVO treatment followed by annealing at 150 °C (UVO-150 °C), the onset potential of the lithium-ion insertion (−0.84 V) in UVO-150 °C a-Nb_2O_5 thin films is comparable to the thin films annealed at 300 °C. A larger potential bias might be required to operate ECDs which use a-Nb_2O_5 thin films annealed at 100 and 150 °C as the CEs.[12] As a CE material, a high charge density is desired to balance the charges consumed in the electrochromic layer. The charge densities can be calculated from the integration of the cyclic voltammograms (Figure 1b). Thin films annealed at 100 and 150 °C both have a charge density of ∼4.0 mC cm^{-2}, while UVO-150 °C a-Nb_2O_5 thin films have a charge density of 7.2 ± 0.9 mC cm^{-2}, which is comparable to the charge density of thin films that were annealed at 300 °C (6.8 ± 0.8 mC cm^{-2}). Fourier-transform infrared spectroscopy (FTIR) studies were performed to get insight into the effect of UVO treatment and annealing temperature (Figure 1c). A very strong absorption peak from the glass substrate was centered at ∼900 nm^{-1} and influenced the observation of the other peaks (Figure S2). Thus, the spectra are shown from 4500 to 1200 nm^{-1}. The broad absorption peak at ∼3300 nm^{-1} is associated with the −O−H stretching of molecular H_2O and −Nb−OH, and the peak ∼1630 nm^{-1} can be assigned to the bending of H_2O molecules. The small peaks around 1400 nm^{-1} can be related to bending and scissoring of the alkane (−C−H) of the organic residues from the precursor solution.[31] The FTIR spectrum of the as-spun a-Nb_2O_5 thin film showed peaks at ∼3300 and 1630 nm^{-1} and small peaks ∼1400 nm^{-1}, which revealed the existence of both molecular water and organic species. The disappearance of peaks at ∼1400 nm^{-1} of the UVO-treated a-Nb_2O_5 thin film suggests that the organic residues can be completely removed by UVO treatment, while the thin film annealed at 300 °C still showed traces of organic species. Most of the molecular water in a-Nb_2O_5 thin films can be eliminated by annealing at 150 °C and can be completely removed by annealing above 300 °C, as seen by the decrease of both −O−H stretching and scissoring peaks in the FTIR spectrum of a-Nb_2O_5 thin films annealed at 150 °C and the disappearance of them in the FTIR spectrum of a-Nb_2O_5 thin films annealed at 300 °C. The FTIR results suggested that UVO treatment was associated with the photoactivation processes of the solution derived a-Nb_2O_5 thin films. Under the continuous UV irradiation in an oxygen atmosphere, strong oxidants like ozone or atomic oxygen were generated, and the photolysis of organic residues from ligands and organic solvent led to the formation of free radical species. These highly reactive species promoted the formation of the amorphous metal−oxygen network, resulting in the condensation of the metal oxide thin film.[28,32] As a result, the organic residues-free and densified thin films would have higher homogeneity and reversibility in the redox reactions.[33] AFM studies were performed to investigate the change of the surface morphology and thickness after UVO treatment (Figure S3). Compared to the AFM image of the solution-derived a-Nb_2O_5 thin film, the UVO- treated thin film was more granular-like and porous, and the thickness decreased from 53.7 ± 5.5 to 39.2 ± 2.7 nm,

DOI: 10.1021/acsami.8b16154
ACS Appl. Mater. Interfaces 2019, 11, 4169−4177

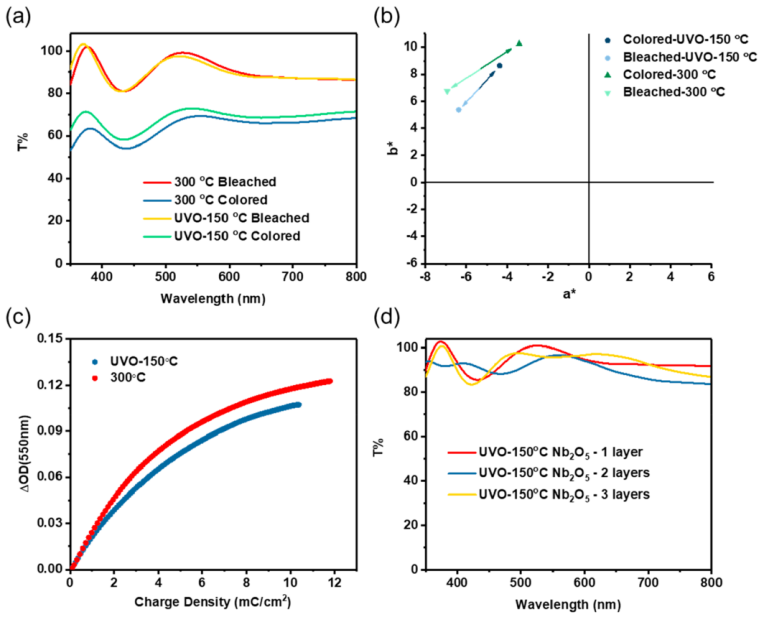

Figure 2. (a) UV−vis spectra and (b) colorimetry a^*b^* (CIE 1976 $L^*a^*b^*$ Color Space) color coordinates of the bleached and colored states of a-Nb_2O_5 thin films processed by annealing at 300 °C and UVO-150 °C. (c) Coloration efficiencies of a-Nb_2O_5 thin films processed by annealing at 300 °C and UVO-150 °C. (d) UV−vis spectra of UVO-150 °C a-Nb_2O_5 thin films with different thickness.

which confirmed the photoactivation process during the UVO treatment. Followed by the low-temperature (150 °C) annealing to remove molecular water, UVO-150 °C a-Nb_2O_5 thin films had a similar reduction onset potential and charge density as the thin films annealed at 300 °C.

In addition, the effect of organic residues on the electrochemical stability of a-Nb_2O_5 thin films was investigated. a-Nb_2O_5 thin films were cycled by double-potential step chronoamperometry between −1.8 and 2.0 V for a time interval of 20 s. The charge density was calculated using the chronoamperomagram for each cycle and normalized by the charge density after the electrochemical conditioning (Figure 1d). The charge density of a-Nb_2O_5 thin film annealed at 150 °C lost ∼80% after 500 cycles, which suggests that organic residues were detrimental to the electrochemical stability of the a-Nb_2O_5 thin films. In contrast, the UVO-150 °C a-Nb_2O_5 thin film lost ∼28% of its original charge density after 1500 cycles. The remaining charge density was sufficient to balance the charges in the electrochromic layer. Additionally, the a-Nb_2O_5 thin film annealed at 300 °C showed better cycling stability than the UVO-150 °C a-Nb_2O_5 thin film during the first 600 cycles but lost ∼50% of its charge density after 1500 cycles. Therefore, using UVO-150 °C treatment can induce a more complete formation of metal−oxide bonds, resulting in a densified thin film which has a better electrochemical stability.

In-situ spectroelectrochemistry was performed to evaluate the hue and transmittance of a-Nb_2O_5 as a MCC-CE material (Figure 2a). In the bleached state, the transmittances of both the UVO-150 and 300 °C-annealed a-Nb_2O_5 thin films are above 85% for most wavelengths ranging from 350 to 800 nm, except the near-UV region (around 430 nm). Because of the antireflection effect of the a-Nb_2O_5 coating or the smoothing of the ITO/glass substrate, the transmittance is larger than 100% in wavelengths around 370 nm.[34,35] When a-Nb_2O_5 thin films were reduced at −1.8 V vs Ag/AgCl, UVO-150 and 300 °C-annealed a-Nb_2O_5 thin films presented a light gray color in the colored state while their transmittances remained larger than 60% in most of the visible-light wavelength region. However, because of its charge density being at least 1.4 times higher than p-type ECPs (i.e., ∼2−5 mC cm^{-2}), only part of the capacity will be utilized to balance the charges on the ECPs during color switching.[36] Thus, a-Nb_2O_5 thin films could preserve its high transmittance in an ECD. The spectra of a-Nb_2O_5 thin films were used to calculate their $L^*a^*b^*$ color space using the Star-Tek colorimetry software. (Note: the negative and positive a^* value correspond to green and red colors, respectively; the negative and positive values of b^* are related to blue and yellow colors, respectively; L^* represents the lightness (Figure 2b).) The UVO-150 °C a-Nb_2O_5 thin film has smaller values of a^* and b^* than the 300 °C annealed a-Nb_2O_5 thin film in both colored and bleached states, which suggests that UVO-150 °C a-Nb_2O_5 thin films have a lower hue. As the CE, UVO-150 °C a-Nb_2O_5 thin films offer a higher color purity in ECDs. Because only a fraction of the charges would be needed to balance the charge consumption in the ECPs, the coloration efficiency of the a-Nb_2O_5 thin film was calculated from the initial slope of the curve of the change of optical density (ΔOD) versus charge density (Figure 2c). The coloration efficiency of UVO-150 °C a-Nb_2O_5 thin film (16.7 cm^2 C^{-1}) was smaller than that of the a-Nb_2O_5 thin film annealed at 300 °C (20.7 cm^2 C^{-1}). Compared to a-Nb_2O_5 thin films annealed at 300 °C, UVO-150 °C a-Nb_2O_5 thin films

DOI: 10.1021/acsami.8b16154
ACS Appl. Mater. Interfaces 2019, 11, 4169−4177

will have less color change to generate the same amount of charges. The charge density of the UVO-150 °C a-Nb_2O_5 thin film can be adjusted by changing its thickness (number of coating layers) (Table 1). Upon increasing the thickness, the a-Nb_2O_5 thin films remain highly transmissive with a low hue indicated by the high value of L^* (>97.0) and small values of both a^* and b^* (<6.0) (Figure 2d). Therefore, UVO-150 °C a-Nb_2O_5 thin films can potentially be paired with a variety of ECPs with different thicknesses in an unbalanced configuration to assemble ECDs that have high optical contrast and color purity. Compared with a-Nb_2O_5 thin films annealed at 300 °C, UVO-150 °C a-Nb_2O_5 thin films have a similar charge density, better long-term cycle stability, less color hue, and smaller coloration efficiency. In the following section, UVO-150 °C a-Nb_2O_5 thin films are demonstrated as MCC-CE material in ECDs.

Table 1. Thicknesses, Charge Densities, and Colorimetry $L^*a^*b^*$ (CIE 1976 $L^*a^*b^*$ Color Space) Color Coordinates of a-Nb_2O_5 Thin Films with Different Thickness Processed by UVO-150 °C

no. of layers	thickness (nm)	charge density (mC cm^{-2})	L^*	a^*	b^*
1	50.0 ± 9.8	7.2 ± 0.9	99.1	−5.1	5.3
2	82.5 ± 8.4	9.4 ± 0.4	97.8	−1.9	3.3
3	143.2 ± 10.0	13.1 ± 1.7	98.6	−1.3	3.7

Two-electrode liquid cells were assembled to further study the performance of a-Nb_2O_5 thin films as the MCC-CE for ECPs. The WE was an ECP-black-coated ITO/glass substrate, the CE was an a-Nb_2O_5-coated ITO/glass substrate, and the electrolyte was 0.2 M LiTFSI in PC. Both WE and CE were electrochemically conditioned by CV cycling prior to the cell assembly. The charge densities of the ECP-black layer and the a-Nb_2O_5 layer were calculated from their CVs to be about 3.0 and 8.0 mC cm^{-2}, respectively. Thus, the two-electrode cell was in an unbalanced electrode configuration (Figure 3a). In the spectroelectrochemistry study, the potential of the two-electrode cell was increased from −1.5 to 2.2 V (Figure 3b). The broad absorption in the visible region (350−800 nm) was mainly inherited from the ECP-black layer. Broad absorptions in the NIR range ~900 nm and beyond 1000 nm are related to polarons and bipolarons, respectively.[37] Upon increasing the potential, the absorption in the visible region decreased; the absorption of polarons first increased and then decreased, and the absorption of bipolarons increased dramatically. These results revealed that the a-Nb_2O_5 layer balanced the charges in the ECP-black layer during the color switching in a two-electrode cell. When the cell was oxidized to its bleached state at 2.2 V, the a-Nb_2O_5 CE was taken out to measure the transmittance spectrum and compared with its spectroelectrochemistry results (Figure 3c). The transmittance spectrum of a-Nb_2O_5 CE in the bleached device was an intermediate between its spectra of the colored and bleached states, which reveals that a-Nb_2O_5 CE was only partially reduced when used as the CE in the two-electrode cell. The partial reduction of the a-Nb_2O_5 thin film was sufficient to balance the charges generated during the oxidation of the ECP-black to a bleached

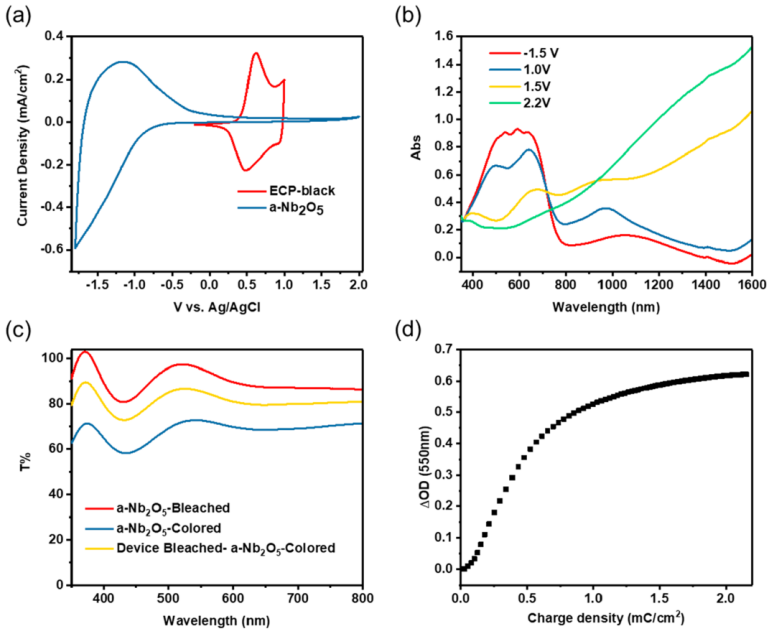

Figure 3. (a) Cyclic voltammograms of thin films of ECP-black and a-Nb_2O_5. (b) Spectroelectrochemistry of the a-Nb_2O_5/ECP-black two-electrode cell. (c) UV−vis spectra of the a-Nb_2O_5 thin film in colored and bleached states and its intermediate state in a bleached a-Nb_2O_5/ECP-black two-electrode cell. (d) Optical density versus charge density of the a-Nb_2O_5/ECP-black two-electrode cell.

DOI: 10.1021/acsami.8b16154
ACS Appl. Mater. Interfaces 2019, 11, 4169−4177

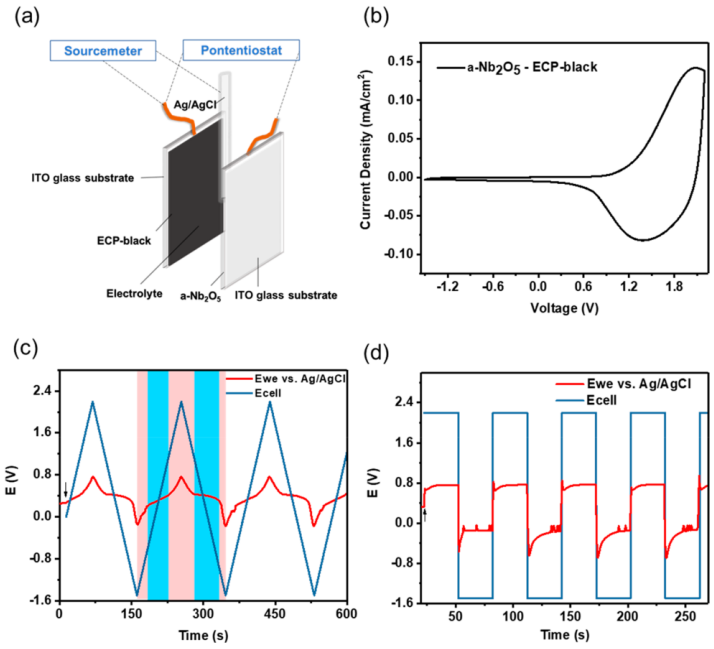

Figure 4. (a) Scheme of the a-Nb_2O_5/ECP-black two-electrode cell with a sourcemeter to monitor the potential at the ECP-black WE vs an Ag/AgCl reference electrode. (b) Cyclic voltammogram of the a-Nb_2O_5/ECP-black two-electrode cell. Change of the potential at the ECP-black WE during the (c) CV experiments and (d) DPSC experiments of the a-Nb_2O_5/ECP-black two-electrode cell. (Note: the potential windows where E_{we} increased quickly have a red background, while the potential windows where E_{we} increased at a slow rate or reached a plateau have a blue background. The black arrows indicate the beginning of the potential measurements.)

state. Therefore, a-Nb_2O_5 thin films maintained high transmittance and low hue and functioned as the MCC-CE during the switching of the electrochromic cell. Moreover, the composite coloration efficiency of the two-electrode cell was calculated to be ~360.0 mC cm^{-2} at the 95% change in optical contrast (Figure 3d).

In a two-electrode system, the potential distribution on electrodes affects the optical contrast (ΔT%), switching time, coloration efficiency, and cycle stability of ECDs.[34] For *in-situ* measurement of the potential distribution, an Ag/AgCl reference electrode was inserted into the two-electrode cell. When the cell potential (E_{cell}) was applied between the a-Nb_2O_5 CE and ECP-black WE by the potentiostat, the change of the potential distribution on the ECP-black WE (E_{we}) versus Ag/AgCl due to the ions intercalation/deintercalation was recorded by a Keithley sourcemeter during the CV and double-potential step chronoabsorptometry (DPSC) experiments (Figure 4a). The CV of the two-electrode cell shows a pair of redox peaks at ~2.00 and ~1.36 V (Figure 4b). After electrochemical conditioning of the two-electrode cell, the potential distribution on the E_{we} was measured versus the Ag/AgCl reference electrode during the CV experiments with the E_{cell} at the scan rate of 40 mV s^{-1} (Figure 4c). In the forward scan, the E_{we} increased with increasing the E_{cell} from −1.50 to 2.2 V at different rates within different potential windows. In the potential windows (with a red background in Figure 4c) where E_{cell} increased from −1.50 to −0.60 V and from 1.33 to 2.20 V, E_{we} increased at rates of 17.2 and 13.8 mV s^{-1}, respectively. While in the potential window (with a blue background in Figure 4c) of E_{cell} from −0.60 to 1.33 V, the E_{we} increased at a relatively slower rate of 4.5 mV s^{-1}. A similar behavior was also observed in the reverse scan of the CV experiments. During the reverse scan, when E_{cell} was scanned from 2.20 to 1.25 V and from −1.00 and 1.50 V, the E_{we} decreased at rates of 12.8 and 34.8 mV s^{-1}, respectively. When the E_{cell} was scanned from 1.20 to −1.00 V, E_{we} reached a plateau at ~0.40 V vs Ag/AgCl. The potential windows where E_{we} responded at a slower rate or reached a plateau suggested that ions cannot intercalate/deintercalate freely into/from the ECP-black WE. These phenomena could be due to the ion-trapping in the electrochromic layer, which requires an overpotential to overcome the trapping.[38−41] In DPSC experiments, the E_{we} was also monitored *in situ* using 2.2 and −1.5 V in accordance with the CV and spectroelectrochemistry of the cell (Figure 4d). When 2.2 V was applied to the cell, the E_{we} stepped to ~0.76 V vs Ag/AgCl. When the E_{cell} was switched from 2.2 to −1.5 V, the E_{we} quickly changed to −0.68 V vs Ag/AgCl and gradually increased, stabilizing at −0.15 V vs Ag/AgCl. Both potentials were within the stable electrochromic window of ECP-black (Figure S4). Therefore, these conditions were used in the cycling test of solid-state ECDs.

A simple fabrication route is vital to lower the production cost. Thus, the performance of the a-Nb_2O_5 electrode without

DOI: 10.1021/acsami.8b16154
ACS Appl. Mater. Interfaces 2019, 11, 4169−4177

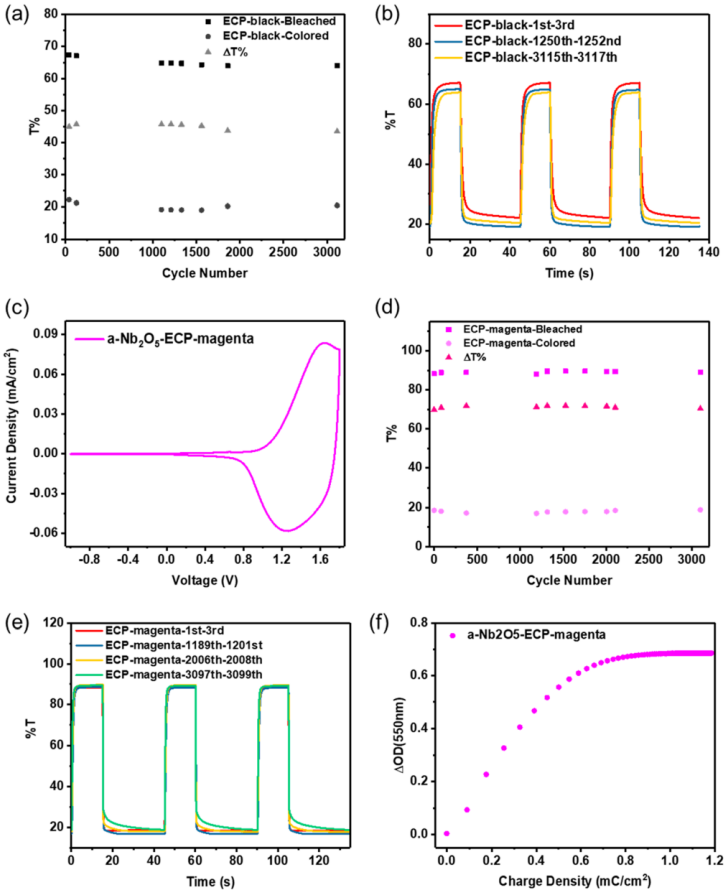

Figure 5. (a) Summary of the transmittance at 550 nm in the bleached and colored states and optical contrast of the a-Nb_2O_5/ECP-black ECD at different cycles. (b) DPSC of the a-Nb_2O_5/ECP-black ECD monitored at 550 nm at different cycles. (c) Cyclic voltammogram of the a-Nb_2O_5/ECP-magenta ECD. (d) Summary of the transmittance at 550 nm in the bleached and colored states and optical contrast of the a-Nb_2O_5/ECP-magenta ECD at different cycles. (e) DPSC of the a-Nb_2O_5/ECP-magenta ECD monitored at 550 nm at different cycles. (f) Change of optical density versus the charge density of the a-Nb_2O_5/ECP-magenta ECD.

any pretreatment and electrochemical conditioning was used in the two-electrode solid-state devices. The two-electrode solid-state device was assembled by using a-Nb_2O_5-coated ITO/glass as the CE electrode, the ECP-black-coated ITO/glass as the WE, and PEGDA plasticized by 50% of the 0.2 M LiTFSI in PC as the gel electrolyte. Because reaching E_{we} equilibrium in the coloring process is slower than the bleaching process, the device was kept at a constant potential of 2.2 V for 15 s and −1.5 V for 30 s to achieve a complete color change (Figure 4d). The device showed a ΔT% of ∼45% and was stable up to 3100 cycles with ∼1.4% decreases of ΔT% (Figure 5a,b). The time to achieve 95% of its full ΔT% is 3.4 and 5.6 s for bleaching and coloring, respectively (Figure 5b). The composite coloration efficiency at 95% of the optical contrast ($\eta_{95\%}$) of the solid-state a-Nb_2O_5/ECP-black ECD was ∼393.3 cm^2 C^{-1} (Figure S5). To extend the scope of this study, the device was also assembled using ECP-magenta as the WE. The ECP-magenta thin film had a charge density of ∼1.8 mC cm^{-2} and was paired with the a-Nb_2O_5 MCC-CE with a charge density of ∼7.2 ± 0.9 mC cm^{-2} to construct an ECD in an unbalanced configuration. The CV result of the ECD showed a pair of redox peaks at ∼1.63 and ∼1.25 V (Figure 5c). Potentials of 1.8 and −1.5 V were used to switch the device during the DPSC cycling test, and no side reactions within this electrochemical window were observed from the cyclic voltammogram of the a-Nb_2O_5/ECP-magenta two-electrode cell (Figure S6). The device can achieve ΔT% of 70% in the first cycle and was able to maintain nearly the same contrast in the following 3100 cycles (Figure 5d,e). The bleaching and coloring times to achieve 95% of its ΔT% are 1.6 and 0.5 s, respectively (Figure 5e). After 3100 cycles, the coloring time increased to 4.8 s, while the bleaching time (∼1.0 s) remained

DOI: 10.1021/acsami.8b16154
ACS Appl. Mater. Interfaces 2019, 11, 4169−4177

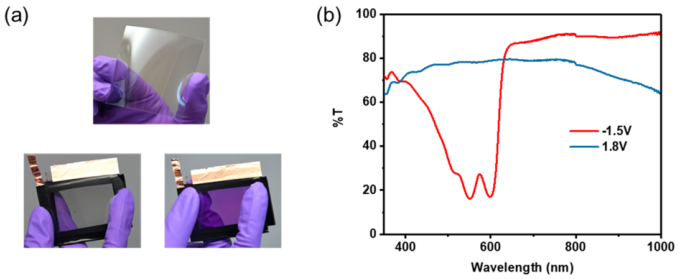

Figure 6. (a) Photographs of a UVO-150 °C a-Nb_2O_5 thin film on ITO/PET substrate and the flexible device of a-Nb_2O_5/ECP-magenta in bleached and colored states. (b) Spectroelectrochemistry of the a-Nb_2O_5/ECP-magenta flexible device.

similar to the first cycle (Figure 5e). At last, the $\eta_{95\%}$ of the a-Nb_2O_5/ECP-magenta was calculated to be ~849.5 mC cm^{-2} (Figure 5f). The high CCE suggests that the ECD can achieve a high contrast by consuming a very small amount of charges. By using a-Nb_2O_5 as the CE materials to balance the charges consumption in electrochromic layers, ECDs of both ECP-black and ECP-magenta showed outstanding cycling stability in double-potential cycling experiments.

Low-temperature (<150 °C) solution processing that is compatible with flexible substrates is the key for large-scale, high-throughput roll-to-roll processing. Thus, a UVO-150 °C a-Nb_2O_5 thin film was fabricated on the ITO/PET substrates with high uniformity and transparency (Figure 6a). The as-assembled flexible device had a $\Delta T\%$ of 62% at 550 nm (Figure 6b). The lower contrast of the flexible device could be due to the higher sheet resistance of ITO/PET substrates (~200 Ω/sq) than the ITO/glass substrates (~8−12 Ω/sq). With the demonstration of the flexible ECD, it is evident that the high-performance a-Nb_2O_5 can be fabricated on flexible substrates and serves as the CE for solution-processed low-cost ECDs.

■ CONCLUSION

In summary, solution-processed UVO-150 °C a-Nb_2O_5 thin films can achieve a similar charge density as that of a-Nb_2O_5 thin films annealed at 300 °C, yet with an improved cycling stability. Because UVO-150 °C a-Nb_2O_5 thin films have a much higher charge density and lower coloration efficiency than ECPs, they were applied as the MCC-CE material to pair with p-type cathodically coloring ECPs. Both a-Nb_2O_5/ECP-black and a-Nb_2O_5/ECP-magenta solid-state ECDs showed a high contrast, fast switching time, high coloration efficiency, and stable cycling performance. With the development of reliable highly transparent CE materials that can be solution processed on flexible substrates, we believe it can benefit the future roll-to-roll manufacturing electrochromic technology.

■ ASSOCIATED CONTENT

Supporting Information

The Supporting Information is available free of charge on the ACS Publications website at DOI: 10.1021/acsami.8b16154.

X-ray diffraction pattern of UVO-150 and 300 °C annealed a-Nb_2O_5 thin films; FTIR spectrum of a bare glass substrate; cyclic voltammogram of the ECP-black in 0.2 M LiTFSI PC; AFM images of the a-Nb_2O_5 thin films (a) before and (b) after UVO treatment; cyclic voltammogram of the ECP-black in 0.2 M LiTFSI PC; the change of optical density versus the charge density of the a-Nb_2O_5/ECP-black ECD; cyclic voltammogram of the a-Nb_2O_5/ECP-magenta two-electrode cell in 0.2 M LiTFSI PC (PDF)

■ AUTHOR INFORMATION

Corresponding Author

*E-mail: jgmei@purdue.edu (J.M.).

ORCID

Jianguo Mei: 0000-0002-5743-2715

Notes

The authors declare the following competing financial interest(s): J.M. is a co-founder of Ambilight Inc.

■ ACKNOWLEDGMENTS

The authors acknowledge Ambilight Inc. for the financial support.

■ REFERENCES

(1) Rauh, R. D. Electrochromic Windows: An Overview. *Electrochim. Acta* **1999**, *44* (18), 3165−3176.
(2) Ma, C.; Taya, M.; Xu, C. Smart Sunglasses Based on Electrochromic Polymers. *Polym. Eng. Sci.* **2008**, *48* (11), 2224−2228.
(3) Baucke, F. G. K. Electrochromic Mirrors with Variable Reflectance. *Sol. Energy Mater.* **1987**, *16* (1−3), 67−77.
(4) Deutschmann, T.; Kortz, C.; Walder, L.; Oesterschulze, E. High Contrast Electrochromic Iris. *Opt. Express* **2015**, *23* (24), 31544.
(5) Amb, C. M.; Dyer, A. L.; Reynolds, J. R. Navigating the Color Palette of Solution-Processable Electrochromic Polymers. *Chem. Mater.* **2011**, *23* (3), 397−415.
(6) Beaujuge, P. M.; Reynolds, J. R. Color Control in π-Conjugated Organic Polymers for Use in Electrochromic Devices. *Chem. Rev.* **2010**, *110* (1), 268−320.
(7) Jensen, J.; Krebs, F. C. From the Bottom Up - Flexible Solid State Electrochromic Devices. *Adv. Mater.* **2014**, *26* (42), 7231−7234.
(8) Jensen, J.; Dam, H. F.; Reynolds, J. R.; Dyer, A. L.; Krebs, F. C. Manufacture and Demonstration of Organic Photovoltaic-Powered Electrochromic Displays Using Roll Coating Methods and Printable Electrolytes. *J. Polym. Sci., Part B: Polym. Phys.* **2012**, *50* (8), 536−545.
(9) Dyer, A. L.; Österholm, A. M.; Shen, D. E.; Johnson, K. E.; Reynolds, J. R. Conjugated Electrochromic Polymers: Structure-Driven Colour and Processing Control. *Electrochromic Materials and Devices.*, 2015; pp 113−184.
(10) Vasilyeva, S. V.; Unur, E.; Walczak, R. M.; Donoghue, E. P.; Rinzler, A. G.; Reynolds, J. R. Color Purity in Polymer Electrochromic Window Devices on Indium-Tin Oxide and Single-Walled Carbon

Nanotube Electrodes. *ACS Appl. Mater. Interfaces* **2009**, *1* (10), 2288−2297.
(11) Vasilyeva, S. V.; Beaujuge, P. M.; Wang, S.; Babiarz, J. E.; Ballarotto, V. W.; Reynolds, J. R. Material Strategies for Black-to-Transmissive Window-Type Polymer Electrochromic Devices. *ACS Appl. Mater. Interfaces* **2011**, *3* (4), 1022−1032.
(12) Takahashi, Y.; Hayashi, N.; Oyaizu, K.; Honda, K.; Nishide, H. Totally Organic Polymer-Based Electrochromic Cell Using TEMPO-Substituted Polynorbornene as a Counter Electrode-Active Material. *Polym. J.* **2008**, *40* (8), 763−767.
(13) He, J.; Mukherjee, S.; Zhu, X.; You, L.; Boudouris, B. W.; Mei, J. A Highly Transparent Crosslinkable Radical Copolymer Thin Film as the Ion Storage Layer in Organic Electrochromic Devices. *ACS Appl. Mater. Interfaces* **2018**, *10* (22), 18956−18963.
(14) Takahashi, Y.; Oyaizu, K.; Honda, K.; Nishide, H. Low-Energy Driven Electrochromic Devices Using Radical Polymer as Transparent Counter Electroactive Material. *J. Photopolym. Sci. Technol.* **2007**, *20* (1), 29−34.
(15) Pittelli, S. L.; Shen, D. E.; Österholm, A. M.; Reynolds, J. R. Chemical Oxidation of Polymer Electrodes for Redox Active Devices: Stabilization through Interfacial Interactions. *ACS Appl. Mater. Interfaces* **2018**, *10* (1), 970−978.
(16) Knott, E. P.; Craig, M. R.; Liu, D. Y.; Babiarz, J. E.; Dyer, A. L.; Reynolds, J. R. A Minimally Coloured Dioxypyrrole Polymer as a Counter Electrode Material in Polymeric Electrochromic Window Devices. *J. Mater. Chem.* **2012**, *22* (11), 4953−4962.
(17) Thakur, V. K.; Ding, G.; Ma, J.; Lee, P. S.; Lu, X. Hybrid Materials and Polymer Electrolytes for Electrochromic Device Applications. *Adv. Mater.* **2012**, *24* (30), 4071−4096.
(18) Hassab, S.; Padilla, J. Using WO_3 as a Transparent, Optically-Passive Counter Electrode in an Unbalanced Electrochromic Configuration. *Electrochem. Commun.* **2016**, *72*, 87−90.
(19) Gillaspie, D. T.; Tenent, R. C.; Dillon, A. C. Metal-Oxide Films for Electrochromic Applications: Present Technology and Future Directions. *J. Mater. Chem.* **2010**, *20* (43), 9585−9592.
(20) Schmitt, M.; Heusing, S.; Aegerter, M. A.; Pawlicka, A.; Avellaneda, C. Electrochromic Properties of Nb_2O_5 Sol−gel Coatings. *Sol. Energy Mater. Sol. Cells* **1998**, *54* (1−4), 9−17.
(21) Pawlicka, A.; Atik, M.; Aegerter, M. A. Synthesis of Multicolor Nb_2O_5 Coatings for Electrochromic Devices. *Thin Solid Films* **1997**, *301* (1−2), 236−241.
(22) Özer, N.; Chen, D. G.; Lampert, C. M. Preparation and Properties of Spin-Coated Nb_2O_5 films by the Sol-Gel Process for Electrochromic Applications. *Thin Solid Films* **1996**, *277* (1−2), 162−168.
(23) Chen, K.-N.; Hsu, C.-M.; Liu, J.; Liou, Y.-C.; Yang, C.-F. Investigation of Antireflection Nb_2O_5 Thin Films by the Sputtering Method under Different Deposition Parameters. *Micromachines.* **2016**, *7*, 151.
(24) Maruyama, T. Electrochromic Properries of Manganese Oxide Thin Films Prepared by Chemical Vapor Deposition. *J. Electrochem. Soc.* **1995**, *142* (9), 3137−3141.
(25) Lee, G. R.; Crayston, J. A. Studies on the Electrochemical Deposition of Niobium Oxide. *J. Mater. Chem.* **1996**, *6* (2), 187−192.
(26) Llordés, A.; Wang, Y.; Fernandez-Martinez, A.; Xiao, P.; Lee, T.; Poulain, A.; Zandi, O.; Saez Cabezas, C. A.; Henkelman, G.; Milliron, D. J. Linear Topology in Amorphous Metal Oxide Electrochromic Networks Obtained via Low-Temperature Solution Processing. *Nat. Mater.* **2016**, *15* (12), 1267−1273.
(27) Zardetto, V.; Brown, T. M.; Reale, A.; Di Carlo, A. Substrates for Flexible Electronics: A Practical Investigation on the Electrical, Film Flexibility, Optical, Temperature, and Solvent Resistance Properties. *J. Polym. Sci., Part B: Polym. Phys.* **2011**, *49* (9), 638−648.
(28) Bretos, I.; Jiménez, R.; Ricote, J.; Calzada, M. L. Low-Temperature Crystallization of Solution-Derived Metal Oxide Thin Films Assisted by Chemical Processes. *Chem. Soc. Rev.* **2018**, *47* (2), 291−308.
(29) Reeves, B. D.; Grenier, C. R. G.; Argun, A. A.; Cirpan, A.; McCarley, T. D.; Reynolds, J. R. Spray Coatable Electrochromic Dioxythiophene Polymers with High Coloration Efficiencies. *Macromolecules* **2004**, *37* (20), 7559−7569.
(30) Shi, P.; Amb, C. M.; Knott, E. P.; Thompson, E. J.; Liu, D. Y.; Mei, J.; Dyer, A. L.; Reynolds, J. R. Broadly Absorbing Black to Transmissive Switching Electrochromic Polymers. *Adv. Mater.* **2010**, *22* (44), 4949−4953.
(31) Verma, A.; Basu, A.; Bakhshi, A. K.; Agnihotry, S. A. Structural, Optical and Electrochemical Properties of Sol-Gel Derived TiO_2 Films: Annealing Effects. *Solid State Ionics* **2005**, *176* (29−30), 2285−2295.
(32) Park, S.; Kim, K.-H.; Jo, J.-W.; Sung, S.; Kim, K.-T.; Lee, W.-J.; Kim, J.; Kim, H. J.; Yi, G.-R.; Kim, Y.-H.; Yoon, M.-H.; Park, S.-K. In-Depth Studies on Rapid Photochemical Activation of Various Sol−Gel Metal Oxide Films for Flexible Transparent Electronics. *Adv. Funct. Mater.* **2015**, *25* (19), 2807−2815.
(33) Spinolo, G.; Ardizzone, S.; Trasatti, S. Surface Characterization of Co_3O_4 Electrodes Prepared by the Sol-Gel Method. *J. Electroanal. Chem.* **1997**, *423* (1), 49−57.
(34) Kim, Y.; Shin, H.; Han, M.; Seo, S.; Lee, W.; Na, J.; Park, C.; Kim, E. Energy Saving Electrochromic Polymer Windows with a Highly Transparent Charge-Balancing Layer. *Adv. Funct. Mater.* **2017**, *27* (31), 1701192.
(35) Kwon, Y.-H.; Jang, G.-E. Effect of SiO_2 and Nb_2O_5 Buffer Layer on Optical Characteristics of ITO Thin Film. *Trans. Electr. Electron. Mater.* **2015**, *16* (1), 29−33.
(36) Hassab, S.; Shen, D. E.; Österholm, A. M.; Reynolds, J. R.; Padilla, J. Exploring Unbalanced Electrode Configurations for Electrochromic Devices. *J. Mater. Chem. C* **2018**, *6* (2), 393−400.
(37) Bulloch, R. H.; Reynolds, J. R. Photostability in Dioxyheterocycle Electrochromic Polymers. *J. Mater. Chem. C* **2016**, *4* (3), 603−610.
(38) Plieth, W.; Bund, A.; Rammelt, U.; Neudeck, S.; Duc, L. M. The Role of Ion and Solvent Transport during the Redox Process of Conducting Polymers. *Electrochim. Acta* **2006**, *51* (11), 2366−2372.
(39) Guan, S.; Elmezayyen, A. S.; Zhang, F.; Zheng, J.; Xu, C. Deterioration Mechanism of Electrochromic Poly(3,4-(2,2-Dimethylpropylenedioxy)Thiophene) Thin Films. *J. Mater. Chem. C* **2016**, *4* (20), 4584−4591.
(40) Huang, J. H.; Hsu, C. Y.; Hu, C. W.; Chu, C. W.; Ho, K. C. The Influence of Charge Trapping on the Electrochromic Performance of Poly(3,4-Alkylenedioxythiophene) Derivatives. *ACS Appl. Mater. Interfaces* **2010**, *2* (2), 351−359.
(41) Wen, R. T.; Granqvist, C. G.; Niklasson, G. A. Eliminating Degradation and Uncovering Ion-Trapping Dynamics in Electrochromic WO_3 Thin Films. *Nat. Mater.* **2015**, *14* (10), 996−1001.

DOI: 10.1021/acsami.8b16154
ACS Appl. Mater. Interfaces 2019, 11, 4169−4177